TEMPORAL AND SPATIAL PROCESSING IN A NONHUMAN PRIMATE MODEL OF NOISE-INDUCED HEARING LOSS

By

Chase A. Mackey

Dissertation

Submitted to the Faculty of

the Graduate School of Vanderbilt University

in partial fulfillment of the requirements

for the degree of

DOCTOR OF PHILOSOPHY

in

Neuroscience

December 17, 2022

Nashville, Tennessee

Approved: Date:

_____ _____

Mark Wallace, Ph.D.

_____ _____

Ramnarayan Ramachandran, Ph.D.

_____ _____

Troy Hackett, Ph.D.

_____ _____

Randolph Blake, Ph.D.

_____ _____

Barbara Shinn-Cunningham, Ph.D.

ACKNOWLEDGEMENTS

To everyone who played a part in my success, I unfortunately cannot do justice to your contributions in words. Trying to communicate my gratitude for all of this using these little sterile 12-point black letters felt like trying to appreciate Yellowstone National Park through the aperture of a confocal microscope. Nonetheless, I tried.

I would like to acknowledge the National Institutes of Health and NIDCD for funding this research, and the Vanderbilt Center for Integrative and Cognitive Neuroscience for supporting me early in my graduate career. Grant support from NIH was as follows: NIH R01 DC 015988 (MPIs R. Ramachandran and B. Shinn-Cunningham), NIH RO1 DC 11092 to RR, NIH T35 DC 008763 to Samantha Hauser (PI Linda J. Hood), and NIDCD F31 DC 019823 (PI Chase A. Mackey).

I have deep, profound gratitude for the time my mentors have spent training me. Their work speaks for itself, and therefore my comments are mostly reserved for their personal impressions on me. My advisor, Ram has left an indelible impression on me as a person and as a scientist. I am a wildly different person than the one who joined his lab. I feel privileged to be taking some of his creativity, careful analytical instincts, and his ever-present sense of humor, wherever I go in my career. Troy Hackett deserves special recognition for being a spectacular model scientist, relentless in his pursuit of scientific accuracy, and for always taking an interest in my wellbeing. To Barbara Shinn-Cunningham, for lending her staggering intellect, quick wit, and inimitable kindness to these projects; it was a privilege. To Randolph Blake, for contributing to my theoretical foundations by spending hours one-on-one reading classic signal detection theory work with me, and always displaying a willingness to be puzzled. Finally, to Mark Wallace for giving me eternal permission to always think bigger, and for setting an example as a tireless mentor and collaborator.

I would also like to acknowledge the excellent veterinary support provided by Drs. Carissa Jones, Michael McKinney, Kate Shuster, and Jeanne Wallace. Special thanks must be given to Mary Feurtado for thoughtful and careful technical support and instruction during every anesthetized procedure mentioned in this work. I would also like to acknowledge Jeremy Parker and the animal care technicians, especially LuAnn Toy and Paula Austin, for countless hours going above and beyond to care for our monkeys.

To Alpha, Bravo, Charlie, Delta, Echo, Gatsby, Aragorn, Bilbo, Celeborn, Durin, Elrond, Frodo, Gandalf, Haldir, Isildur, Dario, Luthien, Nessa, Opal, and Pippin, without whom none of this would be possible.

This work also would not be possible without the data collection and general assistance in the lab from many great individuals in The Ram Lab: Alejandro Tarabillo, Katy Alek, Namrata Temghare, Dr. Jane Mondul, Dr. Amy Stahl, Dr. Rachel Archer, Margit Dylla, Peter Bohlen, Andrew Hrnicek, Julie Choi, Alex McLeod, Jessica Feller, Jackson Mayfield, and Karina Jirik. Thank you all.

To the students I have been fortunate to advise: Natalie Schmidt, Grant Mercer, Julie Choi, Charita Veerapaneni, and Alex McLeod.

To George Wilson III, who, as a graduate student, provided a premium example of what a professional scientist can be, which I am still working to achieve.

To those I met during my time at Vanderbilt, but whose friendship extends beyond the lab, your love and support is invaluable. Andrea, Marina, Ashley, Sarah V., Sarah C., Roark, Amy, Ryan, Monica, John P., Zahra, Patrick, Anna, and everyone else, thank you all.

To Adriana Schoenhaut, whose care and fervent support gave my work new life mid-way through graduate school, and shielded me from my harshest (often self-directed) criticism. A piece of this is yours.

To Dr. Jane Mondul, with whom I was able to live out the phrase “iron sharpens iron,” coming up in this lab together, challenging and supporting each other. I don’t plan on that stopping anytime soon.

To my family, Mom, Dad, Lauren, there are too many to mention in total. Thank you for unconditionally supporting me through the years, and through all my changes.

To my oldest friends, whom I consider family and have supported me through all my changes. Their willingness to discuss science late into the night without ever losing their sense of humor has kept me humble, but only strengthened my resolve to convince all living people of the utility of the nonhuman primate model of auditory perception. Jon, Micah, Micah 2, Josh, Myles, Clare, Michael, Jon L., Cliff, Graham, Sammi, and everyone else, thank you.

To my teachers, particularly Randy Gouge, Mrs. Haddox, Sara Baker, Dr. Peter Kuryla, and Dr. Noel Boyle.

To the memory of Chandler Mackey, Mary Lee Ellis, Peggy Mackey, and Cooper Braun.

TABLE OF CONTENTS

LIST OF FIGURES

LIST OF TABLES

CHAPTER 1 – GENERAL INTRODUCTION

Theoretical foundations for studying hearing in noise

Natural environments are replete with sources of acoustic information. Surviving and communicating in the animal kingdom depend critically on navigating this complex acoustic landscape. This reality has placed the question of how the brain makes hearing in noise possible at the forefront of auditory neuroscience. Different theoretical frameworks are available to break down such problems, and key concepts from these frameworks will be helpful in understanding the theoretical motivation behind the experiments and analyses in this dissertation. First, the concept of levels of analysis will be used throughout (Marr et al., 1979). Briefly, Marr et al. defined three levels of analysis at which information processing can be analyzed: 1) the computational level, which is concerned with the problem being solved by the system (e.g. hearing the signal in the noise), 2) the algorithmic level, which is concerned with the algorithm implemented by the system to solve the problem (e.g. integrate signal over time), and 3) the implementation level, concerned with the physical substrate in which the algorithm is implemented (e.g. sum neuronal spiking activity over time). Measures used in this dissertation will span these levels with the goal of providing converging evidence from multiple levels. Second, insights from signal detection theory (SDT) informed the design of the experiments here (Green and Swets, 1966; Macmillan and Creelman, 2004; Swets, 1973; Tanner and Swets, 1954). The primary theoretical innovation of SDT was to acknowledge the cognitive factors (e.g. decision-making) that affect results in even the simplest perceptual experiments, and to subsequently provide a framework for modeling perceptual performance as a problem of detecting signals in noise. In SDT, analysis proceeds by beginning with these principles, following which two key parameters are extracted from perceptual performance: sensitivity and bias. Sensitivity refers to how well the observer makes correct choices and avoids incorrect ones. Bias refers to how much the observer favors one hypothesis over another, independent of the evidence. This results in descriptions of performance exhibiting low or high sensitivity, and liberal or conservative bias. SDT may appear deceptively simple, but it has been foundational to the understanding of perception and decision-making. Moreover, its rigorous use of nonparametric statistical methods are welcome in an era of problematic

statistical analysis in neuroscience (Garcia-Sifuentes and Maney, 2021; Nieuwenhuis et al., 2011). Specifically for the projects discussed here, SDT's influence was to break down the computational problem of hearing in noise into a sensory encoding component, as well as a decision-making component. This basis in SDT is described mainly to aid in the understanding of this dissertation, rather than to suggest a single optimal approach to understanding hearing. Other frameworks have been instrumental in understanding hearing in complex environments (Bregman, 1994; Shinn-Cunningham, 2008; Yost, 1991), but are not discussed here to provide reasonable scope, and due to the fact that the experiments presented here did not systematically manipulate attention.

Attention will now be turned to how sound features are encoded neuronally, and how that encoding relates to perceptual performance. The focus of this introduction will be the subcortical auditory system, though in specific chapters some implications for the auditory forebrain will be discussed.

Temporal processing

This project is focused on two key sound features that the brain uses to solve the computational problem of resolving signals in noise. The first is a temporal sound feature: amplitude modulation (AM). In natural environments, sound levels (amplitudes) fluctuate quasi-periodically over time (Joris et al., 2004; Richards and Wiley, 1980). AM signals have a few key characteristics. 1) The carrier, the amplitude of which is being modulated, which has its own frequency content distinct from the AM wave by which it is modulated. 2) AM frequency: the frequency at which the carrier's amplitude is modulated. 3) AM depth: the extent to which the signal is modulated, from 0-100%, or in terms of sound level relative to the peaks in AM. 4) AM phase: the phase of the AM wave by which the carrier signal is modulated. The influence of these features on auditory processing has been extensively explored in previous studies, particularly for the segregation of competing sounds (e.g. Bacon and Grantham, 1989; Bohlen et al., 2014; Lentz and Valentine, 2015). AM is a prominent feature of speech (Rosen, 1992). Variations in AM convey several types of linguistic information such as distinguishing consonants from non-consonants, vowel identity, and syllable identity. Sound envelope also has roles in general acoustic processing distinct from linguistic processing (e.g. Prinsloo and Lalor, 2022; Wang et al., 2021).

Given that this temporal sound feature is seemingly ubiquitous, it may be unsurprising to learn of its specialized physiological processing by the auditory system. To understand this processing requires knowledge of a temporally precise chain of events that begins in the peripheral auditory system. Sound, as a pressure wave, enters the ear and is diffracted by the pinnae (external ear), following which it is funneled by the ear canal to the tympanic membrane (Batteau, 1967; Dallos and Fay, 2012). There it vibrates the tympanic membrane, causing displacement of a three-part ossicular chain (malleus, incus, and stapes) in the middle ear, and subsequent transmission to a fluid medium by virtue of the stapes' connection to the round window - an opening in the coiled, fluid-filled cavity that is the cochlea. This fluid movement in the cochlea imparts the basilar membrane with traveling waves, which deflect stereocilia on hair cells, the primary sensory receptors of the auditory system.

Traveling waves along the basilar membrane result in sound frequency being represented tonotopically (spatially organized fashion) by virtue of different places along the cochlear length vibrating maximally to sounds of different frequencies, which is a key feature of the auditory system. Hair cells are polarized neuroepithelial cells with sensory transduction channels at their apical end, and specialized synapses at their basal end. The mechanical gating of the ion channels and specific structural aspects of the synapse at the basal end confer *rapid* and *sensitive* signal transmission, a general characteristic of mechanotransduction (Dallos and Fay, 2012; Tsunozaki and Bautista, 2009). Namely stereocilia are sensitive to nanometer deflections, which can be time-locked to signals of several thousand cycles per second, and the synaptic ribbon at the basal end allows rapid and continuous sound encoding though various vesicle trafficking mechanisms (Becker et al., 2018; Buran et al., 2010; Chakrabarti et al., 2018; Dallos and Fay, 2012; Fuchs and Glowatzki, 2015; Matthews and Fuchs, 2010). Hair cells exhibit two morphologically distinct types, inner and outer hair cells (IHCs and OHCs, respectively). OHCs modify the stiffness of the basilar membrane, enhancing its sensitivity to incoming pressure waves, and contributing to frequency selectivity inherited by the rest of the auditory system (i.e. the membrane vibrates maximally at restricted places depending on the frequency of the incoming sound; Fettiplace and Fuchs, 1999). IHCs are the primary sensory cells of the auditory system, innervated by

90-95% of the auditory nerve fiber (ANF) population, while OHCs are innervated by the remaining 5-10%. Each IHC is innervated by ~10-20 ANFs.

As a result of this highly precise chain of events just described, ANFs are imbued with phase-locked responses to AM stimuli (i.e. spike times are temporally aligned to a particular phase of the AM signal; Joris and Yin, 1992; Joris et al., 2004). The key characteristic of this phase-locking for the purposes of this dissertation is that it is similar across modulation frequencies (i.e. there is no tuning to modulation frequency in the ANF). Tuning to AM frequency becomes increasingly prevalent as the auditory pathway is ascended in the form of a rate code (average firing rate is different in response to different AM frequencies) and a temporal code (spikes aligned to a particular phase of the AM). ANFs innervate the cochlear nuclei (CN), the first station in the central auditory pathway, and bifurcate, with an ascending branch innervating the anteroventral CN (AVCN), and a descending branch innervating the dorsal CN (DCN) and posteroventral CN (Malmierca and Hackett, 2010; Webster and Fay, 2013). The CN are home to many cell types with diverse morphology and response properties (Adams, 1986; Malmierca and Hackett, 2010; Smith and Rhode, 1987). Despite this diversity, a common theme emerges across cell types: tuning to AM frequency is observed for the first time in the auditory pathway, in phase-locking (i.e. spike timing) and, in rare cases, firing rate (Joris et al., 2004; Rhode, 1994; Sayles et al., 2013). Two VCN cell types that are key to precise temporal processing are the spherical and globular bushy cells in the AVCN and rostral PVCN, which, by virtue of being covered by excitatory ANF terminals on their soma, display enhanced temporal precision relative to the ANF (Joris et al., 1994), and project to the superior olivary complex directly (spherical cells) or indirectly through the medial nucleus of the trapezoid body (globular cells; Malmierca and Hackett, 2010). Integration of these highly precise inputs, which are often excitatory and inhibitory, is key to the processing of spatial information in the SOC (discussed below), and to the encoding of AM. This fundamental principle of enhanced processing though the integration of multiple inputs informed the modeling of neuronal responses throughout this work, and is especially important for understanding how cochlear damage can lead to the perceptual deficits associated with hearing loss. The VCN, along with the ANF, also projects to the DCN, where cells with unique anatomical, synaptic, and membrane properties produce a wide variety of response types (e.g. tuning to

spectral notches) subserving functions such as sound localization (see section on spatial processing). Specifically for temporal processing of AM, the DCN generally exhibits similar patterns of phase-locking to AM, just at lower frequencies than the VCN. Anatomically, the DCN shows large interspecies variations, notably in primates; the significance of this variation for perception is unclear, but will be addressed in Chapter 4 (Adams, 1986; Moore, 1980; Moore et al., 1996; Rubio et al., 2008). The DCN's giant cells and pyramidal cells project to the inferior colliculus (IC), which has received a substantial amount of attention specifically for its putative role in temporal processing. Anatomically the IC is divided into central and external nuclei, with investigators commonly identifying a central nucleus, dorsoventral nucleus, and pericentral nucleus (Malmierca and Hackett, 2010; Winer and Schreiner, 2005). The central nucleus is identifiable neurophysiologically (see later chapters) as the tonotopic portion of the IC. The IC is characterized by an exceptional degree of convergence in its ascending inputs (VCN, DCN, SOC, lateral lemniscus), as well as descending inputs from the medial geniculate body and auditory cortex (Malmierca and Hackett, 2010; Winer and Schreiner, 2005). Across studies, the IC has emerged as a particularly interesting station in the auditory pathway for the processing of AM in both its spike rate and spike-timing (e.g. Henry et al., 2016; Langner and Schreiner, 1988; Nelson and Carney, 2007). Modeling studies suggest this emergence of rate-tuning to AM could be due to longer inhibitory time constants in the IC relative to the CN, and provide a simple, three-neuron circuit as an explanation for the emergence of this response property (Hewitt and Meddis, 1994; Nelson and Carney, 2004). Responses to AM in the IC, as well as implications for AM encoding in higher structures will be elaborated upon in Chapter 2.

There is also an abundant literature documenting how AM is processed at the perceptual level, which is a central topic of Chapter 2. One of the simplest behavioral characterizations of AM processing has been termed modulation masking release (MMR). MMR refers to the finding that signal-in-noise detection is improved in AM noise relative to unmodulated noise, reflecting the auditory system's ability to capitalize on the brief troughs in AM when the noise level is lower (e.g. Drullman et al., 1994; Festen and Plomp, 1990; Ihlefeld et al., 2016; Mackey et al., 2021b). In this way, MMR may index a listener's ability to take advantage of the AM in natural sounds and irrelevant speech sounds to segregate different sound sources. More direct behavioral

assays of AM encoding are seen in AM detection and discrimination paradigms. In AM detection experiments, the modulation depth of the signal is varied in order to estimate the shallowest depth a listener can reliably report (Viemeister, 1979). This is thought to provide an estimate of the limit of the auditory system to convey temporal information about stimulus envelope. Discrimination paradigms probe AM encoding fidelity more directly than AM detection paradigms because they typically require listeners to report if two signals are different with respect to a particular feature. This requires a differential perceptual analysis of two signals (Moody, 1994; Moore and Sęk, 2019; Yao et al., 2020), rather than simply listening for the presence or absence of a feature, as in detection tasks, which is particularly important when considering what behavioral assays may be sensitive to different forms of hearing loss (Lentz and Valentine, 2015; Wakefield and Viemeister, 1990). The implications of these differences in informational demands in detection vs. discrimination paradigms will be elaborated in Chapter 2.

Spatial processing

The second sound feature of interest here is space. Sounds arrive at the ears in a spatially unstructured mixture, requiring the brain to rely on various sound localization cues, the encoding of which requires the exquisite temporal precision described above. The first cue of interest originates as sound pressure waves are diffracted by the pinnae (external ear), which impose spectral filtering on broadband sounds. This provides a monaural sound localization cue due to the fact that spectral notches of high frequency sounds differ with sound location across horizontal and vertical planes (Batteau, 1967; Dallos and Fay, 2012; Heffner and Heffner, 2018). These spectral notches are first encoded in the DCN, which also receives projections from the contralateral DCN, affording the DCN two mechanisms for encoding spatial information (Davis, 2005; Mast, 1973). The other two key sound localization cues are interaural time differences (ITDs) and interaural level differences (ILDs; Heffner and Heffner, 2018). Through integration of the highly precise excitatory input from the VCN (described above) and inhibitory input from the contralateral VCN (mediated by the medial nucleus of the trapezoid body), the medial and lateral superior olive (MSO, LSO) exhibit tuning to these two localization cues (Brand et al., 2002; Grothe et al., 2010; Tollin, 2003; Tollin and Yin, 2005). The LSO and MSO then project to the IC. Similar to what is known for

temporal processing, the IC is a center of convergence from regions encoding spectral cues, ITDs, and ILDs (Grothe et al., 2010; Malmierca and Hackett, 2010; Winer and Schreiner, 2005). This anatomical evidence suggests that the IC could be the site of spatial cue integration – perhaps providing a cue-invariant representation of space. However, the neurophysiological evidence is lacking in unanesthetized animal preparations: a study in decerebrate cats suggests that representation of spatial cues remain segregated into parallel streams in the IC (Davis et al., 1999), and a study in awake primates found that IC neurons exhibit weak selectivity to spatial location (Groh et al., 2003). This stands in contrast to studies in primary auditory cortex, where a cue-invariant representation of space was found – neurons encoded *location* rather than spatial cues (Amaro et al., 2021; Wood et al., 2019). Importantly, these cortical recordings took place in animals engaged in localization tasks, in contrast to the subcortical studies of auditory spatial processing.

With the goal in mind of understanding hearing in noise in mind, it is important to strive to synthesize data from the behavioral and neurophysiological levels. Though sensitivity to localization cues provides the neural basis for spatial hearing, it underdetermines spatial processing as indexed by complex behavioral paradigms (Darwin and Hukin, 2000). Namely, higher-order characteristics (e.g. prosody, talker identity) can exert a stronger influence on spatial perception than manipulation of localization cues. Moreover, factors such as working memory influence performance even on simple detection paradigms that index spatial processing (Francis, 2010). Considering spatial hearing from this perspective will be key to interpreting the findings in the simple behavioral paradigm presented in Chapter 5.

Noise-induced hearing loss

This wealth of knowledge about temporal and spatial processing outlined above is valuable in its own right, but it also affords an opportunity to more fully understand noise-induced hearing loss (NIHL). At the global level, NIHL is a healthcare burden (Davis and Hoffman, 2019; World Health Organization, 2018), with substantial impact on mental health at the personal level (Dawes et al., 2015; Griffiths et al., 2020; Lin et al., 2011). The perceptual effects of NIHL are most prominent in environments requiring the use of spatial and temporal sound features (Best et al., 2017; Dai et al., 2018; Festen

and Plomp, 1990; Gelfand et al., 1988; George et al., 2006; reviewed in Moore, 1996), which will be the subject of later chapters. A central goal of this dissertation was to establish neurophysiological and behavioral measures of spatial and temporal processing in a recently developed nonhuman primate (NHP) model of NIHL (Burton et al., 2019a, 2020; Hauser et al., 2018; Mackey et al., 2021b; Stahl et al., 2022; Valero et al., 2017); a revival of a rich line of work in NHPs from decades ago (Hawkins and Stevens, 1950; Hawkins et al., 1976; Lonsbury-Martin and Martin, 1981; Lonsbury-Martin et al., 1987; Moody et al., 1978; Stebbins, 1982). The goal of the current model is to characterize NIHL at the anatomical, neurophysiological, and behavioral levels and to provide quantitative links between these levels. This linking process capitalizes on the high translational potential of NHPs, which can serve as a bridge between small animal studies and diagnostic/therapeutic work in humans (Burton et al., 2019a). It will be shown here that this approach can yield knowledge of the role of different sensory receptors (e.g. outer hair cells, inner hair cells, ribbon synapses) in auditory perception through the use of noise exposure that differentially affects each of these. This approach has shown that high level noise exposures typically result in permanent elevation in audiometric threshold (an estimate of the lowest audible sound level), loss of outer hair cells, variable inner hair cell loss, and ribbon synapse loss (Burton et al., 2019a; Valero et al., 2017; Wu et al., 2020).

Hidden hearing loss

The perceptual effects of NIHL are well established for people with overt hearing loss (e.g. elevated audiometric thresholds). However, an estimated 10-20% of people with normal audiometric thresholds report difficulty hearing in noise (Cooper and Gates, 1991; Hind et al., 2011; Parthasarathy et al., 2019), and such *normal-hearing* listeners display large individual differences in complex temporal and spatial tasks (Bharadwaj et al., 2015; Festen and Plomp, 1981; Parthasarathy et al., 2020a; Ruggles et al., 2011). This large percentage by definition does not include those who do not seek treatment for their deficits, so the real figure may be more staggering. Typical treatments of hearing loss such as hearing aids and cochlear implants were largely developed to recover threshold performance, and thus are unlikely to remedy this

problem. Moreover, hidden hearing loss emerges in *suprathreshold* environments (i.e. normal conversational sound levels) which indicates that devices designed to restore audibility, in their current form, are an unlikely solution. But understanding the origin of hidden hearing loss in the auditory pathway could result in its eventual treatment. One candidate cause of hidden hearing loss has emerged in the past decade: cochlear synaptopathy. Synaptopathy refers to the loss of inner hair cell ribbons synapses following a peripheral insult such as noise exposure or pharmacological manipulation. Synaptopathic noise exposures result in peripheral deafferentation, and have reliable neurophysiological effects – reduction of Wave I of the auditory brainstem response (ABR), and altered excitatory-inhibitory interaction along the auditory pathway (Asokan et al., 2018; Furman et al., 2013; Kujawa and Liberman, 2009; Resnik and Polley, 2017; Shaheen and Liberman, 2018; Song et al., 2016). Inhibition sculpts neuronal responses, facilitating the encoding of spatial and temporal information (Brand et al., 2002; Burger and Pollak, 1998; Davis, 2005; Davis et al., 1999; Ingham and McAlpine, 2005; Mowery et al., 2019). As a result, synaptopathy alters temporal coding of AM, and binaural interaction as measured by contralateral suppression by noise (Shaheen and Liberman, 2018; Shaheen et al., 2015). Despite this compelling theoretical link, it is unclear if the neurophysiological consequences of synaptopathy could explain human hidden hearing loss. Studies of synaptopathy have primarily taken place in rodents, which exhibit differences from primates in anatomical organization of the auditory pathway (Hackett et al., 1998; Kavanagh Moore, 1980; Moore et al., 1996; Rubio et al., 2008), auditory nerve frequency tuning (Joris et al., 2011; Verschooten et al., 2018), neurophysiological measures of temporal coding (Hoglen et al., 2018), and perceptual measures of temporal processing (Kelly et al., 2006; Mackey et al., 2021a; Moody, 1994). Thus, primate studies of spatial and temporal processing are positioned to greatly advance our understanding of synaptopathy, and more generally, NIHL.

CHAPTER 2 - GENERAL METHODS

Details about specific methods and monkeys are included in each chapter. This section is devoted to methodological details that span most of the experiments included in this dissertation.

2.1 Subjects

Subjects in these studies were macaque monkeys (*Macaca mulatta* and *Macaca radiata)*, housed in a primate facility at Vanderbilt University. Macaques were housed in specially designed primate cages (Primate Products, Miami FL). Macaques were fed a commercial diet (LabDiet Monkey Diet 5037 and 5050, Purina, St Louis, MO) supplemented with fresh produce and foraging items. Macaques were also provided manipulanda as well as auditory, visual, and olfactory enrichment on a rotational basis. Macaques were fluid restricted for the study and received filtered municipal water averaging at least 20 ml/kg of body weight/day (typically closer to 25 ml/kg/day). Their weight was monitored at least weekly (typically 4 – 5 days each week) and stayed within bounds of the reference weights set to index the animal's health while on study. Macaques were maintained on a 12:12-h light:dark cycle and all procedures occurred between 8 AM and 6 PM, during their light cycle. After repeated behavioral assessments to attempt to identify compatible social partners, some of these macaques were individually housed (due to incompatibility for social housing with available cohorts) with visual, auditory, and olfactory contact with conspecifics maintained within the housing room. The housing room was located in an AAALAC-accredited facility in accordance with the *Guide for the Care and Use of Laboratory Animals,* the Public Health Service Policy on Humane Care and Use of Laboratory Animals, and the Animal Welfare Act and Regulations. Macaques in this colony received routine health assessments and tuberculosis testing twice yearly. All research procedures were part of protocols that were approved by the Institutional Animal Care and Use Committee at Vanderbilt University Medical Center (VUMC).

2.2 Surgical procedures

Monkeys were prepared for chronic experiments using standard techniques employed in nonhuman primate studies, and as reported in previous studies (Dylla et

al., 2013; Rocchi and Ramachandran, 2018, 2020). Anesthesia was induced via administration of ketamine and midazolam, and maintained via isoflurane. A custom designed headpost was implanted on the skull in order to restrict head movement during head fixation, minimizing sound pressure level changes at the ear as a result of positioning across behavioral sessions. The headpost was secured to bone using 8 mm titanium screws (Veterinary Orthopedic Instruments) and encapsulated in bone cement (Zimmer Biomet). Multimodal analgesics (pre- and post-procedure), intra-procedure fluids, and antibiotics (intra-procedure) were administered to the monkeys under veterinary oversight. The other two surgeries implanted recording chambers (Crist Instruments, Hagerstown, MD) on the skull around craniotomies at stereotaxically guided locations. The recording chambers were angled to fit on the skull – the midbrain chamber was tilted lateral 20˚, and the brainstem chamber was angled posterior 26˚. The chambers were chosen with bases that fit the cranial curvature, and secured to the skull using bone cement and screws. Pre- and postsurgical analgesics were administered, and the monkey was monitored carefully until complete recovery had occurred.

2.3 Apparatus and Stimuli

The behavioral apparatus has been described in detail elsewhere (e.g., Dylla et al. 2013; Rocchi et al. 2017). Monkeys were seated in a primate chair designed and constructed in-house, and situated inside a sound treated booth (IAC, model 1200A and Acoustic Systems model ER 247). Stimuli (tones and noise) were presented in the free field via a speaker (Rhyme Acoustics NuScale 216 or Selah speakers) located in the frontal field at a distance of 90 cm from the center of the monkey's head. The speaker in each booth was calibrated with a ¼ inch microphone (378C01, PCB Piezotronics, Depew, NY) positioned at the location where the monkey's ear canal would be during experiments. The speaker in each booth was calibrated to ensure that outputs were within 3 dB across the macaque audible range. Experimental flow was controlled by a computer running OpenEx software (System 3, TDT Inc., Alachua, FL). Tones and noise were generated using a sampling rate of 97.6 kHz. The monkey pushed and pulled a lever (P3 America, San Diego, CA) to perform the task. The lever state was sampled at

24.4 kHz. More details about the setup can be found in Dylla et al. (2013) and specific stimulus details are found in each chapter here.

2.4 Detection Task Structure and Data Collection

Monkeys performed a lever-based reaction time Go/No Go tone detection task, the design of which is referred to in multiple chapters here. Details of the task have been reported in previous publications (e.g., Dylla et al. 2013; Rocchi et al. 2017). Figure 2.1 details the task structure and reward contingencies.

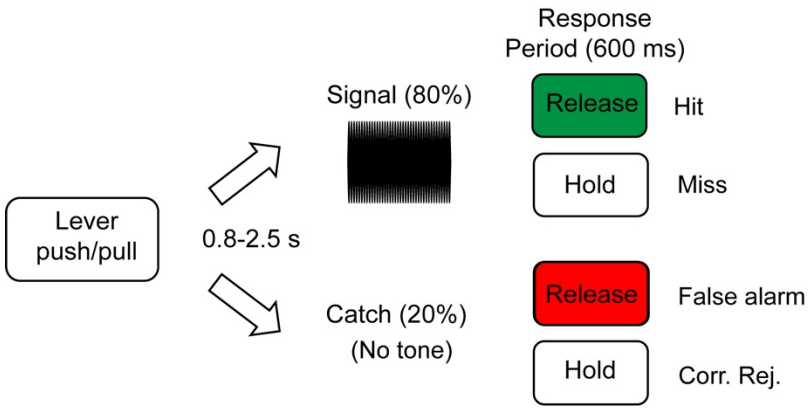

Figure 2.1 Tone detection task design and reward contingencies.

Briefly, monkeys initiated a trial by pulling a lever. Trials could be signal trials (80%) in which a tone signal of fixed duration was played after a random delay period of 0.8-2.5 seconds after lever was pulled, or they could be catch trials (20%), in which no tone signal was played. The monkey was required to release the lever within a response window (600 ms after tone onset) to indicate detection on signal trials, and was required to continue to hold the lever on catch trials. Lever release on signal trials (hits) was rewarded with fluid. Lack of lever release within 600 ms of the onset of the tone on signal trials (misses) was taken to indicate non-detection and was neither rewarded nor punished. Lever release on catch trials (false alarm) resulted in a 6-10 s timeout in which no trial could be initiated. Correct rejections (lack of release on catch trials) were not rewarded. Experiments were blocked by tone frequency and different variables of interest (duration, speaker location etc; see specific chapters for details), while tone level was varied randomly trial by trial, using the method of constant stimuli. Tone

levels in a given experimental block ranged +/- 30 dB from a experimenter-defined threshold estimate, which could be any level from -10 dB to 80 dB SPL in 2.5 dB increments. The levels presented in each block were spaced out in a telescoping fashion around the threshold estimate: the seven tone levels in the center were separated by 2.5 dB steps, while the two just above and below those were separated by 7.5 dB steps, and the outermost two, on the upper and lower edges, were 15 dB above/below the nearest level presented (see Figure 3.1). Each tone level was repeated 15-20 times, resulting in blocks containing ~200-265 trials. On a typical day, each monkey would complete ~1,500-2,000 trials before reaching satiety, resulting in 7-10 experimental blocks. Experiments were performed after extensive audiometric and non-invasive electrophysiological characterization (e.g., otoscopy, tympanometry, ABRs, DPOAEs). All of these measures confirmed normal hearing status.

2.5 Neuronal recordings

Single-unit recordings were made in the CN and in the tonotopic portion of the IC (putative central nucleus). A glass coated tungsten electrode (Alpha Omega Engineering, Alpharetta, GA; tip length ~7-10 μm, diameter ~5 μm; Thomas Recording GmbH, tip impedance 2 – 4 MΩ) was placed in a stainless steel guide tube near the surface of the brain. The guide tube was advanced manually 10 mm into the brain when approaching the central nucleus of the inferior colliculus (IC; all reference to IC in text and figures refers to the central nucleus) and about 15 mm when approaching the CN. The electrode was advanced further into the brain by means of a remotely controlled hydraulic micromanipulator (MO-97, Narishige Inc., Hampstead, NY). The electrode traveled through the cortex to reach the IC, and through the cortex and cerebellum to reach the CN. As the electrode was driven into the brain, bursts of noise were used as probe stimuli to assess proximity to auditory structures. Proximity to CN or IC was indicated by changes in background responses to the noise bursts. The IC was identified as the auditory structure posterior to the superior colliculus (identified by superficial visual drive, deep layer eye movement sensitivity) and anterior to the cerebellum (identified by simple and complex spikes). Further criteria to identify IC (after Nelson et al. 2009) included: (i) short latencies (≤ 20 ms); (ii) reliable, non-habituating responses; and (iii) identification of presence in tonotopic gradient, encountered by

several groups, including the present authors (Nelson et al., 2009; Rocchi and Ramachandran, 2020; Ryan and Miller, 1978; Shaheen et al., 2021). The CN was identified as the region of auditory responses medial to the flocculus (identified by simple and complex spikes, and eye movement sensitivity to ipsiversive and downward eye movements observed over the video monitor). Histological verification of the locations of electrode penetrations in the IC and CN were reported previously (Mackey et al., 2022; Rocchi and Ramachandran, 2020). Once the electrode moved into the CN or IC, single units were isolated using tones (Ramachandran et al., 2000; Rhode et al., 2010; Rocchi and Ramachandran, 2018). The electrode was advanced through the CN or IC until the signal from the electrode was predominantly from one unit. Single units were verified based on visual inspection, and principal component analysis available in the TDT System 3 software suite. The filtered waveform of the electrode signal and the waveforms of spikes that exceeded a user-defined threshold were sampled at 24.4 kHz and stored for offline analysis. Once a single unit was isolated, its characteristic frequency (CF: the frequency with the lowest threshold) was estimated and used to derive the frequency tuning of the unit via a frequency response map (FRM). A FRM was obtained by measuring the responses of the unit to tones as a function of frequency and sound pressure level. Frequency was varied over a 2 or 4 octave range around the estimated CF in 100 logarithmically spaced steps and at three or four sound levels, starting near CF threshold values, and proceeding in 20 dB steps. FRMs were also used to classify the response type of the CN or IC units (Evans and Nelson, 1973; Ramachandran et al., 1999). Sound pressure levels used for the FRMs ranged from 10 - 15 dB below estimated threshold to as high as 74 dB SPL.

2.6 Noise exposure inducing permanent threshold shifts

The parameters of the 141/146 dB SPL noise exposure have been described elsewhere (Hauser et al., 2018). Briefly, following characterization of baseline behavior and physiology (audiograms, masked thresholds, ABRs, DPOAEs) three macaques (*Macaca radiata* E and G, and *Macaca mulatta* L) were subjected to noise exposure. Monkeys were treated with atropine and anesthetized with a mixture of ketamine (10 mg/kg) and midazolam (0.05 mg/kg). They were then intubated, following which anesthesia was maintained with isoflurane (1.5 – 2%). The exposure noise was delivered

through a closed acoustic system. MF1 speakers (TDT Inc.) coupled with probe tips were inserted into the ear canal. The exposure noise was a 50 Hz band of Gaussian noise around 2000 Hz played for four hours at 146 dB SPL for monkeys E and G, and 141 dB SPL for monkey L.

2.7 Noise exposure inducing temporary threshold shifts

Using the same stimulus delivery apparatus and anesthetic preparation described above, macaques were exposed to a lower level noise exposure that induced temporary threshold shifts, with the goal of inducing cochlear synaptopathy without hair cell loss (see Appendix). The exposure noise was an octave-band (2000-4000 Hz) of noise played for four hours at 120 dB SPL.

2.8 Cochlear histology

Following completion of the study, monkeys were euthanized and cochlear tissue was harvested for dissection and immunohistochemistry. Immunolabeling and confocal imaging of cochlear whole mounts was conducted to quantify IHC and OHC counts, IHC and OHC ribbon counts and sizes, and efferent terminal densities (Valero et al., 2017). Data from noise-exposed subjects were compared to unexposed subjects to assess anatomical integrity along the cochlear length. The results of the histological analysis were originally reported in Chapter 7 of the dissertation of Dr. Jane Mondul (2022). These results are integral to the hearing loss sections of this dissertation, and are included in the Appendix.

CHAPTER 3 – TEMPORAL INTEGRATION

Sections of this chapter appear in: Mackey, C., Tarabillo, A., & Ramachandran, R. (2021). Three psychophysical metrics of auditory temporal integration in macaques. *The Journal of the Acoustical Society of America*, *150*(4), 3176-3191.

3.1 INTRODUCTION

The process by which sensory evidence is summed up over time is characterized by a variety of different models across visual, auditory and somatosensory systems (Heil et al., 2017; Hernández-Pérez et al., 2020; Huk and Shadlen, 2005; Liu et al., 2015; Viemeister and Wakefield, 1991; Watson, 1979). This previous work shows that models of temporal integration account for a wide variety of behavioral data, and its explanatory success emphasizes the importance of relying on converging lines of evidence from modeling, psychophysics, and neurophysiology to characterize perceptual processes. Within the auditory domain, temporal integration has often been studied by characterizing the effects of tone duration on detection threshold (Costalupes, 1983; O'Connor et al., 1999; Watson and Gengel, 1969), and the clinical utility of temporal integration has been well characterized in studies of short-tone audiometry (Chung and Smith, 1980; Chung, 1981; Chung, 1982; Sanders & Honig, 1967). Stimulus duration also has effects on reaction time (Hernández-Pérez et al., 2020; Hildreth, 1973; Raab, 1962). The *rate* at which threshold changes with duration is typically used to quantify integration, and has been the subject of many behavioral, neurophysiological, and modeling studies.

Behavioral studies have been conducted in a wide range of species including chinchillas, cats, birds, and macaque monkeys (Macaques: Clack, 1966; O'Connor et al., 1999; Chinchillas: Clock et al., 1993; Cats: Costalupes, 1983; Budgerigars: Wong et al., 2019; Humans: Gerken et al., 1990; Heil et al., 2017; Plomp and Bouman, 1959; Watson and Gengel, 1969). Heil et al. (2017) and O'Connor et al. (1999) presented meta-analyses that conflicted. O'Connor et al. found that macaque temporal integration was five times slower than humans, while Heil et al. (2017) reported that all vertebrate species studied to date are essentially the same. This motivated the comparative analysis of behavioral data in this chapter.

Neurophysiological investigations of auditory temporal integration have differed in their conclusions regarding where neuronal integration rates match behavioral integration rates (i.e. where is the sensory evidence represented?). Heil et al., (2008) provided evidence from cat auditory nerve fiber (ANF) recordings suggesting a peripheral origin. Studies in anesthetized chinchillas suggest otherwise (Clock-Eddins et al., 1993; Clock-Eddins et al., 1998; Viemeister et al., 1992). Clock et al. (1993) found integration rates based on detection theoretic neural thresholds in the cochlear nucleus approximate those derived from psychophysical measures more closely than ANFs (Clock et al. 1998; Viemeister et al. 1992). Electroencephalographic data in humans have been used to argue that the evidence is represented even higher than primary auditory cortex (Lütkenhöner, 2011). Similarly, another study suggests long-latency neurons in auditory cortex may reflect temporal integration on a time-scale similar to certain perceptual measures (Jufang, 1997). Different still, one of the only auditory temporal integration studies in awake animals implicates auditory cortex and parietal cortex. Investigators pharmacologically inactivated projections from auditory cortex to parietal cortex (PPC) in gerbils performing an AM frequency discrimination task, and found that the duration required for above-chance performance was increased (Yao et al., 2020). This is consistent with previous studies finding auditory modulation of visual responses in area LIP (Cohen et al., 2004; Gifford and Cohen, 2005). Finally, the SC may represent a neural integrator of auditory information, as studies of sensorimotor integration suggest (Jay and Sparks, 1987; Rajala et al., 2017; Wallace et al., 1996). Despite these compelling theoretical links, it is unclear if integration of auditory information happens *de novo* in such regions, or is inherited from earlier stations in the pathway (e.g. the cochlear nucleus, the inferior colliculus) as Clock et al. suggested.

Conclusions about the contribution of the CN and IC to temporal integration are complicated by the use of anesthetized animal preparations, lack of studies in nonhuman primates, and most studies measuring responses to stimuli presented in unnaturally quiet environments. Anesthetized/passive-listening preparations are limited because task engagement affects neuronal encoding along the auditory pathway (Downer et al., 2015; Niwa et al., 2012a; Rocchi and Ramachandran, 2020; Ryan and Miller, 1977; Slee and David, 2015). The exclusive use of rodents and cats in previous studies begs the question of how these results translate to humans, because primate

auditory systems differ from rodents and cats in anatomical organization (Hackett, 2011; Hackett et al., 2014; Kavanagh Moore, 1980b), neurophysiological measures of temporal coding (Hoglen et al., 2018), auditory nerve frequency tuning (Joris et al., 2011; Verschooten et al., 2018), and perceptual measures of temporal processing (Kelly et al., 2006; Moody, 1994). Finally, only presenting stimuli in quiet poses a problem of ethological validity. Regarding the relevant brain regions in these studies, previous studies have found that performance at short durations requires integration of populations of ANF inputs (Lopez-Poveda and Barrios, 2013; Stevens and Wickesberg, 1999), a requirement that, at the anatomical level, is met by CN and IC (see Introduction). Thus, previous findings taken together suggest recordings from the central nervous system in task-engaged primates, while presenting stimuli in noise, could significantly advance knowledge of the neuronal mechanisms of temporal integration. This opportunity was addressed here by comparing psychometric and neurometric measures of temporal integration derived from single-unit responses in the cochlear nucleus and inferior colliculus of macaques performing a tone detection task in quiet and in noise. It was hypothesized that the IC would more closely approximate behavioral estimates of temporal integration relative to the CN, reflecting the higher degree of neuronal convergence observed in the IC (see Introduction).

Motivation for the second part of this study stems from the fact that many *normal-hearing* listeners report auditory perceptual deficits and display large individual differences in complex psychoacoustic tasks (see Introduction on Hidden Hearing Loss). Cochlear synaptopathy (CS; the selective loss of inner hair cell synapses) has been posited as an explanation for such deficits, which is consistent with its neurophysiological effects on stimulus encoding (Asokan et al., 2018; Furman et al., 2013; Kujawa and Liberman, 2009; Shaheen and Liberman, 2018; Shaheen et al., 2015; Suthakar and Liberman, 2021). Specifically, CS reduces ANF population responses as indexed by the auditory brainstem response (ABR), without altering ABR thresholds. Theoretically this could lead to perceptual deficits. However, perceptual deficits in animals with histologically confirmed CS have not been demonstrated, and many human studies are equivocal on this issue (Bramhall et al., 2019; DiNino et al., 2021; Grose et al., 2019; Guest et al., 2018; Harris et al., 2021). Temporal integration may be impaired by CS, as others have hypothesized, but have yet to find (Marmel et al., 2020;

Trevino et al., 2022; Wong et al., 2019). And the previous mentioned models of the perception of short duration stimuli predict that deafferentation from CS should alter the perception of short duration stimuli (Lopez-Poveda, 2014; Lopez-Poveda and Barrios, 2013; Stevens and Wickesberg, 1999). This led us in the present study to test the hypothesis that psychophysical measures of temporal integration would be degraded by CS.

3.2 METHODS

3.2.1 Subjects

Seven adult male rhesus macaques (*Macaca mulatta*) participated and, at the beginning of the study ranged in age from 5 – 10 years old with body weights ranging from 10 – 12 kg. Macaques were implanted with headposts (all) and recording chambers (Alp, Bi, Br, Ch, De). Information on surgical procedures, institutional welfare requirements, social housing, food etc. is in the General Methods section. Monkeys Alp, Br, Ch, and De participated in the simultaneous neural and behavioral recordings (the detection task described below using 200 ms tones). Monkeys Bi (not monkey Br), Ch, De, and Ga, and Ha participated in the behavioral experiments described below, where tones of different durations were used. Confounds were generally not anticipated in comparing the neuronal responses to the behavioral responses from these different experiments for two main reasons: 1) the overlap between groups (i.e. Monkeys Ch and De were in both), and 2) Monkeys A and Br had experience detecting short duration tones in a set of experiments not reported here.

Female rhesus macaques Lu, Ne, Op and Pi participated in the behavioral experiments before and after noise exposure. At the beginning of the study, ages ranged from 6-8 years old, and body weights ranged from 5.5-7 kg. All monkeys (male and female) were 6-8 years old at the time of noise exposure.

Names in the figures are often restricted to a single letter, but in this section and in figure captions more letters will be used to enable readers to know monkey identity across chapters in this dissertation.

3.2.2 Stimuli

The behavioral apparatus is described in the General Methods. Tones and noise were generated using a sampling rate of 97.6 kHz. Tone frequencies were 0.5, 1, 2, 2.828, 4, 5.656, 8, 16, 24 and 32 kHz. Tone durations were defined as the time during which tone envelope was greater than 0. Tone durations were 3.25, 6.5, 12.5, 25, 50, 100, and 200 ms. Linear rise/fall times for tones were 1.25 ms for 3.25 ms tones, 2.5 ms for 6.5 ms tones, 4 ms for 12.5 and 25 ms tones, and 10 ms for all other tone durations. Noise was broadband (5-40,000 Hz), 76 dB SPL (30 dB SPL spectrum level), and presented continuously from the same loudspeaker as the tones. For the simultaneous behavioral and neurophysiological experiments, tones were 200 ms in duration, of varying sound level (see Task Design in General Methods), with 10 ms linear gate times. Noise was broadband, 44 dB SPL, continuous, and broadband. Noise was presented from the same loudspeaker as the tones.

3.2.3 Psychometric and neurometric data analysis

Detection theoretic methods were used to analyze behavioral and neuronal responses, as well as simulated data from a model (Macmillan and Creelman, 2004; Swets, 1973; Tanner and Swets, 1954). Behavioral data were analyzed initially in terms of *d'* to facilitate comparison with O'Connor et al. (1999) and were subsequently analyzed in terms of probability correct to facilitate comparison with neuronal responses, detailed below.

Behavioral performance from each block of data was analyzed to calculate hit rate at each tone level (*H(level)*) and false alarm rate (*F*). Sensitivity was calculated as $d'(level) = \big(z(H(level)) - z(F)\big)$, where z represents calculation of the z-score of the value, implemented in MATLAB via the function "norminv." From *d'*, probability correct in a two-alternative forced-choice experiment was given by *pc(level)*, as $pc(level) = z^{-1}(d'(level)/2)$, where z^{-1} represents the transformation from a standard normal variate to probability correct. Calculation of *pc,* rather than a more common *d'* measure, permitted comparison with our distribution free (ROC) calculation of probability correct based on neuronal responses (Rocchi and Ramachandran, 2018, 2020). Psychometric and neurometric functions were fit with a modified Weibull cumulative distribution function (CDF) as others have done in both detection and discrimination tasks (Britten

et al., 1996; Christison-Lagay and Cohen, 2014; O'Connor et al., 1999). The modified equation was: $pc(level) = c - d * e^{-(level/\lambda)^{\kappa}}\ for\ level \geq 0$, where c represents saturation and d represents the range of the function, and λ and κ represent the threshold and slope parameters respectively. Often levels were presented that were below zero, and in these cases the Weibull fit was translated to higher levels before fitting, and translated back to the original levels after fitting. The threshold was calculated as that tone level at which $pc_{fit}(level)$=0.76, and in the cases where *d'* was used, threshold criterion was 1.5 (after O'Connor et al., 1999).

Calculation of reaction time (RT) and psychometric function dynamic range (DR)

Reaction times were calculated for all hit trials. They were calculated as follows:

RT = Time of Lever Release – Time of Tone Onset

RTs as a function of tone level were fit with a line to provide RT slope and intercept, as described in previous studies from this laboratory (Dylla et al., 2013; Rocchi and Ramachandran, 2018).

The dynamic range of each psychometric function was calculated as the range of tone levels over which $pc_{fit}(level)$ spanned, from saturation minus 90% of that range, to saturation minus 10% of that range. This was done by using the *c* parameter as an estimate of saturated performance, and *d* as the total range, or amplitude of the psychometric function.

3.2.4 Statistical analyses and curve-fitting

In all cases, curve fits were attained via non-linear least squares method implemented in MATLAB. Bayesian information criterion was calculated in MATLAB (2018a; Mathworks Inc.) using the non-linear model fit function, "fitnlm," which returns multiple information criteria (including BIC), as well as goodness of fit measures R-squared and p-values. All time constants (τ, the rate parameter), exponents (*m*, the rate parameter) and constants of proportionality (I_k the range parameter) reported were taken from significant fits to the data ($p<0.05$).

The power law function can be expressed as

$$[\text{Eq. 1}]\ I_T = I_k\, t^{-m} + I_\infty$$

The exponential function can be expressed as

$$[\text{Eq. 2}]\ I_T = I_k \exp(-t/\tau) + I_\infty$$

Statistical analysis of the effects of tone frequency, noise masker, and duration were conducted using linear mixed effects models ("fitlme") in MATLAB 2018a. This allowed us to accommodate datasets with missing points, a common reason for avoiding repeated measures ANOVA in cases such as these (Krueger and Tian, 2004). The dependent variable in the models assessing the effects of tone frequency or noise masker was either τ or I_k, the rate and range parameters, respectively. Background noise, tone frequency, and an interaction term between the two were entered as fixed effects into the model, while intercepts for individual macaques were entered as random effects. The effects of duration on threshold and DR were constructed by entering tone duration as a fixed effect, and the individual monkey as a random intercept term. Detection threshold or DR were entered as dependent variables. In all cases p-values were obtained by likelihood ratio testing of the model with the effect in question against the model without the effect in question.

2 sample Kolmogorov-Smirnov tests were used to assess differences between time constant distributions between brain structures, and between quiet and noise conditions ("kstest2" in MATLAB).

3.2.5 Time window analysis

Neuronal responses were analyzed using different time windows, to facilitate comparison with the tone durations used in the behavioral experiments. The latency of the response to a 200 ms tone ~5 dB above detection threshold was estimated using the point at which the cumulative spike function significantly deviated from a 250 ms baseline period (after Rowland and Stein, 2007; Rowland et al., 2007). Starting at the latency, responses were then calculated using time windows of 100, 50, 25, 12.5, 6.5, and 3.25 ms. Using each of these time-windows, neurometric probability correct could be

calculated at each tone level, using previously mentioned ROC analysis. Assessing how neurometric performance (e.g. threshold) changed as a function of time/duration provides a measure of temporal integration analogous to behavior when fit with a three-term exponential function (Eqn. 2).

3.3 RESULTS

3.3.1 Effects of tone duration on detection performance in quiet

Psychometric threshold and dynamic range

For each tone duration, the hit rate at each tone level and false alarm rate were used to compute sensitivity (*d'*) as a function of tone level. The *d'* vs. tone level plots (psychometric functions) were used to compute detection threshold (*d'* = 1.5, after O'Connor et al. 1999) at that tone duration. The effect of tone duration can be seen in Figure 3.1, which contains a large *subset* of the psychometric functions from the detection in quiet data set. The psychometric functions were shifted to lower tone levels for longer tone durations (Figure 3.1), resulting in detection thresholds that decreased

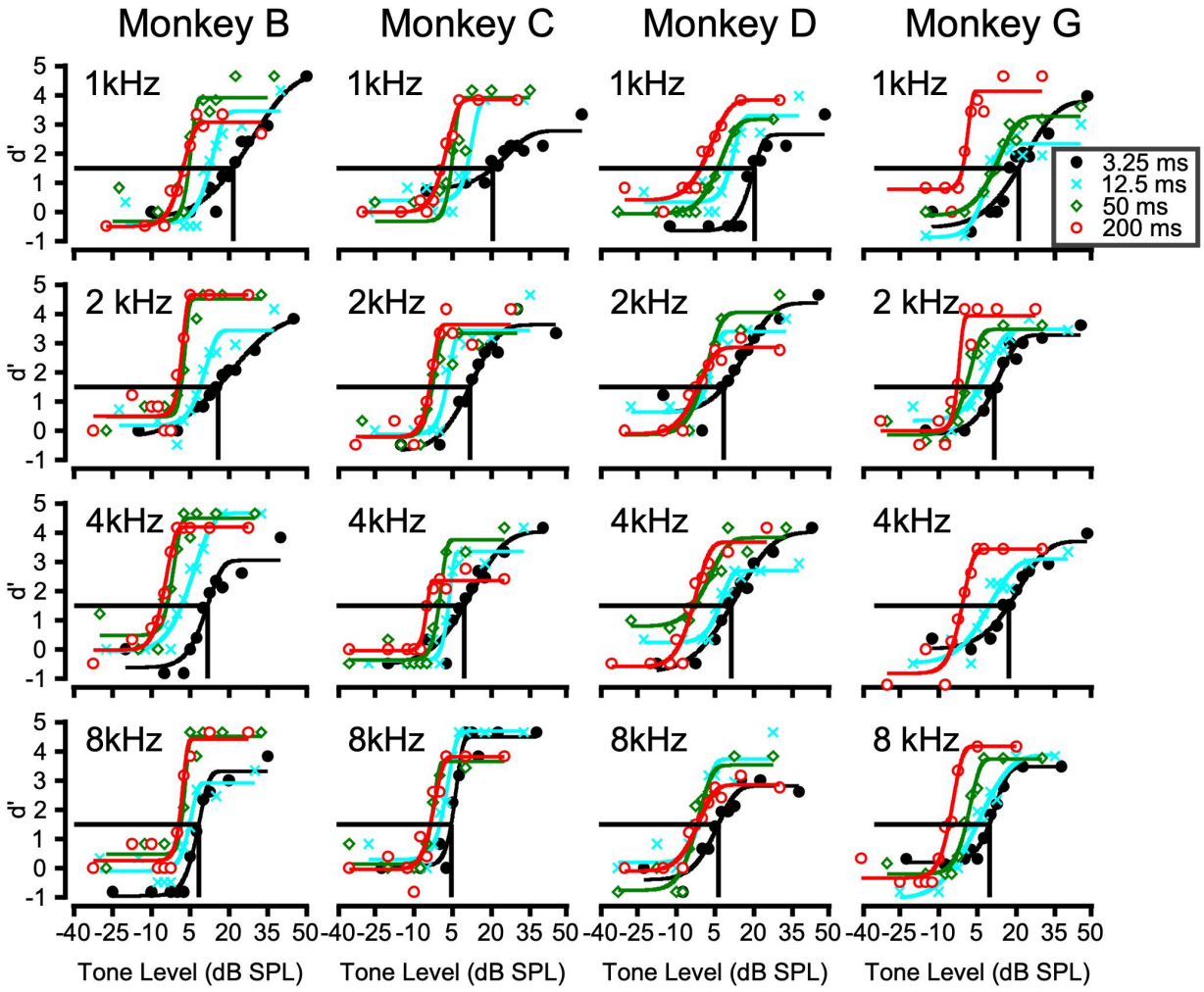

FIGURE 3.1 – Psychometric functions for all monkeys at 1, 2, 4, and 8 kHz. Different tone durations are indicated by different symbols and colors. The colored curves represent Weibull fits to the threshold vs. level trend. Threshold, indicated by the solid vertical lines, was taken to be the level at a *d'* of 1.5. Four of the seven tone durations used in this study are displayed to preserve the visibility of the data. *Monkeys: B = Bi, C = Ch, D = De, G = Gan.*

as tone duration increased (Figure 3.2). The effect of tone duration on detection threshold was confirmed by a mixed effects model that incorporated all of the detection thresholds in the detection in quiet dataset (t = -7.6, df = 257, $p = 4.7*10^{-13}$). The model took the form *Threshold ~ Duration + Frequency + Frequency*Duration + (1|Monkey)*. An interaction between tone duration and frequency was not significant ($p = 0.7$). This suggests that while tone frequency shifts threshold up/down, the effects of duration are

not significantly different across tone frequencies, which can be seen in the mean thresholds shown in Figure 3.2.

It was also a goal of the present work to characterize the effect of tone duration on psychometric function slope. In general, slope increased as tone duration increased, which was quantified using the dynamic range, or width, of the psychometric function. The dynamic range was inversely related to the slope (see Methods), and was consistently less variable than psychometric slope, likely due to the large fluctuations in *d'* that occur at ceiling performance in well trained animals (Figure 3.1). The effect of duration on dynamic range/slope can be seen in the individual data in Figures 1 and summarized in Figure 3.2. Dynamic range decreased as tone duration increases. The effect of duration on dynamic range was confirmed using a mixed effects model that contained all of the data from the detection in quiet data set ($t = -4.2$, $df = 257$, $p = 3.4*10^{-5}$). In the mixed effects model, an interaction between tone frequency and duration was not significant ($p > 0.05$), confirming that the effects of duration were not significantly different across tone frequencies.

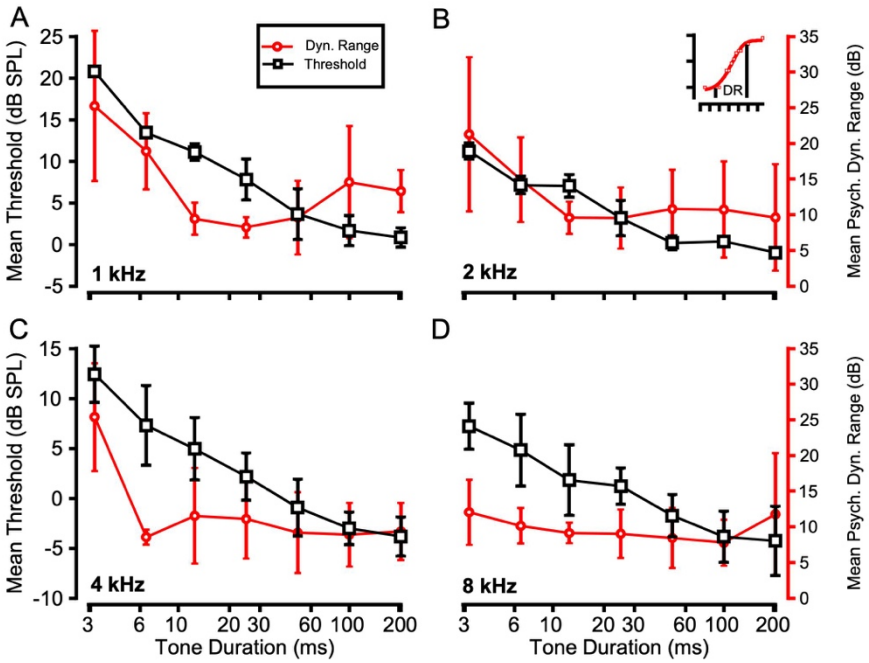

FIGURE 3.2 – Psychometric thresholds (*d'* = 1.5) and psychometric function dynamic range (tone levels spanned by the dynamic portion of the function), averaged across monkeys, as a function of duration, at various frequencies (A-D). Error bars represent one standard deviation.

False alarm rates and reaction times

In an effort to fully characterize the effects of duration on performance, reaction times (RTs) were measured as the time elapsing from the onset of the tone to the release of the lever on signal trials (see Methods). Many precautions were undertaken to ensure that RTs were reliable (see Discussion of RTs). False alarm rates were inspected and analyzed as a function of stimulus duration, and only RTs to suprathreshold tones (35 dB SPL) were used to investigate the effects of duration. False alarm rates suggest very conservative decision criteria, making the likelihood of contamination of RT data by guesses unlikely (see Discussion). Figure 3.3 shows the false alarm rates from all of the sessions used in these quiet and masked detection experiments (532 blocks of ~200-265 trials per block, over 100,000 trials). Figure 3.3 shows that false alarm rates were usually 0-6 % (over 65% of blocks), and false alarm rates did not exceed 18%. Consistent with this, stimulus duration did not affect false alarm rate, suggesting that any effects of stimulus duration on performance (e.g. RTs) resulted from the stimulus, an issue which is elaborated on in the Discussion section. No effect of duration on false alarm rate was observed in a mixed effects model analysis that included false alarm rate as a dependent variable, tone duration and frequency as fixed effects, and individual monkeys as a random effect (Effect of duration: t = 0.18, df = 516, p = 0.85).

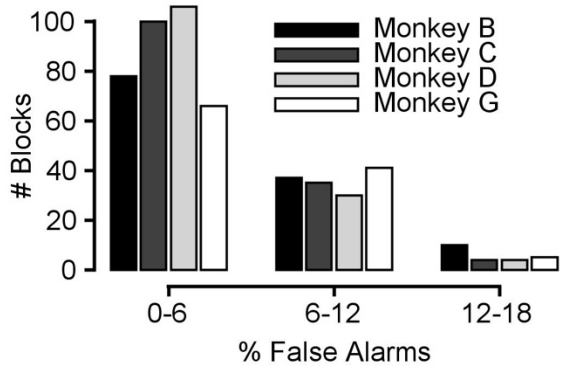

FIGURE 3.3 – False alarm rates from all sessions (516 blocks of 200-265 trials, n > 100,000 trials), in quiet and noise. Total number of blocks for each monkey were 125 (Monkey B), 112 (Monkey G) and 139 (Monkey C), and 140 (Monkey D). *See Fig 3.1 for monkey names.*

In general, RTs were longer for shorter tone durations, when controlling for the effects of tone level. Figure 3.4 shows cumulative distributions of RT for each duration. RTs were to

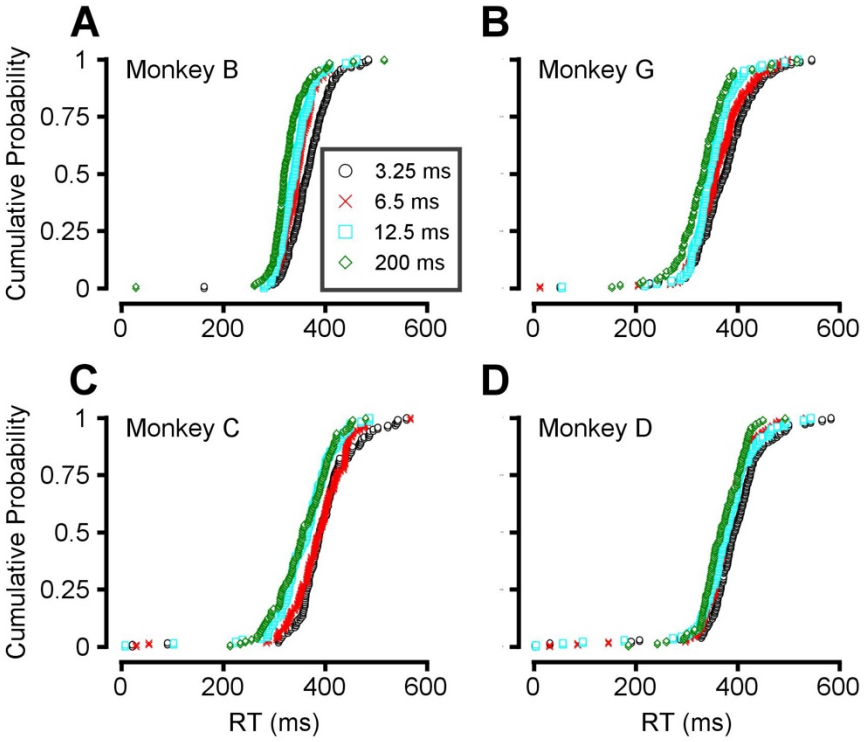

FIGURE 3.4 – A-D. Cumulative reaction time distributions for each monkey, pooled across frequency. Tones were 35 dB SPL. RTs to 3.25 (○), 6.5 (×), 12.5 (□) and 200 (◇) ms are shown. *See Fig 3.1 for monkey names.*

suprathreshold tones presented at 35 dB SPL across all tone frequencies tested. The effect of duration on RTs was confirmed by constructing a mixed effects model that incorporated tone frequency and duration as fixed effects, and individual subjects as a random intercept term. The effect of duration on RTs was significant ($t = -6.3$, $df = 3697$, $p = 3.3*10^{-10}$), as was the effect of tone frequency ($t = 4.36$, $df = 3697$, $p = 1.3*10^{-5}$), but not the interaction between duration and frequency ($p = 0.76$). To facilitate comparison with threshold by duration functions that are typical in the literature, median reaction-times, pooled across monkeys were plotted as a function of duration, and are shown in Figure 3.5.

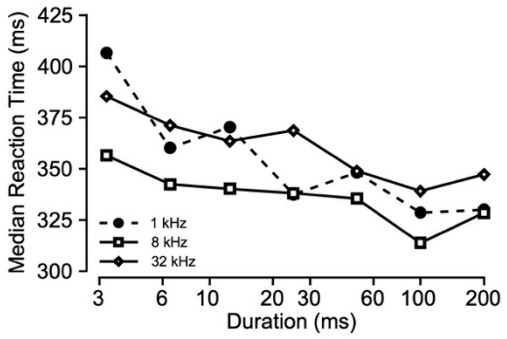

FIGURE 3.5 – Median reaction times to 35 dB SPL tones, pooled across monkeys, as a function of tone duration. The RT by duration trend was consistent across frequencies, which are shown in different symbols (1 kHz as ●, 8 kHz as □, and 32 kHz as -).

3.3.2 Effects of tone duration on masked tone detection

Psychometric threshold and slope

Masked detection experiments were conducted to assess the effects of continuous, broadband, 76 dB SPL noise (BBN) on temporal integration. Detection threshold decreased as tone duration increased, as with the detection in quiet data. The threshold by duration trends were remarkably similar in quiet and noise, illustrated in Figure 3.6. Mean thresholds (averaged across monkeys), normalized to the threshold to 200 ms tones (usually the minimum threshold), are shown as a function of duration in Figure 3.6 to illustrate how performance in quiet compared to performance in noise. This similarity held across tone frequencies. The effect of duration was confirmed with mixed effects model analysis ($p = 2.0*10^{-34}$), which contained an interaction term between duration and frequency. As with the detection in quiet data, the interaction between duration and frequency was not significant ($p > 0.05$). Psychometric function slope increased as tone duration increased, as with the detection in quiet data. This effect was quantified using the dynamic range (DR, the tone levels spanned by the dynamic portion of the psychometric function). Noise appeared to decrease DR, but only at shorter durations (3.25-12.5 ms). An

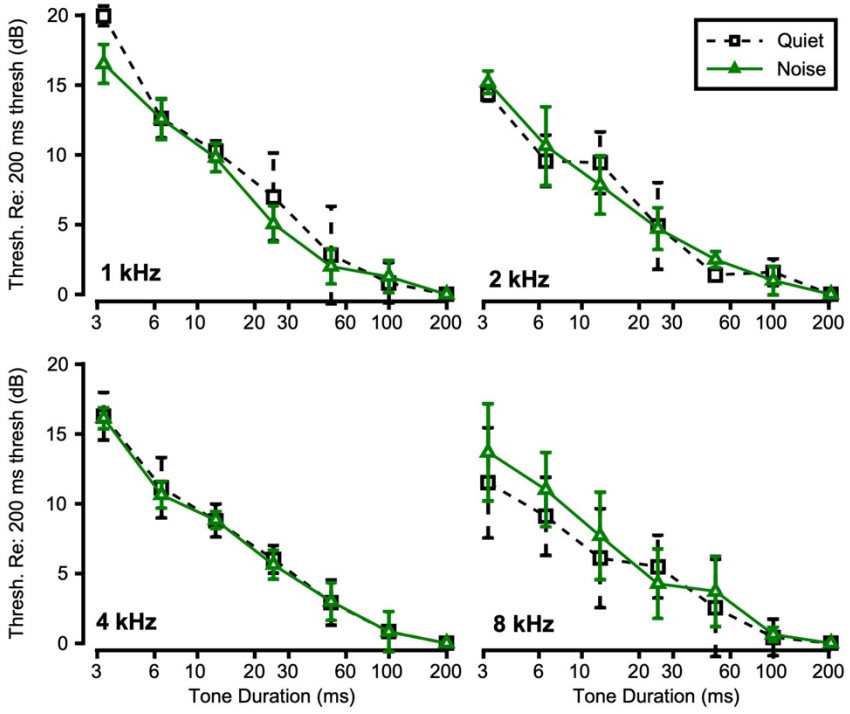

FIGURE 3.6 - Average psychometric thresholds (tone level at *d'* = 1.5) from all monkeys, normalized to the 200 ms threshold, plotted as a function of tone duration. Quiet data are in black dashed traces, while thresholds in noise are shown as solid green traces. Error bars represent one standard deviation. Color available online.

example of the effect of masking noise on DR is shown in Figure 3.7A/3.7D. This effect of masking noise on slope was confirmed with a mixed effects model containing DR as the dependent variable, tone frequency, duration, and noise as fixed effects, and individual monkeys as a random intercept term (Effect of noise: t = 8.56, df = 514, p = $1.2*10^{-16}$). The interaction between background noise and duration in a mixed effects model was also significant, consistent with the observation that noise only affected DR at a subset of tone durations (p = 0.005).

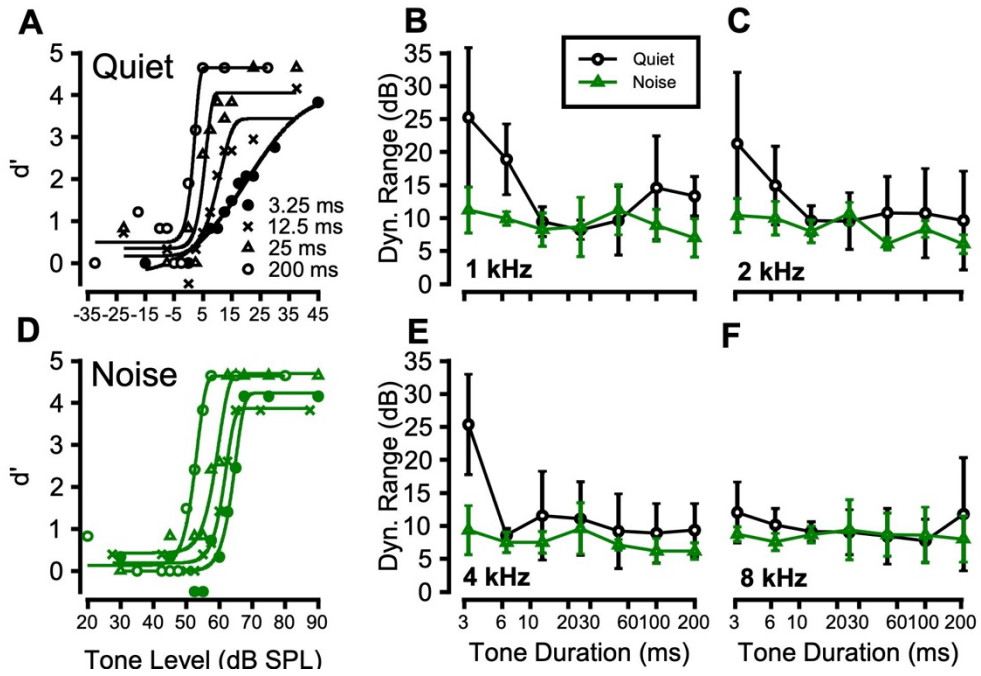

FIGURE 3.7 – Effect of background noise on dynamic range. A. Psychometric functions (d' vs. level) for detection of 2 kHz tone of various durations in quiet by monkey B. B. Exemplar psychometric functions when monkey B detected 2 kHz tones of various durations in continuous 76 dB SPL noise. C – F. Summary figures showing mean DRs across all four monkeys as a function of duration for 1 (C), 2 (D), 4 (E), and 8 kHz (F). Color available online.

Reaction times

RTs were also calculated for masked detection performance. RTs at 85 dB SPL (+/- 5 dB, ~20-35 dB above threshold) were separated by duration and monkey, and medians calculated to provide an initial estimate of speed in the task. Figure 3.8 displays median RTs to 1 and 8 kHz tones pooled across frequency, compared to RTs in quiet (black traces). RTs decreased with increasing duration, though qualitatively the effect of duration appeared weaker than suggested by RTs to tones in quiet. RTs were lower in noise, likely due to the well characterized effects of sound level on RT (Kemp, 1984; Dylla et al., 2013). Specifically, RTs decreased with increasing tone level, even when signal to noise ratio is held constant. Thus, it is likely that the higher tone levels used in the masked detection experiments resulted in lower RTs. As with the detection in quiet data, the effect of duration on RTs was confirmed by constructing a mixed effects model that incorporated tone frequency and duration as fixed effects, and individual monkeys as a random intercept term. As with RTs in quiet, reaction times during masked detection decreased with increasing duration ($t = -4.59$, $df = 3163$, $p = 4.6*10^{-6}$) and increased with increasing tone frequency ($t = 10.3$, $df = 3163$, $p = 1.7*10^{-24}$).

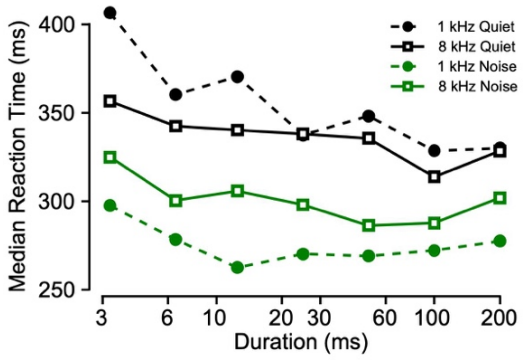

FIGURE 3.8 - Median reaction times (RTs) as a function of duration to 85 dB SPL tones in 76 dB, continuous, broadband noise (green traces), compared to RTs to 35 dB tones in quiet (black traces). Open symbols show 1 kHz data, while filled symbols represent 8 kHz data.

3.3.3 The power-law and exponential functions

Thresholds from both the detection in quiet and masked detection data sets were fit with exponential and power law functions to provide estimates of the rate and range of temporal integration. We could find no systematic differences in goodness of fit between the power law and exponential models, across monkeys and tone frequency, similar to the results of O'Connor et al. (1999). This is illustrated by the scatter plot in Figure 3.9 showing Bayesian information criterion (BIC) from each monkey at each frequency for the two models. The points generally cluster around the unity line,

suggesting the two models have approximately the same goodness of fit. Moreover, both models provided similarly good fits in terms of root-mean-square error (~1.5 dB on average, Eqn. 3 in Methods). For this reason, the exponential model was used for estimation of different aspects of temporal integration to facilitate comparison to previous macaque data, where the exponential function was found to be "most strongly descriptive of temporal integration" (O'Connor et al. 1999).

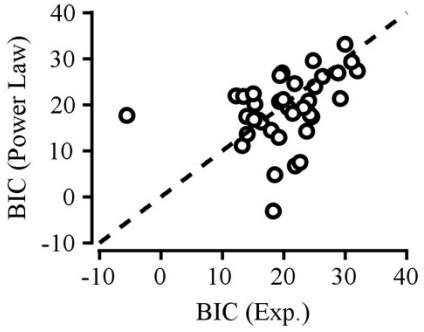

FIGURE 3.9 – Bayesian information criterion (BIC) for power law vs exponential functions, for each monkey at each tone frequency, to assess the goodness of fit of each power law or exponential function fit to threshold data.

3.3.4 Comparison across species

Three term exponential functions (Eqn. 2; see Methods) were fit to the threshold vs. duration data from the data sets obtained for detection in quiet and in broadband noise. An example can be seen in Figure 3.10A. The rate parameter τ, which is traditionally taken to be an estimate of the rate of integration, was extracted for each monkey at each frequency. Figure 3.10B and 10D show these values for detection in quiet and in noise, respectively. The constant of proportionality, I_k, provides an estimate of the range of thresholds from each exponential fit. These values are shown in Figure 3.10C. As it was a goal of this study to characterize the effects of noise on temporal integration, exponential functions were fit to the masked detection threshold data as well, and τ and I_k were similarly extracted for the data obtained in continuous background noise. The time constant and constant of proportionality values estimated during masked detection can be seen in color in Figure 3.10D and 10E, overlaid on the estimates obtained from the detection in quiet data. Qualitatively, the estimates of temporal integration rate (τ) and range (I_k) in quiet and in noise look similar, suggesting noise does not have effects on these parameters. To validate this observation statistically, the effects of frequency and masking noise on the exponential model's estimates of temporal integration rate were assessed by constructing a mixed effects model. Frequency and noise were entered as fixed effects, as well as an interaction term between the two, to assess whether effects of tone frequency might be restricted to only one data set (quiet or noise). Time constants were not significantly different between quiet and noise conditions ($t = -1.17$, $df = 70$, $p = 0.25$). Time constants were not significantly affected by tone frequency ($t = -1.15$, $df = 70$, $p = 0.24$). The interaction between frequency and noise was not significant, confirming that effects of frequency were not present in the quiet or noise data sets ($t = 1.19$, $df = 70$, $p = 0.24$). Similarly constructed mixed effects models confirmed that constants of proportionality, which provide an estimate of the range of thresholds, were similarly unaffected by frequency ($t = -1.7$, $df = 70$, $p = 0.09$) or masking noise ($t = -0.45$, $df = 70$, $p = 0.65$). The interaction term between the two was not significant, indicating that the lack of effect of frequency held true for both the quiet and noise data sets ($t = -0.96$, $df = 70$, $p = 0.34$). Figure 3.10F compares the time constants of the present study to time constants estimated

from previously published data. The macaque time constants of the present study (open circles, Figure 3.10F) were noticeably lower than chinchillas, mice, cats, and previously published macaque (black line) time constants. The present data most closely resemble human and budgerigar data (see Discussion).

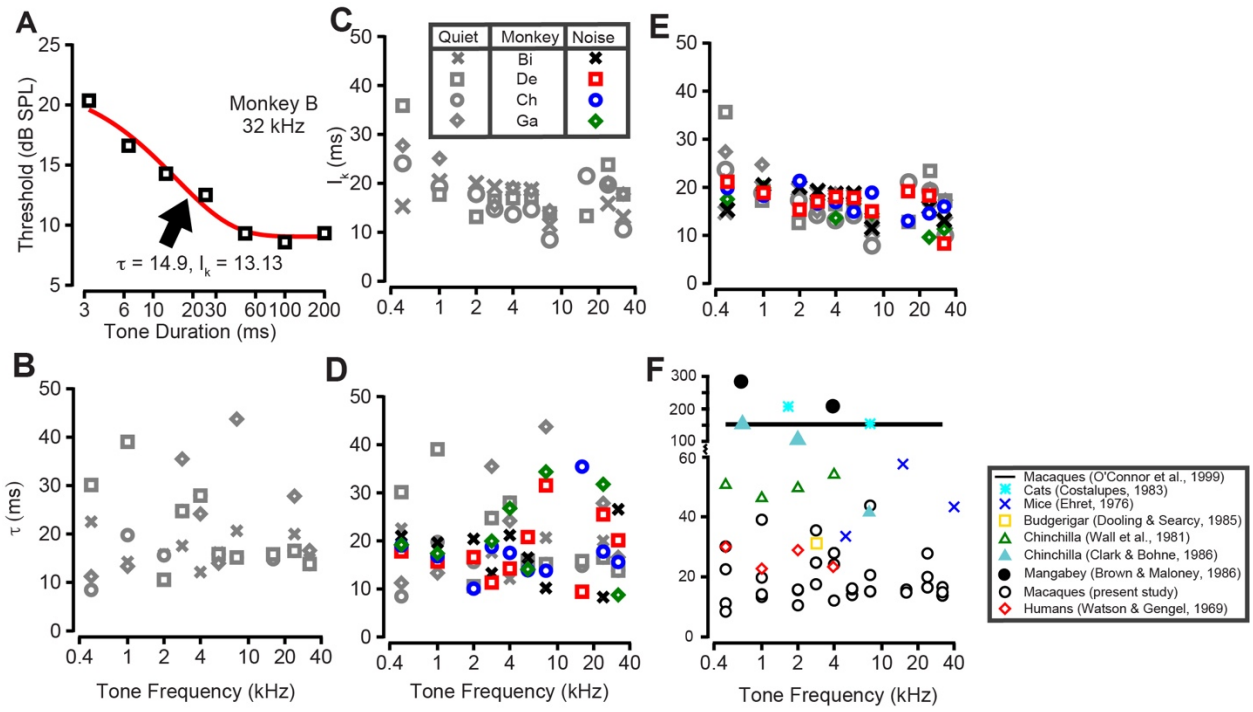

FIGURE 3.10 – A. Example of detection threshold decreasing with increasing tone duration, fit with an exponential function. **B, D**. Temporal integration rate estimates (the time constant, τ) from each exponential function, as a function of tone frequency for all monkeys in quiet (B) and in noise (D). Symbols follow conventions in the legend in **C**. C, E. Estimates of the range of thresholds from each exponential function, based on the parameter, I_k. Parameters from exponential fits to quiet data are in grey (C), and parameters from fits to masked detection data (E) are in color (available online). **F**. Temporal integration rate estimates (the time constant, τ) compared to previously published data from a range of species. Time constants to the previously published data were attained by curve-fitting with the exponential function (Eq 2) to thresholds in Fay (1988), for uniformity of methods and ease of comparison with O'Connor et al. (1999). Color available online.

3.3.5 A probabilistic Poisson process model

Though exponential and power law models are commonly used to describe temporal integration, they have limitations which have been described previously (Heil et al., 2017; Viemeister and Wakefield, 1991). In particular, they were not formulated based on neurophysiological processes. This stands in contrast to process models such as the probabilistic Poisson model (PPM) formulated by Heil et al. (2017). Heil et al. described how the PPM could be used to model performance in a yes-no task using standard signal detection theoretic methods. Using their methods, the present data were also compared to simulated data generated using this model. Poisson probability density functions were generated using different rate parameters (Figure 3.11A) to simulate differences in the response evoked by stimuli of different intensity/duration combinations. Detection theoretic methods (receiver operating characteristic analysis, ROC) were then used to model detection performance that could be based on such responses. Namely, placement of a decision criterion at a given event rate, and calculation of the area under the signal distributions, to the right of the decision criterion (*c*), yielded hit rates (Figure 3.11). The area under a noise distribution (Figure 3.11A), to the right of the decision criterion, yielded false alarm rates. The decision criterion (10 events per second) and rate parameter of the noise distribution (5 events per second) were selected to produce a

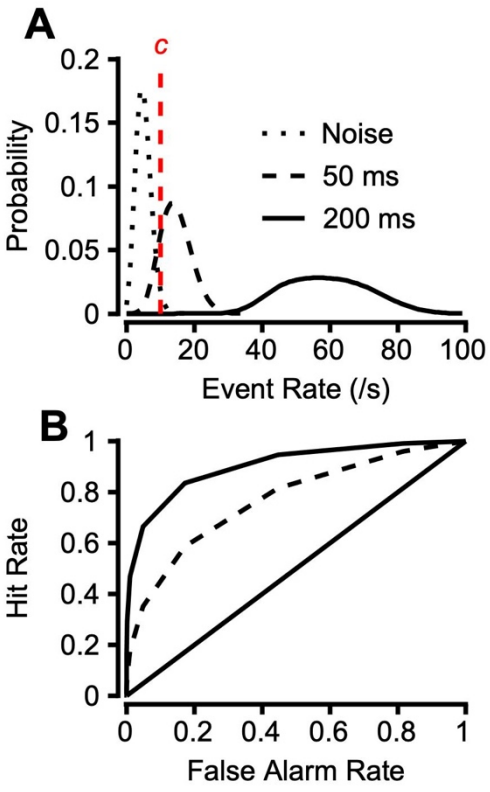

FIGURE 3.11. Example analysis using Poisson distributions to model the effects of duration. **A**. Poisson probability density functions (PDFs) with rate parameters corresponding to the noise (no stimulus) distribution, and responses to 200 and 50 ms stimuli. "c" is the decision criterion used in standard detection theoretic analyses to calculate hits and false alarms. **B**. Receiver operator characteristic (ROC) curves generated by integrating the area under Poisson PDFs at different decision criteria (*c*).

false alarm rate that matched our typical false alarm rates of ~5%. This parameter choice is very similar to Heil et al. (2017), who used very low-rate noise distributions that matched low-spontaneous rate auditory nerve fibers, to provide the best match to behavior. The choice of low event rates for noise distributions poses an interesting theoretical issue. Namely, it is widely held that high-spontaneous rate fibers, not low-spontaneous rate fibers, support detection of quiet signals (e.g., Costalupes, 1985). Model psychometric performance similar to what we report could still be achieved with higher event rate noise distributions that would mimic a combination of low- and high-spontaneous rate auditory nerve fibers. Use of such a noise distribution simply required an increase in the rate of the signal distributions (suggestive of integration of larger numbers of auditory nerve fibers), but the same psychometric threshold and slope trends that held with low event rate noise distributions held for this case also (data not shown).

The event rate of the signal distributions (Figure 3.11A) was selected to most closely evoke simulated performance similar to what we observed in our behavioral experiments, at a range of intensity/duration combinations. This was done by manipulating the rate parameter as a means of generating more simulated events, or spikes. For longer durations (100 and 200 ms), simulated behavioral performance could be generated using spike counts of about 200, which, assuming a maximum firing rate of 350 spikes per second, suggests integration of three to five auditory nerve fibers (ANFs; see Discussion). For shorter durations, greater firing *rates* (not total spike counts) were used to increase the number of spikes to 75 for 50 ms stimuli, ~60 for 25 ms stimuli, and about 20 for 12.5, 6.5, and 3.25 ms stimuli. For 3.25 ms stimuli, given a maximum firing rate of about 350 spikes per second for each ANF, ceiling psychometric performance suggests the integration of ~20-25 ANF firing rate distributions (see Discussion). This suggests that later stations in the auditory pathway may display integration properties more similar to behavior (e.g. cochlear nucleus). To facilitate the comparison with behavior such as shown in Figure 3.1, it was desirable to display model performance as a function of tone level, instead of firing rate or spike count. To accomplish this, we related event rate to tone level with the rate-level model of Sachs and Abbas (1974). This allowed the generation of psychometric functions (Figure 3.12B) that showed

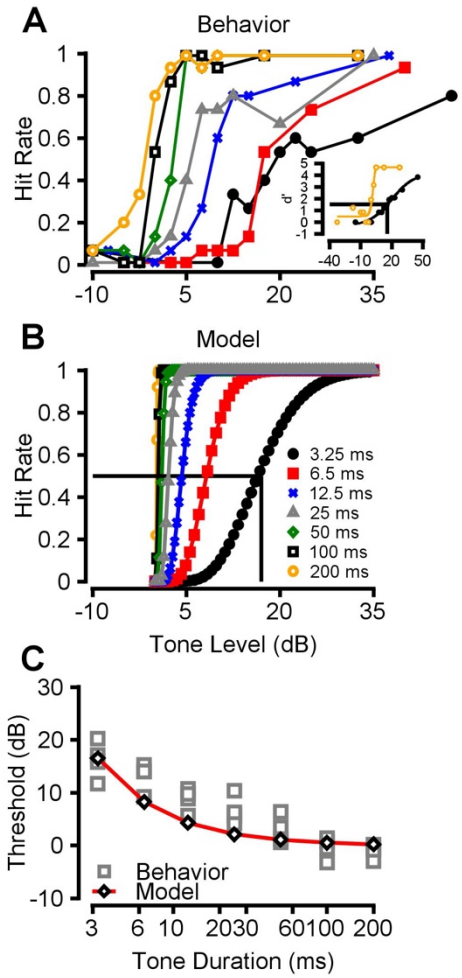

FIGURE 3.12. Results from the Poisson model compared to behavior. A. Example psychometric functions from Monkey B at 2 kHz (x-axis range limited to facilitate visual comparison with model data; original axes are shown as an inset). Hit Rate, used to calculate *d'* in previous figures, is displayed to facilitate comparison with model data. **B**. Psychometric functions generated using the probabilistic Poisson model outlined in Figure 3.11. Threshold is the tone level that evoked Hit Rate = 0.5. **C**. Comparing model thresholds to behavioral thresholds. Model thresholds are displayed as black diamonds connected by red lines, while behavioral thresholds from all monkeys at 2 kHz are displayed as grey squares. Color available online.

the same threshold and slope trends as our empirical psychometric functions (example in Figure 3.12A). In this specific case, psychometric functions are displayed in terms of hit rate, rather than *d',* to facilitate visual comparison with model data in the subsequent panels in Figure 3.12. Hit Rate in Figure 3.12B corresponds to the area under the Poisson distribution. A more typical *d'* measure was not used because *d'* assumes an underlying normal distribution, which does not apply to this model. Threshold was taken to be the tone level that evoked 0.5 hit rate (area under the curve), a common threshold criterion when extracting threshold from hit rate functions (Beitel et al., 2003; O'Connor et al., 1999). Psychometric thresholds (in terms of *d'*) for all monkeys detecting 2 kHz tones in quiet and model thresholds (hit rate = 0.5) are compared in Figure 3.12C. A related question is whether the PPM could be adapted to mimic behavior in noise, with the main finding in the present report being that noise decreases psychometric DR. To some degree this is predicted by the model. By shifting the distributions to higher baseline rates to simulate

the presence of noise, the dynamic ranges contracted for short duration stimuli, similar to what was observed behaviorally. However, the actual thresholds did not, at least when a necessary, realistic parameter of noise induced changes in nerve fiber responses was imposed upon the model. Specifically, Costalupes et al. (1984) and Gibson et al. (1985) documented that background noise caused a 0.61 – 0.79 dB/dB threshold shift in ANFs that does not match the 1 dB/dB behavioral threshold shift that macaques and humans exhibit (Dylla et al., 2013; Hawkins and Stevens, 1950). Thus, the model captures one aspect of the behavioral data in background noise.

The PPM consistently yielded slightly worse fits than the exponential and power law models, indicated by greater RMS error values (Eqn. 3 in Methods), which were consistently around 1.0-1.5 dB for the exponential and power law models, whereas the PPM fits were more consistently 2-3 dB for the PPM (Table 3.1).

TABLE 3.1: Final parameters for fitting the probabilistic Poisson model to psychometric data. The key parameter for fitting the model to various sets of data (the range of the rate-level function used for sound level conversion, see Results E) is indicated for thresholds at a range of different tone frequencies. The range parameters that gave the lowest average root-mean squared error (RMSE) is indicated, along with the average RMSE for all four monkeys. The RMSE for the exponential fits were consistently 1-1.5 dB (no effect of tone frequency).

Tone Frequency (kHz)	*Tone level range (dB)*	*Poisson model RMSE (dB)*	*Exponential model RMSE (dB)*
1	*0-45*	*3.19*	*1.28*
2	*0-25*	*2.9*	
4	*-5-25*	*2.98*	
8	*-5-20*	*2.39*	
16	*-5-15*	*2.59*	
32	*10-60*	*1.89*	

Interim summary

To summarize thus far, behavioral estimates of macaque temporal integration closely match humans, and modeling suggests this behavior may require integration of ~20 ANF inputs. Such integration is known to occur in the cochlear nucleus and inferior colliculus (see General Introduction on temporal processing). This motivated the following analysis of neuronal responses in the CN and IC.

3.3.6 Hierarchical differences in temporal integration emerge only in masking noise

Tone evoked responses from the cochlear nucleus (CN) and inferior colliculus (IC) of macaques performing a tone detection task were analyzed using a time-window analysis. These recordings are part of a previously published dataset (Preprint: Mackey et al., 2022; Conference proceedings: Ramachandran, 2018).

From the tone evoked response (Figure 3.13A), the latency was calculated (Figure 3.13B), and neurometric accuracy (Probability Correct, see Methods) was then calculated via ROC analysis as a function of time elapsing after neuronal latency. This time after latency will be referred to as duration. Neurometric functions resembled psychometric functions: threshold and slope changed as a function of duration, which can be seen by comparing Figure 3.13C to Figure 3.12.

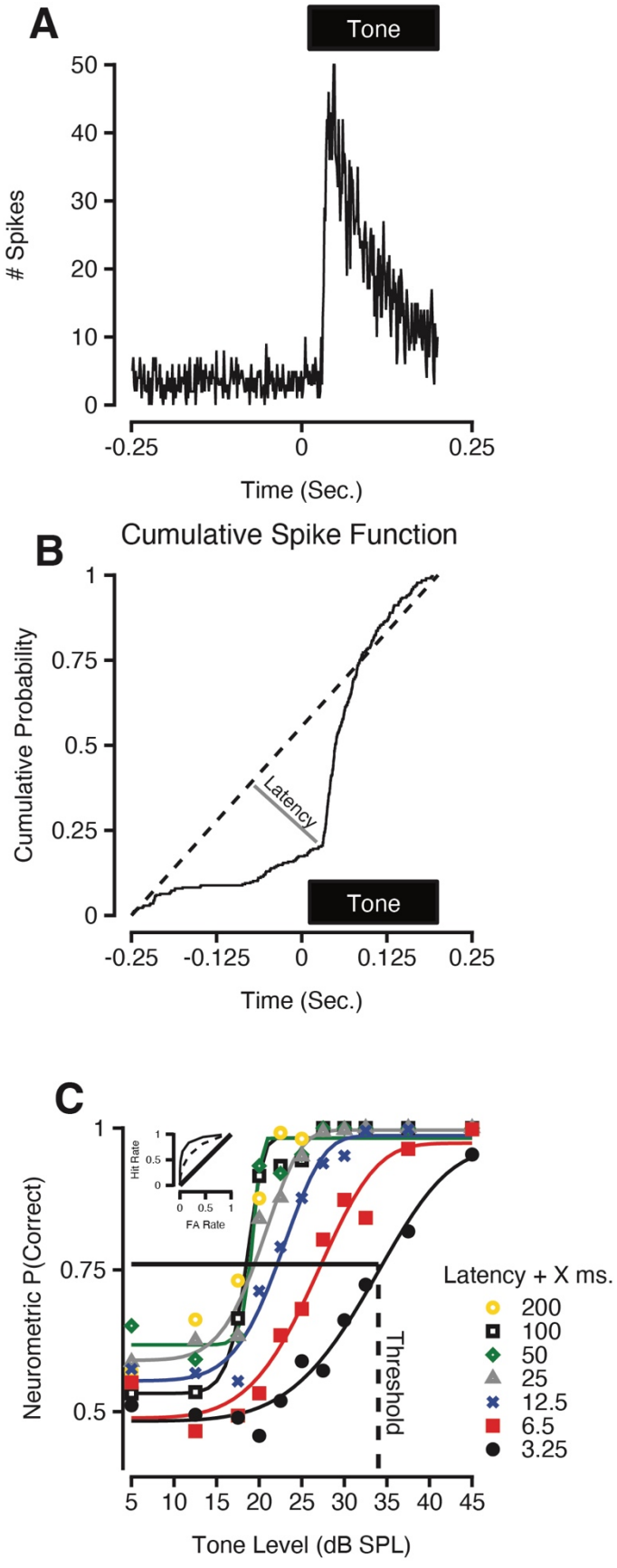

FIGURE 3.13 – Time window analysis on single-unit responses. A. Example peristimulus time histogram from a neuron in the IC. **B.** Example cumulative spike function (CSF) based on the response in A. The CSF was used to estimate neuronal latency. **C.** Example neurometric functions calculated via ROC analysis (inset) at different durations, as indicated by the symbols in the legend. Threshold was the conventional value of PC = 0.76.

Neurometric thresholds from each neuron were plotted as a function of duration and fit with an exponential function (Figure 3.14), to compare neuronal and behavioral temporal integration time constants, which are inversely related to the rate of temporal integration. The effect of duration was consistent across the CN and IC, and the trend resembled behavioral trends in that threshold decreased exponentially as a function of duration. Figure 3.14A-B shows median neurometric thresholds in quiet and in noise, in both brain regions, normalized to the lowest threshold (200 ms). Figure 3.14 C-D illustrates how thresholds were fit

with exponential function to extract the neurometric time constant, and representative neurons are shown. While the form of the exponential function (and thus the time constant) did not differ between quiet and noise conditions for the CN, an increase in the time constant by masking noise was regularly observed in the IC population (Figure 3.14C & D). Hierarchical differences (between the IC and CN) in temporal integration were not apparent in quiet conditions, as can be seen in the green time constant distributions, plotted as cumulative probability distributions in Figure 3.14E and F. The CN and IC distributions were not significantly different in quiet, which was confirmed with a 2-sample Kolmogorov-Smirnov test ($p = 0.29$). However, in noise, a slower subpopulation emerged in the IC, which more closely approximating behavioral time constants, as can be seen in Figure 3.14F. This effect of brain region was validated with a two sample

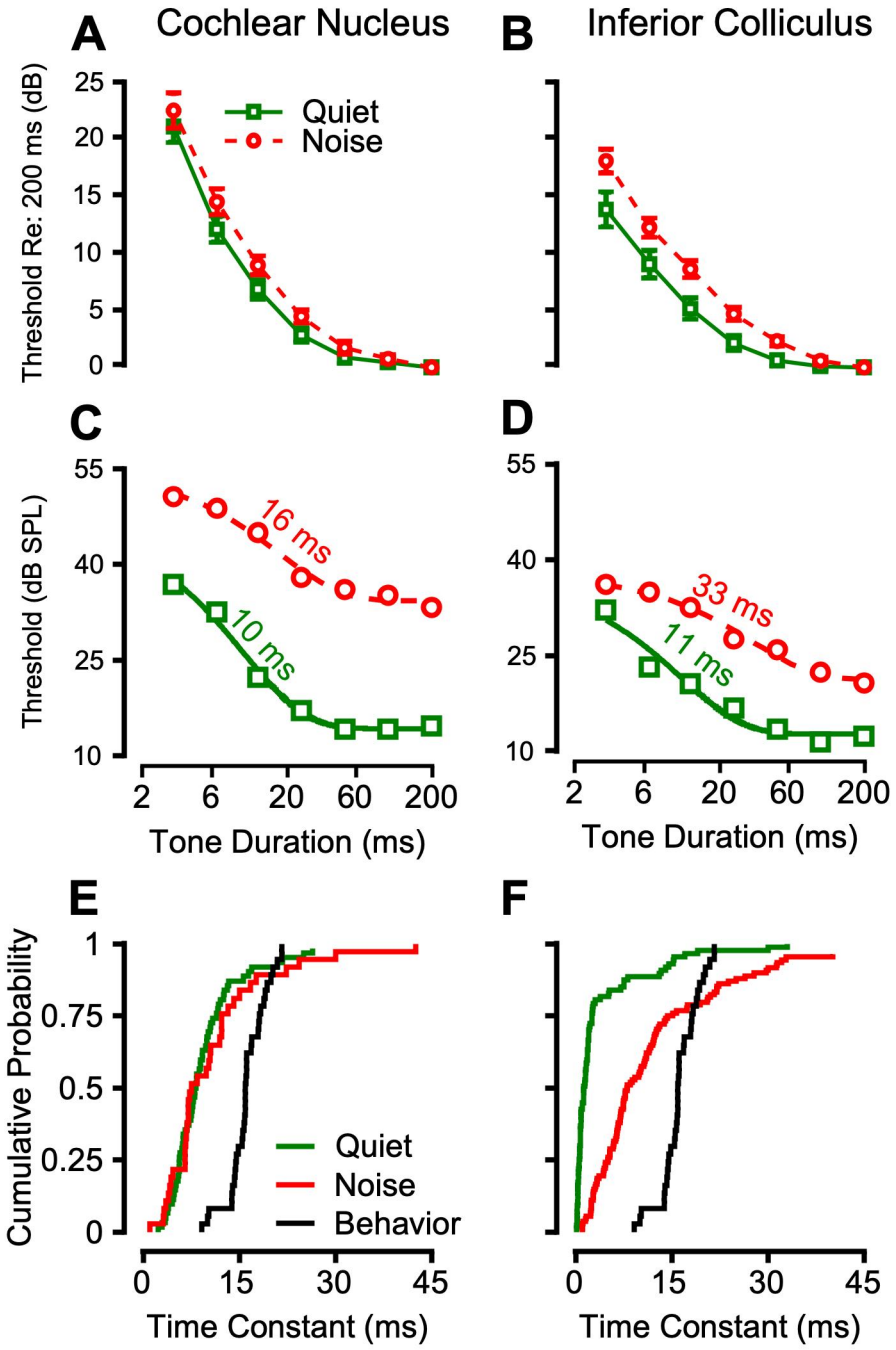

Figure 3.14 – Neurometric measures of temporal integration reveal a hierarchical effect of noise. A. Median (+/- standard error) neurometric thresholds in the CN as a function of duration, in quiet (green squares) and in noise (red circles). **B.** Median neurometric thresholds in the IC. **C,D.** Example neurometric thresholds from the same neuron in quiet and in noise, fit with three term exponential functions. Temporal integration time constants are listed above each trace for the CN (C) and the IC (D). **E, F.** Time constants of all neurons in quiet (green) and noise (red) plotted cumulatively for the CN (E) and IC (F), along with the distribution of behavioral time constants (black). The effect of noise on time constants was significant in the IC as assessed by a 2-sample Kolmogorov-Smirnov

Kolmogorov-Smirnov test (p = 0.022), and the effect of noise in the IC was significant (p = 0.017).

3.3.7 Effects of noise exposure

Psychophysical measures of temporal integration

To understand why many normal-hearing human listeners display perceptual deficits in complex acoustic environments, we tested the hypothesis that psychophysical measures of temporal integration would be impaired by moderate noise exposure in male and female macaques. Cochlear histological analysis so far indicates that this 120 dB noise exposure (see General Methods) causes temporary inner hair cell ribbon synapse loss, and permanent synapse enlargement (see Appendix), which may result in lasting synaptic dysfunction. Following this noise exposure, detection thresholds were rarely elevated after the relaxation of the temporary threshold shift associated with these moderate noise exposures. However, 4-7 months post exposure, psychometric function slopes exhibited reliable changes at durations of 6-25 ms, quantified using psychometric dynamic range (DR; Figure 3.15). This effect was confirmed with a mixed effects model (Table 3.2), and lasted the duration of the study (9-11 months post noise exposure). The effect of noise exposure was significant, as well as interactions of exposure with tone frequency and duration (Table 3.2). In the female cohort, the effect of noise exposure was significant, as well as an interaction with tone duration (Figure 3.16; Table 3.2). In a mixed-effects model incorporating both male and female data, effects of noise exposure were significant, as well as interactions of noise exposure and sex, reflecting the fact that noise exposure impaired performance in both cohorts, but

did so differently across frequency and duration. The magnitude of the effect was substantial, with the joint male/female model predicting an 8.1 dB increase in DR after noise exposure, which in many cases was a doubling in DR (Figure 3.15, Figure 3.16). The effect of sex was that DR was larger in the female cohort at baseline, indicated by a positive t-statistic, and a model coefficient estimate of 3 dB (Table 3.2). Another key difference in the male and female cohort was that thresholds were permanently elevated in female monkeys Pi and Lu by 8-15 dB, at short durations (3-25 ms) following noise exposure, which can be seen in Figure 3.16. Surprisingly, this effect was not restricted to the tone frequency at which DR was elevated. Thus, thresholds at different frequencies are shown in Figure 3.16 (bottom row) for the female cohort, where occasional permanent threshold shifts (restricted to short durations) were observed.

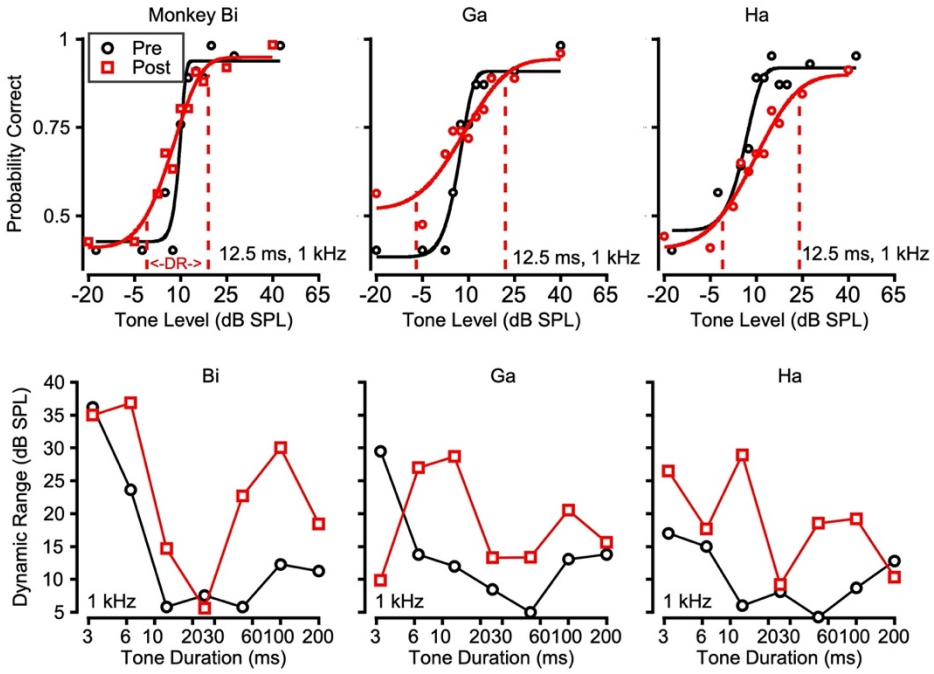

Figure 3.15. Change in psychometric function dynamic range following noise exposure. Top row, Psychometric functions from Monkeys Bi, Ga, and Ha detecting 12 ms, 1 kHz tones, pre (black circles) and post (red squares) exposure. Dynamic range is indicated by the dashed red traces on each function. **Bottom row,** dynamic range of 1 kHz psychometric functions as a function of tone duration pre and post exposure for each monkey.

Reaction-times also changed following noise exposure. To quantify this effect, reaction time slope and intercept were used. Previous work has characterized how RTs increase with sound level, and signal-to-noise ratio (Dylla et al., 2013; Kemp, 1984). These effects have been quantified using a linear fit to RT as a function of tone level

(Bohlen et al., 2014; Dylla et al., 2013; Rocchi and Ramachandran, 2018). The two parameters of the RT vs. level function (slope and intercept) were used in the present analysis to assess two potential effects of synaptopathy on RTs: a change in the growth of loudness (slope change), or an overall change in the speed of auditory processing (intercept change). To test these hypotheses, the slope and intercept of each RT vs. level fit were calculated for each monkey, at each tone frequency and duration, in quiet and in noise. The intercepts and slopes of the reaction time vs. tone level linear regressions were entered into a mixed effects model as the response variable, with tone frequency, sex, duration, and pre vs. post noise exposure status as fixed effects. Individual monkeys were entered into the model as random effects. Reaction time intercept was slightly lower after noise exposure, indicating faster RTs, possibly a result of training (Coefficient estimate: -29.97 ms, $t = -4.17$, $p = 4*10^{-5}$), and reaction time slope was slightly increased at certain tone durations following noise exposure, indicated by a significant positive interaction between noise exposure status and tone duration ($t = 2.0$, $p = 0.043$). Thresholds and reaction time measures from the masked detection experiments did not significantly differ before and after noise exposure as assessed by mixed effects model analysis, and the dynamic range of the psychometric function slightly decreased following noise exposure, possibly another beneficial effect of training ($t = -0.23$, $p = 0.004$).

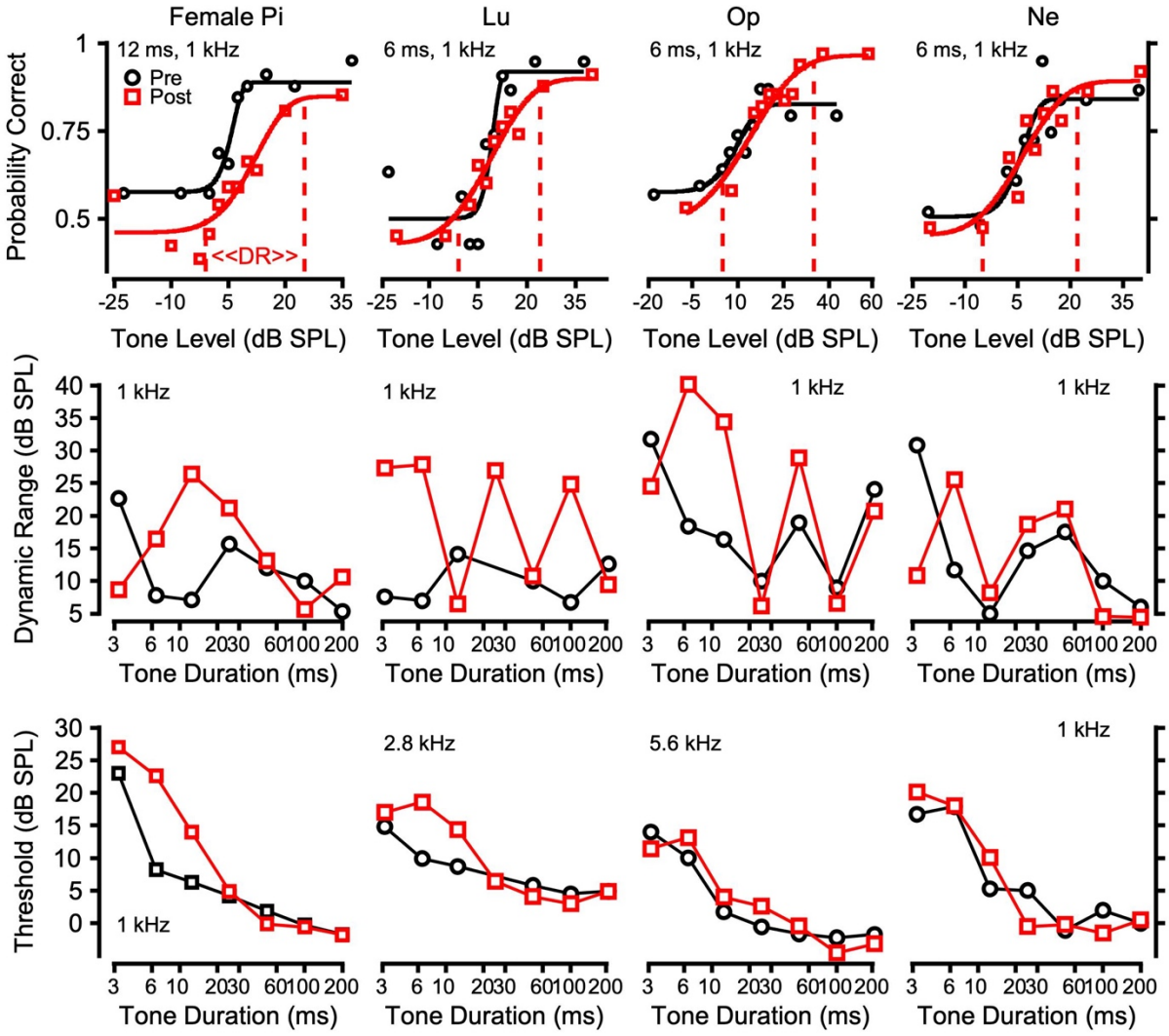

Figure 3.16. Change in dynamic range and threshold following noise exposure in a female cohort. Top row, examples of DR change following noise exposure. Psychometric functions from monkeys Pi, Lu, Op, and Ne are shown. Formatting follows conventions in the last figure. **Middle row,** DR as a function of duration at 1 kHz for each monkey. **Bottom row,** detection threshold as a function of tone duration for each monkey at select frequencies exhibiting threshold shifts.

TABLE 3.2. Mixed effects model analysis of the effects of noise exposure and sex on psychometric function dynamic range (DR).

MODEL	**Effect of noise exposure (t-stat, *p-value)***	**Effect of sex (t-stat, *p-value)***
Male cohort Psychometric DR ~ Noise Exposure*Tone Frequency + Noise Exposure*Duration + Tone Frequency + Duration + Noise Exposure + (1|Monkey)	Noise Exposure: t = 1.23, p = 0.0019 Noise Exp*Tone Freq: t = -2.3, p = 0.019 Noise Exp*Duration: t = 2.26, p = 0.024	N/A
Female cohort Psychometric DR ~ Duration* Tone Frequency*Noise Exposure Status + Duration + Tone Freq + Noise Exposure Status + (1|Monkey)	Noise exposure: t = 2.4, p = 0.01 Noise Exp*Duration: t = -2.1, p = 0.039	N/A
Male & Female Psychometric DR ~ Noise Exposure*Sex*Tone Frequency + Noise Exposure + Sex + Tone Freq + Duration + (1|Monkey)	Noise exposure: t = 3.28, p = 0.001	• Sex: t = 2.8, p = 0.005 • Noise Exposure*Sex = t = -2.12, p = 0.034

Modeling deficits with a Poisson process model

In the absence of neuronal measures of temporal integration from the noise exposed animals, computational modeling was used to conceptualize how deficits in temporal integration after noise exposure could emerge from neuronal activity. The Poisson process model from section 3.3.5 predicted the psychometric threshold and DR trends in normal hearing monkeys, and was then adapted to produce changes in DR putatively due to synaptopathy. Figure 3.17 shows model psychometric functions in response to a 6.5 ms stimulus with and without simulated cochlear synaptopathy/ANF loss ("SYN"). Key assumptions of the model are outlined in section 3.3.5. To produce deficits in DR, the rate at which firing rate changed with tone level (i.e. recruitment) was decreased, and the decision criterion was lowered (i.e. made more liberal). The change in criterion was necessary to produce a change in DR without a substantial change in threshold. Figure 3.17 shows model psychometric functions, with dashed lines pointing to the hit rate evoked by 9 dB tones, and with the number of simulated auditory nerve fibers recruited. The 9 dB point was chosen 1) for illustrative purposes, as the number of ANFs recruited for detection increased with level (e.g. for the normal hearing model: 8 ANFs for 9dB, 17 for 30 dB; for the SYN model: 2 ANFs recruited for 9dB, 3 ANFs required for 30 dB), and 2) because the loss of 6 ANFs is roughly equivalent to the maximum synapse loss observed at the early post exposure time point (see Appendix), which will be discussed later.

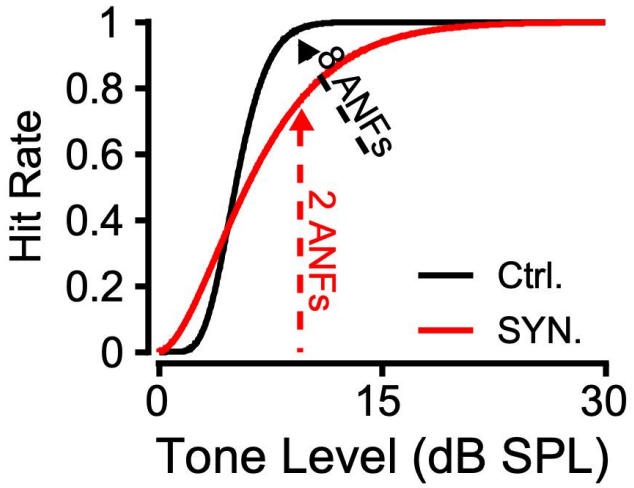

Figure 3.17. Poisson process modeling predicts synaptopathic deficits in temporal integration. Model psychometric functions are displayed with (black) and without (red) simulated cochlear synaptopathy (SYN). The dashed lines point to the proportion of responses at 9dB, and list the number of ANFs recruited for detection.

3.4 Discussion

These results contribute in many ways to the understanding of how acoustic evidence is accumulated over time. Analysis at the behavioral, neurophysiological, and computational levels indicate that 1) macaques are well-positioned to model human temporal integration, 2) there is a hierarchical effect of noise on temporal integration in the subcortical auditory system, and 3) hidden hearing loss may be in part due to noise-induced synaptic dysfunction, and subsequent reduction in the rate of temporal integration.

Similarity between macaque and human behavior

Consistent with other studies of the effect of signal duration on detection across a variety of species, we found that threshold decreased exponentially as tone duration increased (e.g., Macaques: Clack, 1966; O'Connor et al., 1999; Humans: Plomp & Bouman, 1959, Watson & Gengel, 1969; Budgerigars: Wong et al., 2019). Though the threshold data in the current report are in agreement with many aspects of these studies, τ values (temporal integration time constants) in the current report were 10-40 ms, in contrast to the macaque data of Clack (1966) and O'Connor et al. (1999), who found τ values in the range of 140 – 150 ms. Those earlier data suggest that macaques exhibit drastically slower temporal integration than humans (human mean of ~30 ms Watson & Gengel, 1969; Clack, 1966; O'Connor et al., 1999). The present data suggest macaque data resemble the data from humans and budgerigars. Evaluation of this claim is critical to determining the extent to which the macaque serves as a model of human auditory perception. The strongest candidate explanation for the difference in the current report and the two earlier macaque studies seems to lie in the range of tone durations the monkeys were trained to detect. The current study used 3.25 - 200 ms tones while O'Connor et al. (1999) used 25 – 800 ms tones. The time constants reported here do not change if thresholds of 25-200 ms are used (data not shown), suggesting the difference is not because of the analysis, rather these short duration tones may have caused the monkeys to integrate at faster rates due to being trained on shorter duration stimuli.

Consistent with human psychophysical studies in the visual system (Hildreth, 1973; Kietzman and Gillam, 1972; Miller and Ulrich, 2003), somatosensory system

(Hernández-Pérez et al., 2020), and a single study in the auditory system (Raab, 1962), we found that reaction time (RT) increased as stimulus duration decreased. This extends the currently available data in animal models to show that insofar as these behavioral paradigms index temporal integration, the process also occurred at suprathreshold levels. To the best of the authors' knowledge this has not been shown before in any animal model of auditory perception. Data from chinchillas and cats demonstrate a lack of effect of sound duration on RT (Clark, 1979; Costalupes, 1983), and thus RTs serve as the second line of evidence suggesting human-macaque perceptual similarity.

A hierarchical effect of noise on subcortical auditory temporal integration

Building on the Poisson process model (Figure 3.12) and previous work suggesting the pooling of auditory nerve fiber (ANF) responses is necessary to explain auditory perception (Clock Eddins et al., 1998; Lopez-Poveda, 2014; Stevens and Wickesberg, 1999; Viemeister et al., 1992), the present results investigated temporal integration in the CN and IC. In contrast to a previous study of anesthetized chinchilla CN (Clock et al., 1993), the CN time constants presented here did not resemble behavior in quiet or in noise. It was hypothesized that temporal integration in the IC would resemble behavioral temporal integration, as IC responses provide reliable estimates of psychometric threshold and slope, and exhibit significant choice-probabilities (Mackey et al., 2022). These neurometric-psychometric correlations may be due to the high degree of convergence in the midbrain, and consequent reduced variability of neuronal responses. However, IC temporal integration time constants only resembled behavioral time constants in the presence of noise. This wider range of timescales at which neurons encode sound may be of utility in noisy, suprathreshold environments, and/or for the encoding of complex sounds that exhibit fluctuation on multiple timescales (e.g. species specific communication sounds). The hierarchical differences between CN and IC are consistent with a study of IC, thalamus, and primary auditory cortex (Asokan et al., 2021), which characterized how progressively longer timescales are encoded in these regions. Asokan et al. did not explicitly relate neural measures to behavioral measures, but the CN and IC results presented here may suggest that auditory cortex time constants would more closely resemble behavioral measures of temporal integration.

Further downstream, parietal cortex integrates acoustic evidence (Yao et al., 2020, 2022), and sensory evidence more generally (e.g. Cohen et al., 2004; Huk and Shadlen, 2005). Alternatively, the superior colliculus can integrate acoustic evidence, as multiple studies indicate (Jay and Sparks, 1987; Rajala et al., 2017; Wallace et al., 1996), and there is causal evidence for its role in evidence accumulation in the visual domain (Jun et al., 2021). Future studies can empirically address how neural measures of temporal integration in these regions relates to perceptual measures.

Effects of noise exposure causing temporary threshold shift, synaptic loss and dysfunction

Previous studies have investigated temporal integration as a candidate behavioral assay of cochlear synaptopathy (Marmel et al., 2020; Wong et al., 2019) and reported null results. Here it was shown that temporal integration was impaired by noise exposure that preferentially targets the IHC synapse. The discrepancy between these studies may be due to a few methodological differences. Marmel et al. (2020) and Wong et al. (2019) measured threshold using an adaptive procedure, and psychometric function slope/DR are not reported. It may be that subjects in these studies had perceptual deficits not evident in detection threshold, as many of the monkeys in this study did. Another difference is that Wong et al. used a glutamate analog, kainic acid, to mimic the effects of synaptopathic noise exposure. While kainic acid causes substantial synaptic loss compared to our noise exposure, there may still be differences in the two methods of inducing cochlear damage. Finally, Marmel et al. measured temporal integration in humans with *putative* synaptopathy. The lack of histological verification makes it unclear if their null result was due to lack of synaptopathy, or that synaptopathy doesn't impair detection of short tones.

Interestingly, it was shown here that noise exposure's effect on DR was not largest for the detection of 3.25 ms tones, (which sometimes even showed enhancement), but rather for 6-25 ms (see Results). While counterintuitive, this may be explained by a companion study from this lab, and from a study of mice ANF. Specifically, Suthakar and Liberman (2021, 2022) found that the onset response in mice ANF, and ABR Wave-I amplitudes were increased following synaptopathic noise

exposure, and NHPs from this lab displayed the same increase in ABR amplitude following noise exposure (Dissertation by Dr. Jane Mondul, 2022).

Finally, the Poisson model introduced here offers an explanation of how synaptopathic noise exposure could cause perceptual deficits. Namely, a loss of auditory nerve fiber input, coupled with a more liberal decision criterion was able to reproduce deficits in psychometric DR for short duration stimuli without elevating threshold. This reduced ANF input could be conceptualized as a synaptopathy on par with what was observed histologically (see Appendix), but an essential component of reproducing the deficit was the more liberal decision criteria in the model. This aspect of the model, based on a basic insight of signal detection theory (Tanner and Swets, 1954), may be a key consideration in future studies of hidden hearing loss.

CHAPTER 4 – TEMPORAL SOUND ENVELOPE PROCESSING

Sections of this chapter appear in the following:

Mackey, C. A., McCrate, J., MacDonald, K. S., Feller, J., Liberman, L., Liberman, M. C., Hackett T.A. & Ramachandran, R. (2021). Correlations between cochlear pathophysiology and behavioral measures of temporal and spatial processing in noise exposed macaques. *Hearing Research*, *401*, 108156.

Mackey, C. A., Hauser, S., Schoenhaut, A. M., Temghare, N., & Ramachandran, R. (2022). Psychometric and subcortical neurometric measures of temporal discrimination in rhesus macaques. *bioRxiv*.

4.1 INTRODUCTION

Temporal sound envelope fluctuations are critical for navigating complex acoustic environments (Bregman, 1994; Festen and Plomp, 1990; Vélez et al., 2012; Yost, 1991). Specifically, amplitude-modulation (AM) aids in the processing of species-specific communication sounds, including speech (Boemio et al., 2005; Drullman et al., 1994; Hauser, 1989; McDermott and Hauser, 2007; Richards and Wiley, 1980; Rosen, 1992; Zion Golumbic et al., 2013). Consequently, many studies have investigated AM processing at the psychophysical and neurophysiological levels. AM processing tasks have described human and nonhuman animal capacity for detecting and discriminating features of AM (Beitel et al., 2020; Dooling and Searcy, 1981; Fay, 1982; Formby and Muir, 1988; Kelly et al., 2006; Lee, 1994; Lemus et al., 2009a; Moody, 1994; O'Connor et al., 2011; Viemeister, 1979; Wakefield and Viemeister, 1990; Yao and Sanes, 2021). Primates and songbirds, specifically budgerigars, display enhanced perceptual sensitivity to AM relative to rodents (Kelly et al., 2006; Moody, 1994; O'Connor et al., 2011), positioning them as ideal models to investigate the neural basis of AM perception. A similarly wide range of species have been studied in another AM processing paradigm, modulation masking release (MMR; Humans: Arlinger and Gustaffson, 1991; Bacon and Grantham, 1989; Macaques: Dylla et al., 2013; Mackey et al., 2021b; Treefrogs: Vélez et al., 2012; Gerbils: Ihlefeld et al., 2016). MMR describes the finding that detection thresholds are lower in modulated maskers relative to unmodulated maskers, and that detection threshold increases as modulation frequency increases. MMR is thought to index a listener's ability to track rapid changes in a masker's modulation; an ability that is likely important in understanding speech in noisy, social settings (see General Introduction).

Neuronal responses to AM have been well characterized along the auditory pathway (Bartlett and Wang, 2007; Beitel et al., 2003, 2020; Bendor and Wang, 2008; Downer et al., 2017; Joris et al., 2004; Langner and Schreiner, 1988; Nelson and Carney, 2007; Niwa et al., 2013; Rhode et al., 2010; Sayles et al., 2013; Wang et al., 2008). In early stages (e.g. auditory nerve and cochlear nucleus) neurons respond with synchronized firing to AM, and in later stages (inferior colliculus and above) average rate-tuning becomes increasingly prevalent (reviewed in Joris et al., 2004). Consistent with this, the average neuronal sensitivity based on spike-timing in the cochlear nucleus (CN) and inferior colliculus (IC) correlated with AM detection performance (Henry et al., 2016; Sayles et al., 2013), while the average rate of simulated populations in auditory cortex (A1) correlated with AM detection performance (Johnson et al., 2012). Such population analyses have revealed that the decrease in spike-timing precision in auditory cortex (A1) may be recovered at the population level (Downer et al., 2021; Johnson et al., 2012), and can test predictions of modulation filter-bank models (Dau et al., 1997; Maxwell et al., 2020; Verhulst et al., 2018; Viswanathan et al., 2022), which factor heavily in current thinking of auditory perception.

Current knowledge of subcortical AM processing draws heavily from rodent, cat, and budgerigar studies; however, a potential concern is the lack of subcortical AM processing studies in primates. Nonhuman primates bear exceptional similarity to humans in CN and cortical neuroanatomical structure (Hackett, 2011; Moore, 1980, 2000; Moore et al., 1996; but see Rubio et al., 2008), perceptual measures of temporal processing (Kelly et al., 2006; Mackey et al., 2021a; Moody, 1994), auditory nerve frequency tuning (Joris et al., 2011; Verschooten et al., 2018), and cortical AM encoding (Hoglen et al., 2018). It is unclear to what degree the enhanced (relative to rodents) AM encoding in auditory cortex (Hoglen et al., 2018) is inherited from subcortical stations, because studies of subcortical AM processing in primates have been conducted under anesthesia (e.g. Rhode et al., 2010). Subcortical data from awake primates could enhance the understanding of human and nonhuman primate perception and speak to the validity of models suggesting that CN populations converge on IC neurons to confer AM sensitivity (Hewitt and Meddis, 1994; Nelson and Carney, 2004). Finally, animal studies of the subcortical basis of AM processing have generally focused on detection paradigms, in contrast to cortical studies where the use of different paradigms has

illuminated differences in their computational demands (See General Introduction; Beitel et al., 2003; Lemus et al., 2009a, 2009b; Niwa et al., 2012b; Yao and Sanes, 2021). These opportunities for furthering knowledge of the neural processing of AM were addressed in the present study through single-unit recordings in the CN and IC of awake macaques, and an AM frequency discrimination paradigm, in contrast to more typical detection paradigms.

In addition to understanding the subcortical basis of AM processing using the temporal discrimination paradigm described above, the experiments described in this chapter were designed to advance the understanding of permanent noise-induced hearing loss as well as hidden hearing loss (see General Introduction). Specifically, we sought to establish perceptual correlates of specific cochlear pathophysiology (e.g. hair cell and synapse loss vs. selective synaptic pathophysiology) using behavioral paradigms that index different forms of temporal processing. Temporal processing has been hypothesized to be compromised by synaptopathy by previous neurophysiological studies in animals and humans (see General Introduction). This was addressed in this chapter through the use of an MMR paradigm, and the above mentioned AM discrimination paradigm. Together, these results provide complementary descriptions of macaque temporal processing at the behavioral level, and demonstrate clinical utility of the basic knowledge of temporal processing at the computational and neurophysiological levels.

4.2 METHODS

4.2.1 Subjects

Data from eleven adult male macaques (*Macaca mulatta, n = 9; Macaca radiata, n = 2*), and four female macaques (*Macaca mulatta)* are reported here. Macaques were implanted with headposts and, in some cases (Ch, De, Ec, and Li) recording chambers. Information on surgical procedures, institutional welfare standards, social housing, food etc. is in the General Methods section. Groups are described below. Names in the figures are often restricted to a single letter, but in this section and in figure captions more letters will be used to enable readers to know monkey identity across chapters in this dissertation.

Modulation masking release (MMR)

Experiments were performed on normal-hearing macaques (*Macaca mulatta*, n=7), noise-exposed macaques (Monkey Li, *Macaca mulatta*, n=1; Monkey Ga, *Macaca radiata, n=1*), and one macaque before and after noise exposure (Monkey E, *Macaca radiata,* n=1). The noise exposure described for these monkeys was the permanent threshold shift (PTS) inducing exposure described in the General Methods. Body weights ranged from 10-12 kg. For PTS monkeys, ages at the time of noise exposure were as follows: 10 years (Monkey L), 9 years (Monkey G), and 11 years (Monkey E). Normal-hearing monkeys presented for comparison to L, G, and E were from Monkeys aged 5-9 years old.

MMR data will also be presented from monkeys exposed to a lower-level noise than the one to which L, G, and E were exposed, which only caused a temporary threshold shift (TTS; see General Methods). TTS monkeys participated in the MMR experiments before and after noise exposure, and did not overlap with the noise exposed group described above. Male monkeys B, G, H were 10-12 kg, female monkeys L, N, O, and P were 5.5-7 kg. All monkeys (male and female) in this group were 6-8 years old at the time data collection began, and at the time of noise exposure.

Temporal discrimination experiments

At the beginning of the study macaques ranged in age from 7-8 years old, with body weights ranging from 11-13 kg. The behavior group consisted of Monkey Is and Da, who were not implanted for neuronal recordings. The electrophysiology group consisted of Monkeys C and D. Monkey Is was 7 years old at the time of noise exposure, while Monkey Da was 8.

4.2.2 Experimental procedures

General information about the detection task is reported in the General Methods section. Specific details of the MMR task are described below.

Modulation masking release task

The monkeys detected a tone signal in continuous unmodulated and sinusoidally amplitude modulated broadband noise masker (Figure 4.1). The noise level typically

used was 30 dB SPL spectrum level (76 dB SPL); in some cases, 40 dB SPL spectrum level (86 dB SPL) noise was used as a masker to verify that deficits observed in the noise-exposed monkeys were not dependent on audibility. Tone frequencies used were 0.5, 1, 2, 2.828, 4, 8, and 16 kHz. The noise modulation frequencies were either 10, 20, 40, 80, 100, or 150 Hz. Noise modulation depth was 100%. Monkeys also reported detection in unmodulated noise for comparison. Onset phase of modulation was set at -90°. Tone levels used were based on individual macaque masked audiograms; tone levels were chosen to straddle expected threshold. Noise level and modulation frequencies were blocked. Example stimuli are shown in Figure 4.1, from the 80 Hz and 20 Hz modulated masker conditions.

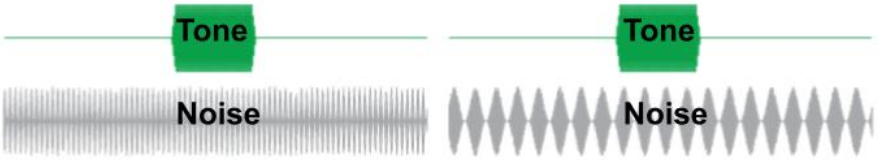

Figure 4.1. Example stimuli from the modulation masking release experiments. Tones were 200 ms, and example broadband, continuous noise waveforms are shown from the 80 Hz (left) and 20 Hz (right) conditions.

Temporal discrimination task

Broadband noise was 76 dB SPL, 500 ms in duration (unless otherwise specified), ramped on/off using a 20 ms cosine squared function (10 ms ramp for durations less than 250 ms), and sinusoidally amplitude-modulated at different frequencies (2-1024 Hz). The speaker was calibrated with a ¼ inch microphone (378C01, PCB Piezotronics) positioned at the location where the entry to the monkey's ear canal would be during experiments. The speaker was calibrated to ensure that outputs were within 3 dB across all frequencies. Monkeys Is and Da performed a lever-based reaction time Go/No-Go discrimination task (Figure 4.2A). Trials were initiated by pulling a lever, following which a delay of 1.5-2 seconds elapsed and two noise bursts modulated at 100% depth were presented without an interstimulus interval (ISI). Trials could be signal trials (50%) in which two AM noise bursts of differing AM frequency were presented, or they could be catch trials (50%), during which identical AM noises were presented. Lever release was required within a response period of 1 second (after the second noise onset)

to indicate discrimination on signal trials, and animals were required to continue to hold the lever on catch trials. All reward contingencies followed convention established in previous studies (e.g. Beitel et al., 2003, 2020; Moody, 1994). Lever release on signal trials (hits) were rewarded with fluid. Lack of lever release within 1 second of the onset of the second noise onset on signal trials (misses) was punished with a time-out of 4-6 seconds in which no trial could be initiated. Lever release on catch trials (false alarm) also resulted in a 4-6 s timeout. Correct rejections (lack of release on catch trials) were rewarded with fluid. Rewarding correct rejections and punishing misses was necessary to balance reward contingencies across trial types, and we empirically determined these reward contingencies to be optimal for performance. The green and red in Figure 4.2A indicate fluid reward and time-out punishment, respectively. MF was varied trial-to-trial, over a range of 1-64 Hz Δ MF. Each MF was repeated 30 times, resulting in blocks containing ~300-420 trials. Experiments were performed after confirming normal hearing status through extensive audiometric and physiological characterization (ABRs, DPOAEs, otoscopy, and tympanometry), ensuring that all measures were within the range of normative values as reported in our previous work (Burton et al., 2019b; Hauser et al., 2018; Stahl et al., 2022; Valero et al., 2017). Figure 4.2B shows how monkeys Is and Da learned to discriminate amplitude modulation frequency (MF) at various MFs in about ten sessions. These data were collected using a cage-training apparatus. A speaker, lever, and waterspout were mounted to the front of the primate cage for short periods each day, permitting the monkeys to learn to interact with the lever for a food reward. Gradually, monkeys were transitioned into pulling the lever for fluid, and, eventually, to releasing the lever for signal trials, but not catch trials.

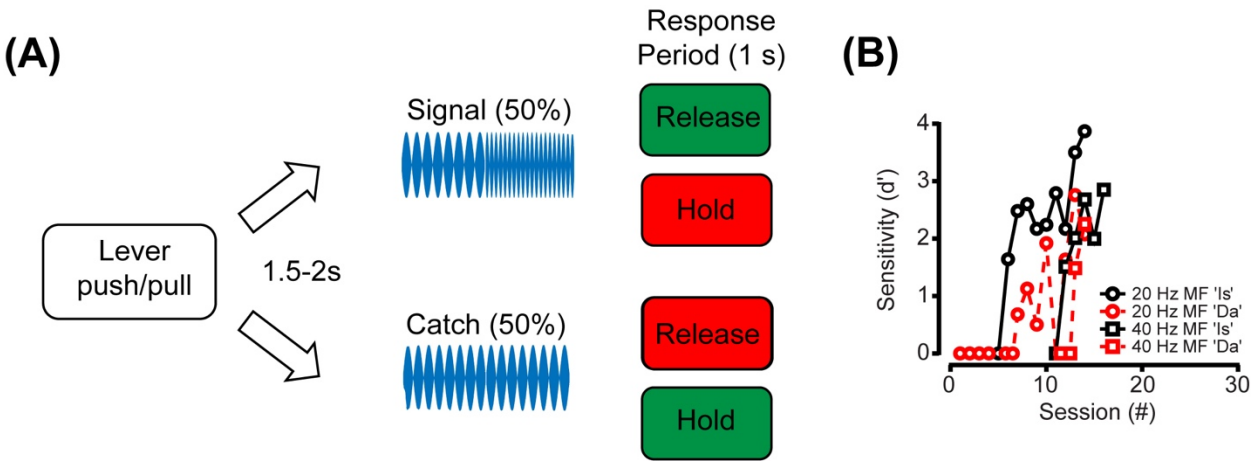

FIGURE 4.2 – Task design and learning trends. A. A diagram of the go/no-go procedure used to measure temporal discrimination performance in this study (see Methods). Monkeys initiated a trial by pulling a lever. Following a random delay (1.5-2 seconds), stimuli were presented for a signal or catch trial (50/50). Monkeys were rewarded (green boxes) for lever release within the response period (1 second) of a signal trial ("Hit") or holding on catch trials ("Correct rejection"). Monkeys were punished with a timeout (red boxes) on holding the lever through the response period of a signal trial ("Miss"), or for releasing on a catch trial ("False alarm"). **B.** A signal detection theoretic measure of sensitivity (*d'*) is shown as a function of training session for each monkey (shown in different colors). Over the course of training, discrimination performance increased for both monkeys discriminating either 20 Hz (circles) or 40 Hz amplitude-modulated noise (squares).

Neuronal recordings

Monkeys C and D (the electrophysiology group) sat passively during recordings reported here, though they had experience in previously published tone detection tasks, including AM processing tasks (Bohlen et al., 2014; Mackey et al., 2021b). Neuronal recordings were made from the CN and IC (see General Methods). After isolating single-units, responses to 76 dB, 100% amplitude modulated noise (frequencies: 2-1024) were collected.

4.2.3 Data analysis

Calculation of neural responses to amplitude-modulation

Average firing rate was calculated over the entire 500 ms interval that each AM noise burst was presented, at each modulation frequency. Changes in firing rate relative to the response to steady-state noise were plotted, depicting the rate modulation transfer functions (MTFs) as others have previously reported (Krishna and Semple, 2000; Langner and Schreiner, 1988; Nelson and Carney, 2007; Sayles et al., 2013). Spike-timing was measured using classical vector strength (Goldberg and Brown, 1969) and phase-projected vector strength (Yin et al., 2011). The onset response was included for both firing rate and vector strength (VS) calculation (see Discussion).

Analysis of psychometric accuracy, neurometric accuracy, and reaction-time

Detection theoretic methods were used to analyze both behavioral and neuronal responses (Macmillan and Creelman, 2004; Swets, 1973; Tanner and Swets, 1954). Behavioral performance from each block of data was analyzed to calculate hit rate at each modulation frequency (*H(MF)*) and false alarm rate (*F*). Sensitivity at a given modulation frequency (MF) was calculated as $d'(MF) = \big(z(H(MF)) - z(F)\big)$, where z represents calculation of the z-score of the value, implemented in MATLAB via the function "norminv." From *d'*, probability correct in a two-alternative forced-choice experiment was given by *pc(MF)*, as $pc(MF) = z^{-1}(d'(MF)/2)$, where z^{-1} represents the transformation from a standard normal variate to probability correct. Calculation of *pc,* rather than a more common *d'* measure, permitted comparison with our distribution free (ROC) calculation of probability correct based on neuronal responses (Mackey et al., 2022; Rocchi and Ramachandran, 2018, 2020). Psychometric and neurometric functions were fit with a modified Weibull cumulative distribution function (CDF) as others have done in both detection and discrimination tasks (Britten et al., 1996; Christison-Lagay and Cohen, 2014; O'Connor et al., 1999). The modified equation was:

$$pc(MF) = c - d * e^{-(MF/\lambda)^{\kappa}}$$

where *c* represents saturation and *d* represents the range of the function, and λ and κ represent the threshold and slope parameters respectively. The threshold was calculated as that tone level at which $pc_{fit}(MF)$=0.76, similar to common use of *d'=1* threshold criterion. Reaction times (RT) are reported from hit trials and were calculated as follows:

RT = Time of Lever Release – Time of Second Noise Burst Onset

RTs were plotted cumulatively to visualize and to give insight into the effects of modulation frequency difference on discrimination speed, as previous publications of AM processing in animals have rarely reported RTs.

Simulation of population responses

Neuronal responses were analyzed at the population level in a similar fashion to the "across-cell" method described by Johnson et al. (2012). A population (2-35) of neurons was randomly selected with replacement, following which single-trial spike trains were randomly sampled from each neuron. Responses were sampled 20 times with replacement, after determining empirically that neurometric sensitivity could not be enhanced beyond 20 permutations. Rate responses were summed, while vector strength was calculated based on the pooled spike times. The pooling process was repeated 1,000 times. The simulated population response to each modulation frequency calculated in this way served as the basis for ROC calculation described above, permitting the calculation of the population's neurometric probability correct and discrimination threshold. Pooling is not reported for vector strength, as we found that VS only decreased as spike-trains were pooled, likely due to the diverse phase-preferences of subcortical neurons.

Time-window analysis

Neuronal responses were calculated at varying durations to compare neuronal sensitivity to behavioral sensitivity as a function of stimulus duration. This was done by changing the time-window within which spikes were counted. This was initially attempted at exactly the durations used in the behavioral experiments (50, 100, 250, and 500 ms), however, the concentration of spikes at the onset of each cycle of AM in the noise caused highly variable and non-monotonic spike-counts. We then calculated time-windows differently for each modulation frequency, so that the time-window would be rounded up or down to the nearest AM trough. Using this method, and slightly different durations (50, 62.5, 125, 250, 500 ms), more consistent responses were attained as a function of duration. After the time-window was adjusted, ROC analysis

was conducted on the spike-count using the method described above, and in our previous publications (Mackey et al., 2022; Rocchi and Ramachandran, 2018, 2020).

Drift-diffusion model

Data were fit with a drift diffusion model using the HDDM 0.8.0 package (Wiecki et al., 2013), based on previous work modeling Go/No-Go task performance (de Gee et al., 2020). We used some of the code made available by de Gee et al. on Github (https://github.com/hddm-devs/hddm/blob/master/hddm/examples/gonogo_demo.ipynb). Data were fit using RT quantiles, using the G-square method. RTs, along with proportion of go responses at each modulation frequency and duration, contributed to G square, and a single bin of the number of no-go responses (but not the no-go RTs) also contributed to G square, which is conventional for Go/No-Go tasks (de Gee et al., 2020; Ratcliff et al., 2018). Drift rate was allowed to vary across modulation frequency, while non-decision time and decision-threshold could only vary as a function of whether the trial was a catch trial or not, consistent with the finding that high conflict trials can induce rapid changes in these processes (Cavanagh et al., 2014). This model was chosen based on a Bayesian information criterion (BIC) value that was lower than the BIC of other models that were less psychologically plausible (e.g. ones in which drift rate, threshold, and non-decision time could vary across modulation frequency, ones in which drift rate and threshold could vary across modulation frequency, and ones in which drift rate was the only free parameter). All data were fit using Markov-chain Monte Carlo sampling, using 6000 samples and a 1000-sample burn-in. The goodness of fit of the model was quantified with BIC (discussed above), and with a posterior predictive check, which indicated that the 95% confidence intervals around the model estimates of the data captured both the empirical choice proportions and empirical reaction-time data.

Modulation masking release (MMR) calculation

Calculation of accuracy (probability correct) in these tone detection experiments are described in the General Methods section. Measures of MMR are described here. The masking release observed in the task in which tones were embedded in amplitude-modulated noise will be referred to as modulation-based masking release (MMR). In the

MMR task, thresholds were measured for the unmodulated masker condition as well as for the different masker modulation frequencies. Previous studies from this laboratory showed that when the noise was modulated at 10 Hz, the monkeys' detection threshold of a signal tone was lower relative to when the noise was unmodulated (Dylla et al., 2013; Hauser et al., 2018). The relationship between masking release and noise modulation frequency was quantified by fitting a sigmoidal function (a Weibull CDF) to the threshold vs. noise modulation frequency data. The threshold parameter (α) of the MMR Weibull function was taken to be the MMR threshold (the highest noise modulation frequency that caused a significant and reliable reduction in masked tone detection thresholds). To further characterize MMR, the amplitude (*d* parameter of the Weibull CDF) of each of the MMR functions was taken as an estimate of the magnitude of masking release. The MMR threshold and amplitude provide complementary estimates of temporal processing. MMR threshold was taken to be the lowest value measured (10 Hz) if the MMR amplitude was less than 6 dB (termed "MMR Criterion"), as this appeared to be roughly 50% of the typical MMR amplitude observed (see Results).

The control data to this study were not obtained in monkeys G and L before they were noise-exposed. The effects of noise exposure were obtained by comparing with a separate group of unexposed macaques that had normal hearing as assessed by behavioral and audiological (non-invasive physiological) methods.

Statistical analyses and curve-fitting

In all cases, curve fits were attained via non-linear least squares method implemented in MATLAB 2019a (Mathworks Inc.). Two-sample Kolmogorov-Smirnov tests were used to statistically confirm the differences in neurometric threshold distributions ("kstest2" in MATLAB). Statistical analysis of the goodness of fit of the drift diffusion model is discussed above.

Correlations of MMR with audiometric shift and histological data were calculated using the "corrcoef" function in MATLAB, which gives Pearson's correlation coefficient, R and significance value. Additionally, "fitlm" and "fitnlm" were used to assess goodness of fit of each linear or non-linear fit, respectively. Choice of model was always validated

using the “fitlm” and “fitnlm” functions, which gives Bayesian Information Criteria (BIC). Statistical analysis of the differences between noise-exposed and control data were conducted using linear mixed effects models (“fitlme”) in MATLAB 2018a. These models accommodate datasets with missing points. This reason, among others, has motivated many researchers to opt for mixed effects models over repeated measures ANOVA (Krueger and Tian, 2004). The dependent variable in each model was either MMR threshold or MMR amplitude. Noise exposure status, tone frequency, and an interaction term between the two were entered as fixed effects into the model, while intercepts for individual macaques were entered as random effects. P-values were obtained by likelihood ratio testing of the model with the effect in question against the model without the effect in question.

The histological-behavioral models that incorporated frequency (tone frequency and frequency place of the cochlea), inner hair cell survival, synapse survival, outer hair cell survival, and behavioral performance (Δ MMR threshold, MMR amplitude, or SRM) were constructed using “stepwiselm” in MATLAB, which starts with a model that contains all independent variables, and systematically removes independent variables and interaction terms that do not add significant ($p < 0.05$) explanatory power to the model. In all cases the residuals (the error of the model) were compared against the fitted values of the model, and linear regression was only used if the residuals were randomly distributed. For the model using MMR amplitude, the residuals of the stepwise regression were not randomly distributed, and this motivated the use of quadratic terms to fit the data.

The histological-behavioral correlations reported in the permanent noise-induced hearing loss section are presented with the caveat that there was a range of delays (5-22 months) between noise exposure and euthanasia/subsequent histology; a necessary aspect of collecting large behavioral datasets. Despite this limitation, the present analysis contains strong histological correlates of behavior (see Results) that are likely *underestimated* due to the presence of this delay because of the likelihood of progressive deterioration following the behavioral data collection. Evidence is presented here of such deterioration and compared with previous corroborating findings. This suggests to the authors that the present results provide meaningful insight into the dependence of behavior on cochlear function.

4.3 Results

4.3.1 Psychometric measures of modulation masking release (MMR)

To provide complementary behavioral measures of temporal processing, two behavioral paradigms are discussed in this chapter. First, modulation masking release (MMR) is shown in normal-hearing male macaques. Figure 4.3A shows the psychometric functions that demonstrate MMR in normal-hearing macaque D detecting a tone (frequency = 1 kHz). When the masker was modulated at high frequencies (e.g. 150 Hz), the sigmoidal psychometric function had a threshold of about 53 dB SPL. This threshold was similar to that measured in unmodulated noise (triangles). However, when the masker was modulated at low frequencies (e.g., 10 Hz), the psychometric function was shifted to lower SPLs relative to the unmodulated masker (diamonds, Figure 4.3A), with a threshold close to 43 dB SPL, a masking release of 10 dB. MMR achieved at this SAM frequency ranged from ~10 – 20 dB across tone frequencies. This is consistent with previous reports from our group, albeit at lower masker SPLs (Dylla et al., 2013). An example of detection thresholds from Monkey D, detecting 1 kHz tones embedded in maskers of various masker modulation frequencies are plotted as a function of noise modulation frequency in Figure 4.3B. At this tone frequency and every other one tested, detection thresholds were a sigmoidal function of the noise modulation frequency. The thresholds were fit with a Weibull CDF (see Methods 2.6.2). The threshold parameter (α) of the Weibull function provides an estimate of the highest noise modulation frequency that showed reliable MMR. This point was taken to be the MMR threshold, which represents an estimate of the limit of temporal sensitivity. Figure 4.3C shows how MMR threshold varied with the tone frequency in seven normal-hearing (NH) macaques. At low tone frequencies (1 kHz), MMR threshold frequencies were low (mean=40.7 Hz, SD: 1.6); at intermediate frequencies (2.828 kHz), they were higher (mean=48.5 Hz, SD: 3.7), and at the highest frequencies tested (16 kHz), they had a higher mean than at the lowest frequency, but lower than the intermediate frequencies (42.9 Hz, SD: 4.03). The amplitude parameter (d) of the Weibull function was also taken into account, as it provided a measure of the magnitude of the MMR function between 10-150 Hz modulation frequency, and typically represented the maximum release from masking. Figure 4.3D shows each monkey's MMR amplitude across frequency, which provides an estimate of the magnitude of masking release

across modulation frequencies (see Methods). These values clustered around 12 dB (Mean: 12.85, SD: 2.3), consistent with previous data from this lab measured as threshold change (Dylla et al., 2013). Despite the differences in the SPL at which masking release was measured across the two studies, the results converge to suggest MMR is 10-15 dB in these conditions.

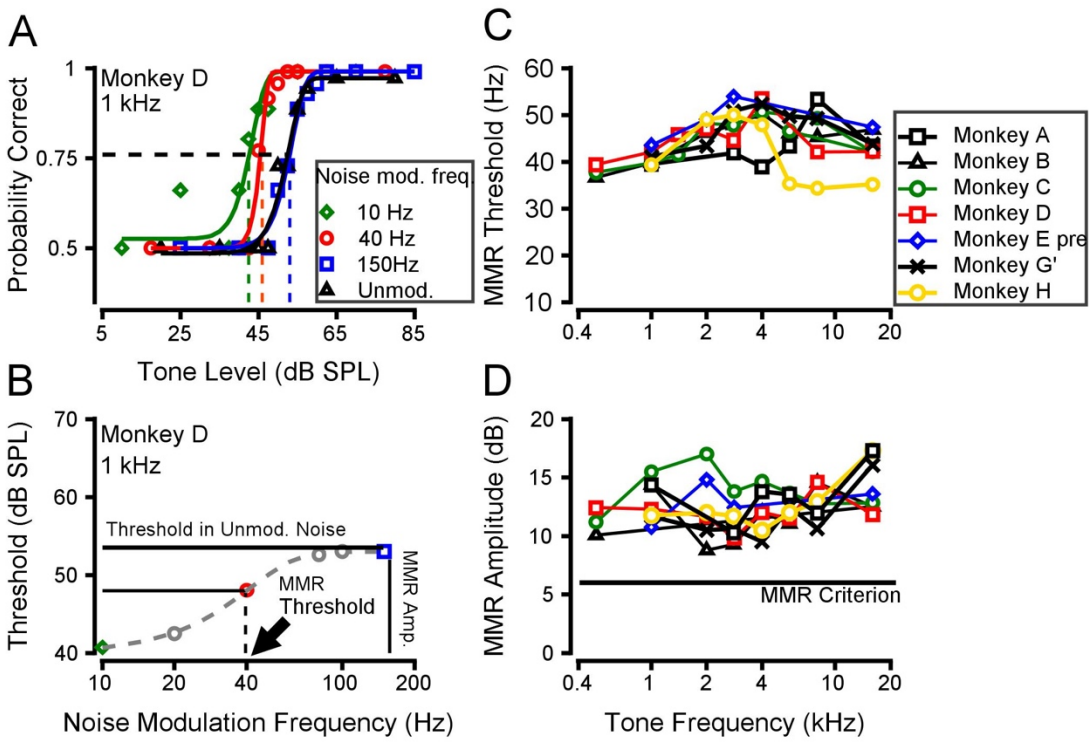

FIGURE 4.3 – Modulation masking release (MMR) in normal-hearing male macaques. A. Exemplar psychometric functions showing probability correct as a function of tone level for Monkey D, detecting 1 kHz tones embedded in noise that was unmodulated (triangles), or amplitude modulated at 10 (◇), 40 (○) or 150 Hz (□). B. An example of detection threshold (*pc*=0.76) as a function of noise modulation frequency, fit with a Weibull function to extract metrics of MMR: MMR threshold (arrow) and amplitude (solid vertical line). C. MMR thresholds of each monkey, at each tone frequency tested. D. MMR amplitudes for each monkey, at each tone frequency tested. *Monkey initials refer to Ar, Bi, Ch, De, Ec, Gan, and Ha.*

4.3.2 Psychometric measures of temporal discrimination

Psychometric measures of discrimination were attained through a Go/No-Go procedure (see Methods, Figure 4.2A). After learning to discriminate between noises with large differences in modulation frequency in their home cages (see Methods, Figure 4.2B), macaques were trained to discriminate AM frequency near discrimination threshold in a sound booth. Figure 4.4 shows psychometric functions (Figure 4.4A-4.3D) and reaction-time distributions (Figure 4.4E, F) from Monkeys Is and Monkey Da. Hit rate and false alarm rate were used to calculate a signal detection theoretic measure, Probability Correct (PC, see Methods). PC was used in favor of more typical measures such as *d'* to facilitate comparison to neurometric measures, consistent with previous studies from this group (Burton et al., 2018; Hauser et al., 2018; Mackey et al., 2022; Rocchi and Ramachandran, 2018, 2020). The psychometric functions and RT distributions in Figure 4.4E and F extend what is currently known about MF discrimination in animals, as previous studies have usually reported only thresholds attained through adaptive procedures. Figure 4.4 shows, for the first time, that response accuracy and speed change coincidently in this task, indicating that performance improved as the change in MF increased.

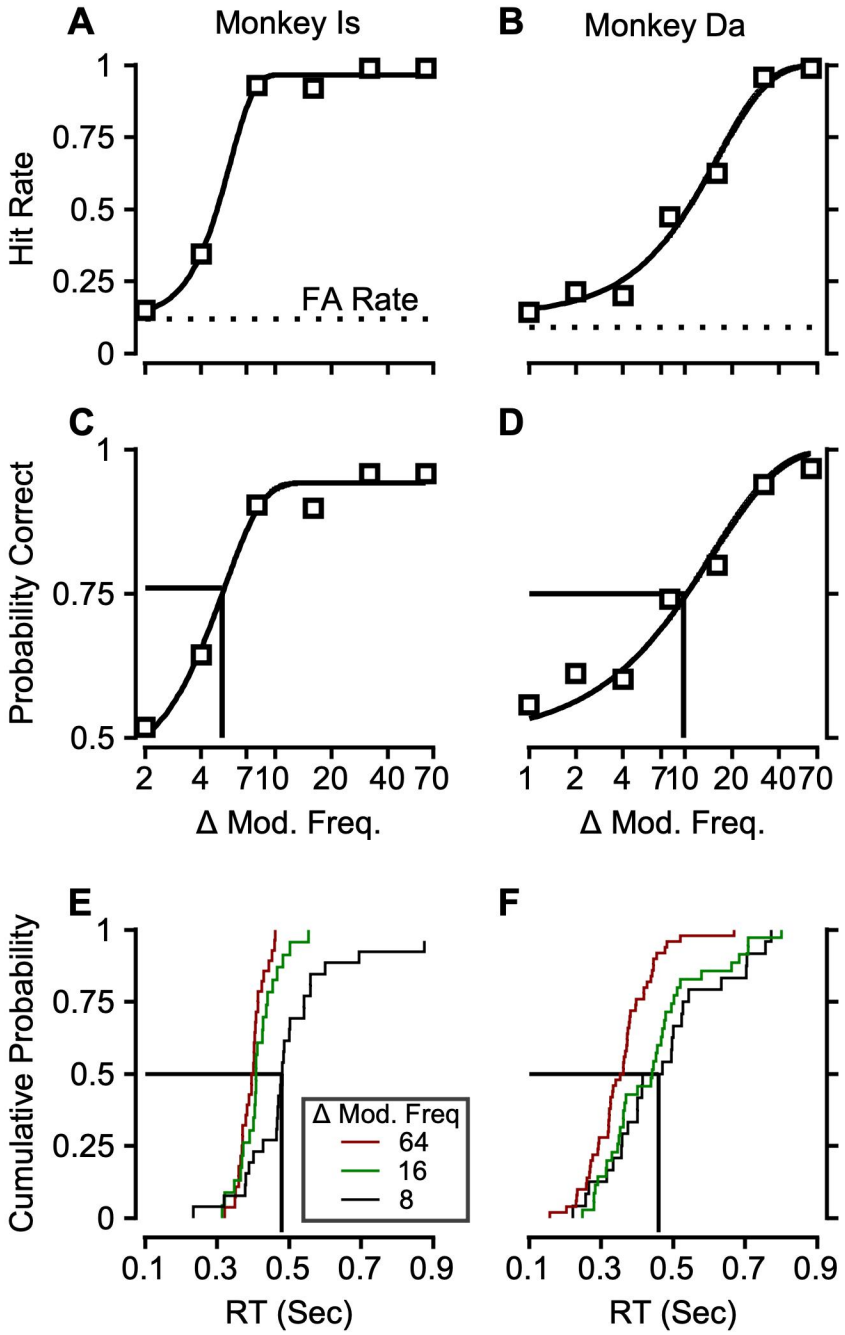
A
Monkey Is
B
Monkey Da
Hit Rate
1
0.75
0.5
0.25
0
FA Rate
C
D
Probability Correct
1
0.75
0.5
2 4 7 10 20 40 70
1 2 4 7 10 20 40 70
Δ Mod. Freq.
Δ Mod. Freq.
E
F
Cumulative Probability
1
0.75
0.5
0.25
0
Δ Mod. Freq
64
16
8
0.1 0.3 0.5 0.7 0.9
RT (Sec)
RT (Sec)

FIGURE 4.4 – Amplitude modulation frequency discrimination performance from the two monkeys. A. Hit rate and false alarm rate for monkey Is, plotted as a function of change in modulation frequency (MF) of a 20 Hz, broadband, amplitude modulated noise. **B.** Hit rate and false alarm rate for monkey Da. **C, D.** A signal detection theoretic measure of sensitivity (Probability Correct, see Methods) calculated from the hit rate and false alarm rate in **A** and B, plotted as a function of change in MF, for monkeys Is (**C**) and Da (**D**). Psychometric functions were fit with a Weibull cumulative distribution function (see Methods), and a conventional value of PC = 0.76 was used as threshold criterion. **E, F.** Reaction times plotted cumulatively at example modulation frequencies for monkeys Is (**E**) and Da (**F**).

The psychometric thresholds attained from monkeys Is and Da are nearly identical to previous reports in macaques (Moody, 1994). Moody (1994) also synthesized and reported data from other species. Figure 4.5 shows discrimination thresholds from those previous studies (black) compared with data in the present study (color).

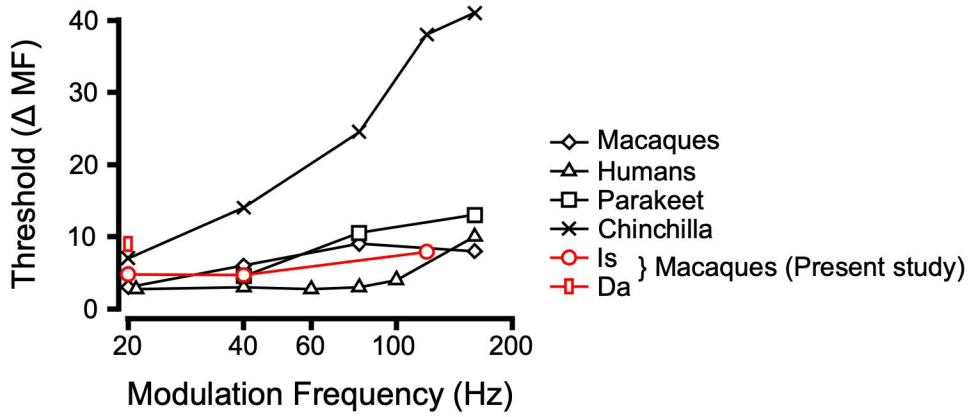

Figure 4.5 – Amplitude modulation frequency discrimination thresholds as a function of the standard frequency across species. Macaque discrimination thresholds from the present study are plotted along with data from a variety of species originally reported by Moody (1994). Monkey Is completed psychometric functions (from which thresholds were extracted) at 20, 40, and 120 Hz, while monkey Da only completed psychometric functions in the 20 Hz condition. Data from the present study are shown in red (circles for Monkey Is, rectangles for Monkey Da).

4.3.3 Neuronal measures of temporal discrimination

Modulation Transfer Functions in the Cochlear Nucleus (CN)

Initial characterization of how single neurons in the auditory pathway respond to temporal sound envelope fluctuations often takes the form of modulation transfer functions (MTFs). MTFs are displayed as changes in average firing rate, or spike-timing (measured using vector strength), as a function of modulation frequency (see Methods).

The present report documents the first MTFs in the subcortical auditory system of awake primates, from Monkeys C and D, (see Methods). Figure 4.6 shows example MTFs from the cochlear nucleus (CN). Figure 4.6 shows units that exhibited typical changes in vector strength as a function of MF, while Figure 4.7 shows units that exhibited changes in firing rate as a function of MF, which were encountered more frequently than expected. A limitation of this study is that only 35 neurons were recorded in the CN, which is a necessary caveat in interpreting the proportions of each form of MTF in the sample. However, the entire tonotopic axis was sampled, shown by the distribution of characteristic frequencies as an inset in the top panel of Figure 4.6 This sample contained mostly band-pass and band-reject temporal MTFs. Figure 4.6 contains the specific percentages of each temporal MTF form. Interestingly, we found many examples of rate-tuning to AM in the putative VCN (based on frequency response maps being exclusively Type I and III in our sample). Figure 4.7 shows examples of these rate MTFs.

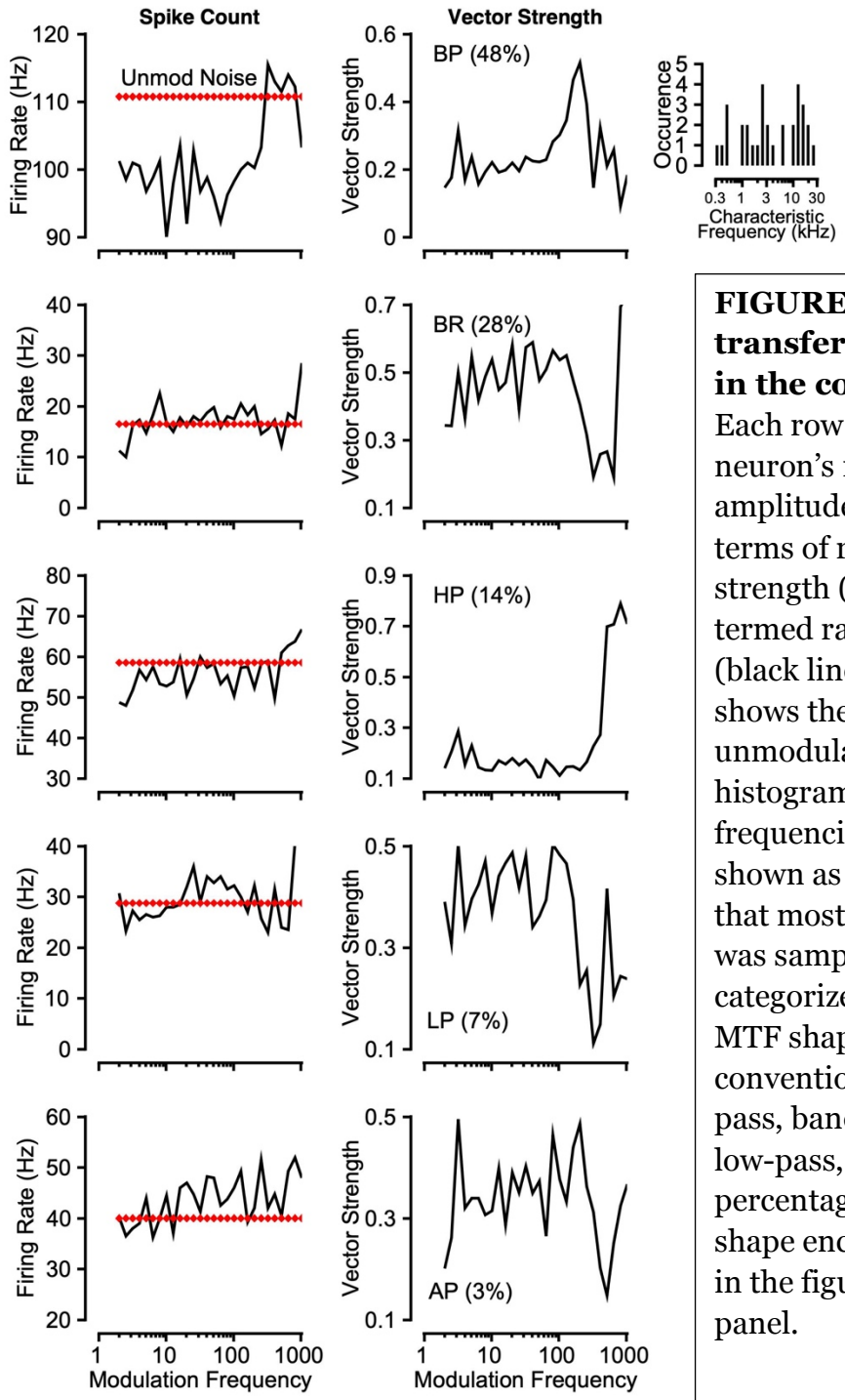

FIGURE 4.6 – Modulation transfer functions (MTF) in the cochlear nucleus. Each row shows an example neuron's responses to amplitude-modulated noise in terms of rate (left) and vector strength (right) which are termed rate and VS MTFs (black lines). Dotted red lines shows the rate response to unmodulated noise. A histogram of the characteristic frequencies encountered is shown as an inset as evidence that most of the tonotopic axis was sampled. Neurons were categorized based on their VS-MTF shape, and exhibited conventional shapes (Band-pass, band-reject, high-pass, low-pass, all-pass). The percentage of each VS-MTF shape encountered is displayed in the figure legend of each panel.

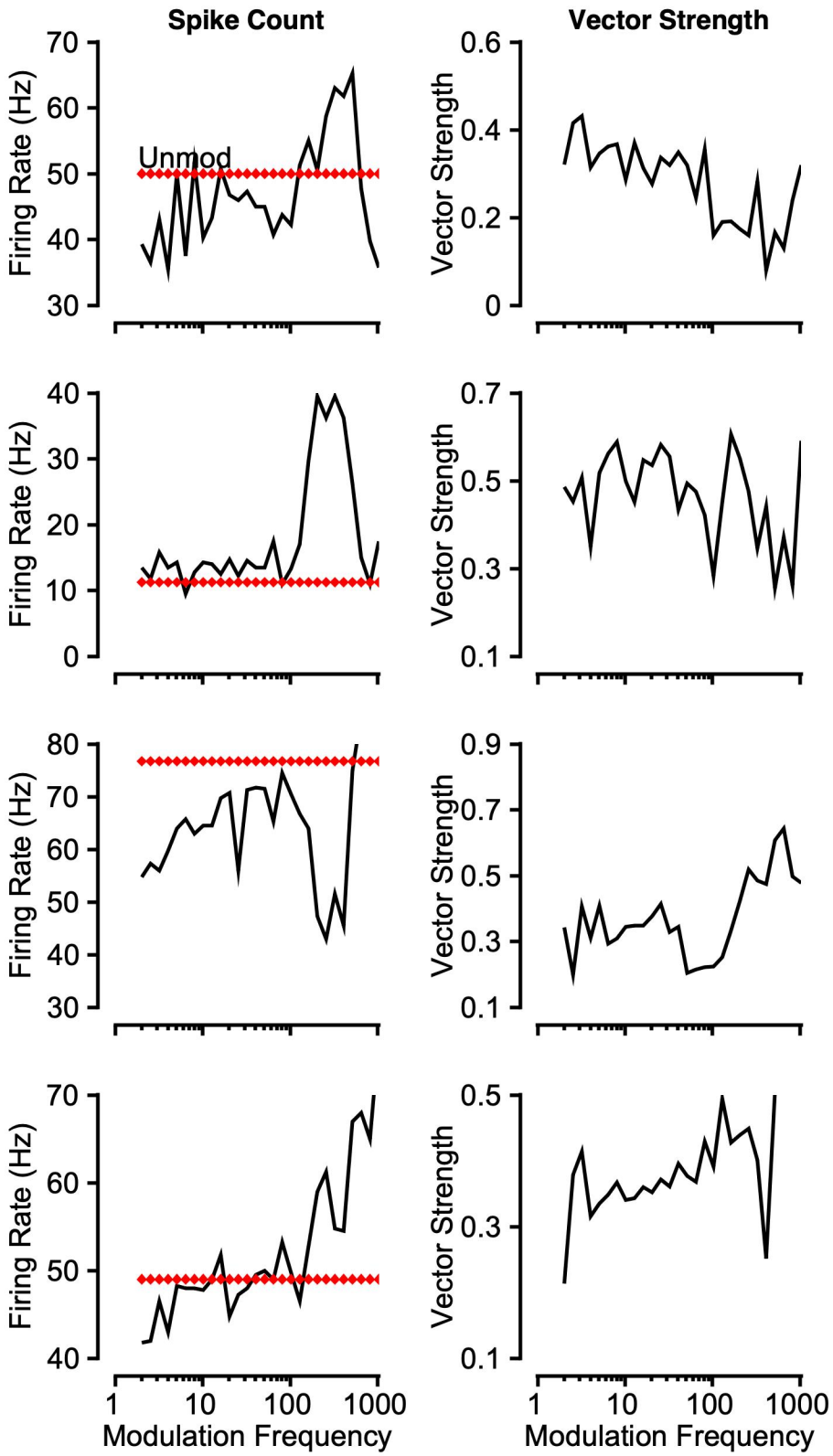

FIGURE 4.7 – Examples of rate tuning in the CN. Each row shows a rate MTF (left) and VS-based MTF of example neurons that exhibited rate-tuning in the VCN. Format is the same as in Figure 4.

Modulation Transfer Functions in the Inferior Colliculus (IC)

Example rate-based and spike-timing (vector strength) based MTFs from the IC are presented in Figure 4.8. Most neurons displayed both rate and VS tuning to MF, in contrast to the CN, where less rate-tuning was present. We observed mainly band-enhance/band-pass, high-pass, and band-suppress/band-reject response types, consistent with previous literature (Henry et al., 2016; Nelson and Carney, 2007). The entire tonotopic axis was sampled, as evidenced by the distribution of characteristic frequencies, shown as an inset in the top panel of Figure 4.8. As is commonly observed, VS tuning to AM was also observed, which facilitated neurometric discrimination analysis described in the following section.

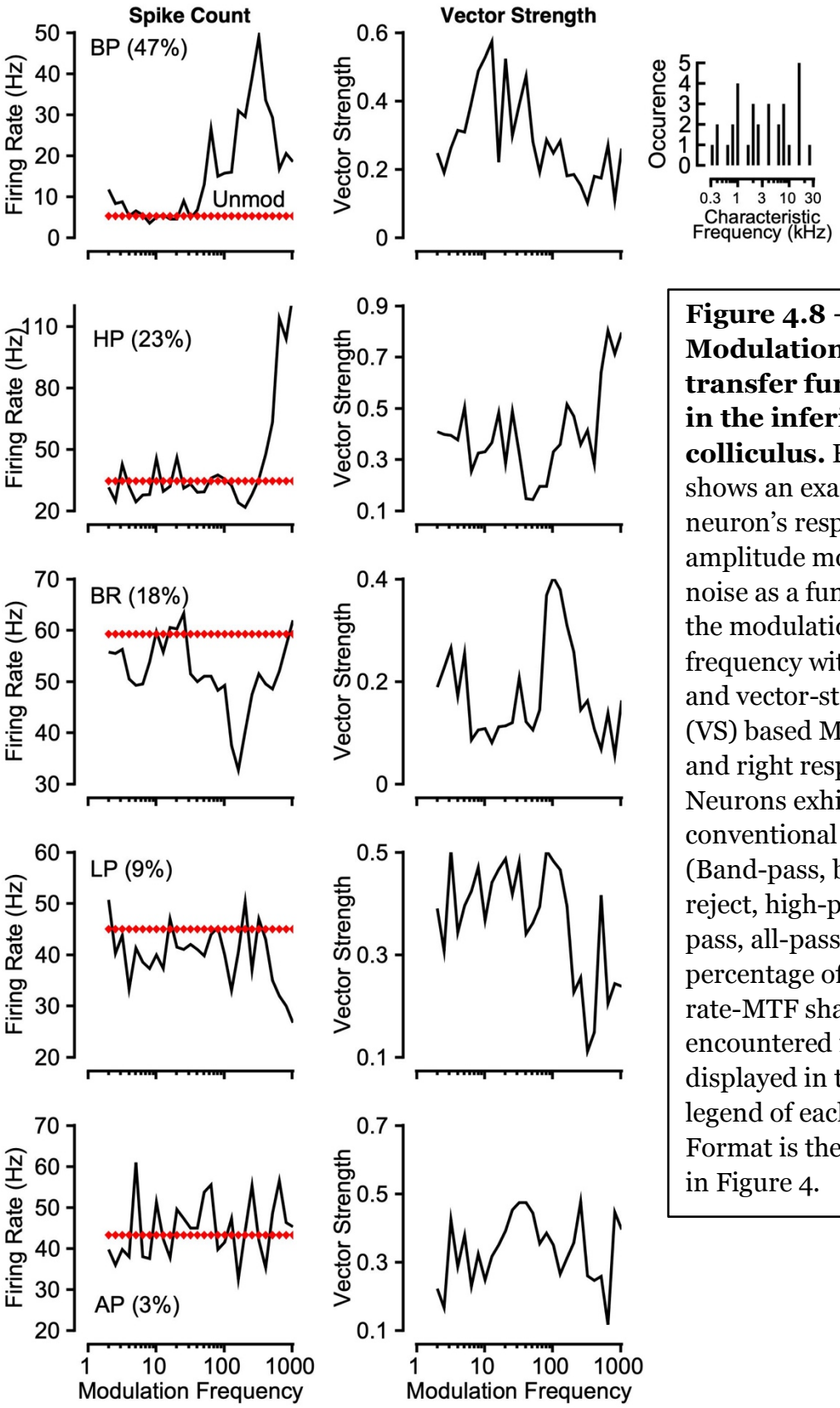

Figure 4.8 – Modulation transfer functions in the inferior colliculus. Each row shows an example neuron's responses to amplitude modulated noise as a function of the modulation frequency with rate and vector-strength (VS) based MTF on left and right respectively. Neurons exhibited conventional shapes (Band-pass, band-reject, high-pass, low-pass, all-pass). The percentage of each rate-MTF shape encountered is displayed in the figure legend of each panel. Format is the same as in Figure 4.

Neurometric measures of temporal discrimination based on single-unit activity

Rate and vector strength tuning to AM in the CN and IC permitted the derivation of neurometric measures of temporal discrimination, as previous studies have done as a function of modulation depth (Henry et al., 2016; Johnson et al., 2012; Sayles et al., 2013). Here this type of analysis is extended to modulation frequency discrimination. Figure 4.9 shows this analysis for an example neuron in the IC. From either the rate or temporal MTF (Figure 4.9A and B), ROC analysis could be conducted on the distribution of responses (see Methods). The area under the ROC curve is reported here as Neurometric Probability Correct (Figure 4.9A'). Neurometric threshold criterion is the conventional value of PC = 0.76 (Mackey et al., 2022; Rocchi and Ramachandran, 2018, 2020). Neurometric functions were fit with a Weibull curve (see Methods) to extract threshold. Figure 4.9A' and B' show the corresponding neurometric functions derived via ROC analysis (shown as inset) on the responses in Figure 4.9A and B. Figure 4.9C and D show neurometric discrimination thresholds extracted from single neurons near their best modulation frequency. Thresholds were plotted cumulatively, revealing that IC rate-based thresholds (green) are lower than CN (black) rate-based thresholds (Figure 4.9C; KS test, $p = 0.005$). Neurometric discrimination thresholds based on vector strength were also calculated in the same way. Discrimination based on classical vector strength is overestimated when spike counts are very low, which motivated Yin et al. (2011) to introduce a measure called phase-projected vector strength (VS_{pp}). We found no significant differences in VS- and VS_{pp}-based neurometric discrimination thresholds (two-sample K-S test, $p = 0.5$), likely due to the high spike counts typically observed in the subcortical auditory system (compare solid to dotted traces in Figure 4.9D). Both VS and VS_{pp} based neurometric thresholds were lower in the IC than the CN, indicating greater sensitivity in the IC (Figure 4.9D), similar to results from rate-based measures (Figure 4.9C). Neurometric sensitivity as assessed by rate or vector strength did not obviously differ by frequency response map type (data not shown). However, correlations between response types and neurometric sensitivity are better suited for larger sample sizes (e.g. Henry et al., 2016; Nelson and Carney, 2007).
It was a concern that differences in neurometric sensitivity were being conflated with differences in the range of modulation frequencies to which each neuron was tuned. To

address this, neurometric thresholds were normalized to the standard (comparison) stimulus frequency (Figure 4.9E and F). The IC still displayed lower rate-based thresholds than the CN after normalization, suggesting this effect was not frequency dependent. However, normalized VS-based thresholds in the CN and IC were nearly identical. To relate neurometric sensitivity to psychometric sensitivity, Figure 4.9 C-F shows monkeys Is and Da psychometric thresholds from the 20 Hz condition in all panels as grey lines. About 40% of IC neurons appear to match or exceed behavioral sensitivity (Figure 4.9A-B) regardless of which code (rate or VS) is used, while only the most sensitive CN neurons approximate behavioral thresholds. Monkey Is also completed the task in the 120 Hz condition, which is shown in grey in Figure 4.9 C and Figure 4.9D. Normalized neurometric thresholds are much higher than monkey Is' psychometric threshold in the 120 Hz condition (and previous macaque psychometric thresholds at high frequencies). This motivated further analysis of the effect of frequency in the next section.

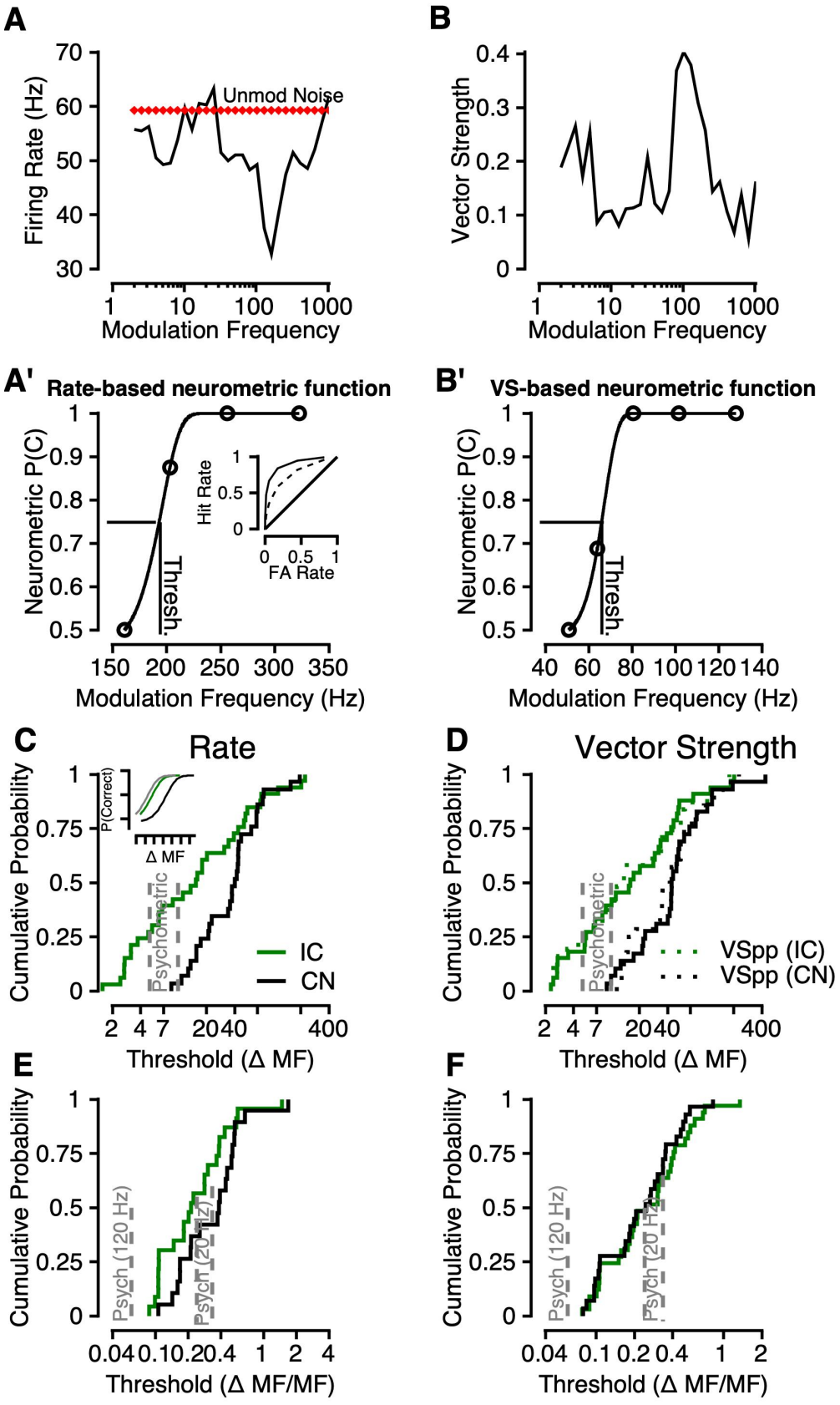
A
Firing Rate (Hz)
Unmod Noise
Modulation Frequency
B
Vector Strength
Modulation Frequency
A'
Rate-based neurometric function
Neurometric P(C)
Hit Rate
FA Rate
Thresh.
Modulation Frequency (Hz)
B'
VS-based neurometric function
Neurometric P(C)
Thresh.
Modulation Frequency (Hz)
C
Rate
Cumulative Probability
P(Correct)
Δ MF
Psychometric
IC
CN
Threshold (Δ MF)
D
Vector Strength
Cumulative Probability
Psychometric
VSpp (IC)
VSpp (CN)
Threshold (Δ MF)
E
Cumulative Probability
Psych (120 Hz)
Psych (20 Hz)
Threshold (Δ MF/MF)
F
Cumulative Probability
Psych (120 Hz)
Psych (20 Hz)
Threshold (Δ MF/MF)

FIGURE 4.9 – Temporal discrimination based on single-unit activity. A. An example band-reject/band-suppress rate-MTF from an IC neuron. **B.** An example VS-MTF from the same IC neuron as in **A. A'.** An example of a derived neurometric function via ROC analysis (see Methods) using the data in A. **B'.** An example of a neurometric function using the data in B. **C.** Firing rate based neurometric thresholds of all units in the sample, plotted cumulatively. IC thresholds are shown in green while CN thresholds are shown in black. **D.** VS and phase-projected VS (VS_{pp}) based neurometric thresholds plotted cumulatively in the same format as in C. **E.** Firing rate based neurometric thresholds of all units in the sample, plotted cumulatively and normalized to the standard/comparison modulation frequency used for discriminant analysis. **F.** VS based neurometric thresholds plotted cumulatively in the same format as in E. In all panels psychometric thresholds are plotted as grey lines.

Neurometric discrimination based on simulated population activity

Interpretation of single-unit data requires implicit assumptions about how population activity is read out. Previous studies have addressed this by pooling responses in various ways to make explicit how single-unit responses may be combined and related to psychometric measures. Johnson et al. (2012) described an "across-cell method," by which responses are sampled indiscriminately, with replacement, across the population (see Methods). This permitted the analyses in Figure 4.10A, which shows that as the number of units in the population increases, the median neurometric discrimination threshold of the population gradually approaches psychometric threshold (Δ5 Hz). While the IC (green squares) was initially more sensitive, CN (black circles) and IC sensitivity converged at 8 units. Once the population size reached 30, both the IC and CN exhibited the same threshold as derived from macaque behavior. This similarity between simulated population and behavioral sensitivity held true for 10-20 Hz, but not for higher frequencies (Figure 4.10B; macaque behavioral data from Moody (1994) and the present study; human data from Formby (1985)). However, by including only the few neurons tuned to the frequency of interest, simulated populations could exhibit the same sensitivity as behavior (Figure 4.10C). This necessity of a more complex form of decoding for higher frequencies has been found in a study of gerbil auditory cortex (Penikis, 2020).

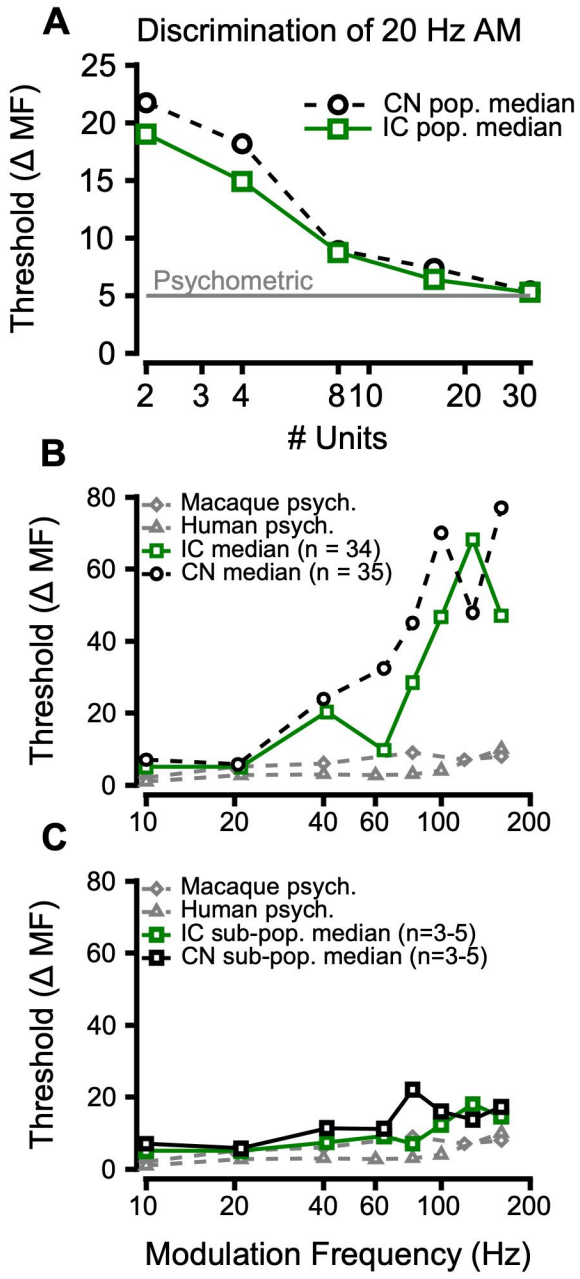

FIGURE 4.10 – Neurometric thresholds of simulated neuronal populations. A. Example trend of neurometric discrimination threshold of indiscriminately sampled populations of neurons (see Methods) as a function of how many neurons were in the population. CN data are shown in black, IC data are shown in green, and behavioral data are shown in grey. **B.** Neurometric discrimination thresholds of indiscriminately sampled neuronal populations in the IC (n = 34 neurons, green trace) and CN (n = 35 neurons, black trace) compared to behavior (grey traces) as a function of the MF of the standard/comparison stimulus. **C.** Neurometric thresholds of small populations (n = 3-5 neurons) compared to behavior. Colors match panel B.

4.3.4 Temporal integration of sound envelope

Neurophysiological studies of envelope processing often use stimuli with a constant duration (Henry et al., 2016; Johnson et al., 2012; Sayles et al., 2013; but see Yao et al., 2020). However, psychophysical studies have gained insight into auditory temporal integration by manipulating duration in AM processing tasks (Dau et al., 1997;

Lee, 1994; O'Connor et al., 2011; Sheft and Yost, 1990). This question is of particular importance in the context of macaque studies, as macaques and budgerigars may exhibit unique similarity to humans in temporal integration (Mackey et al., 2021a; and see Chapter 3). This motivated us to evaluate the effects of duration on performance in the AM frequency discrimination task previously discussed and explore its neural correlates. Figure 4.11 shows discrimination thresholds as a function of duration. As duration became shorter, macaques Is and Da exhibited changes in discrimination threshold consistent with temporal integration. Similarly, neurometric discrimination thresholds changed as the time-window used for spike-count analysis was changed (see Methods). The change in threshold as a function of duration is often quantified by the time constant (τ) of a three term exponential function (Mackey et al., 2021a; O'Connor et al., 1999), and is inversely related to the rate of integration. Thus, Figure 4.11 shows that CN neurons had, on average, slightly longer time constants than IC neurons, and neuronal time constants were longer than behavior. This suggests that behavioral measures of the temporal integration of AM may more closely resemble changes in higher brain structures (see Discussion). In the absence of data from such structures, some of which may serve as neural integrators of sensory evidence, we modeled the evidence accumulation process using a drift-diffusion model (DDM).

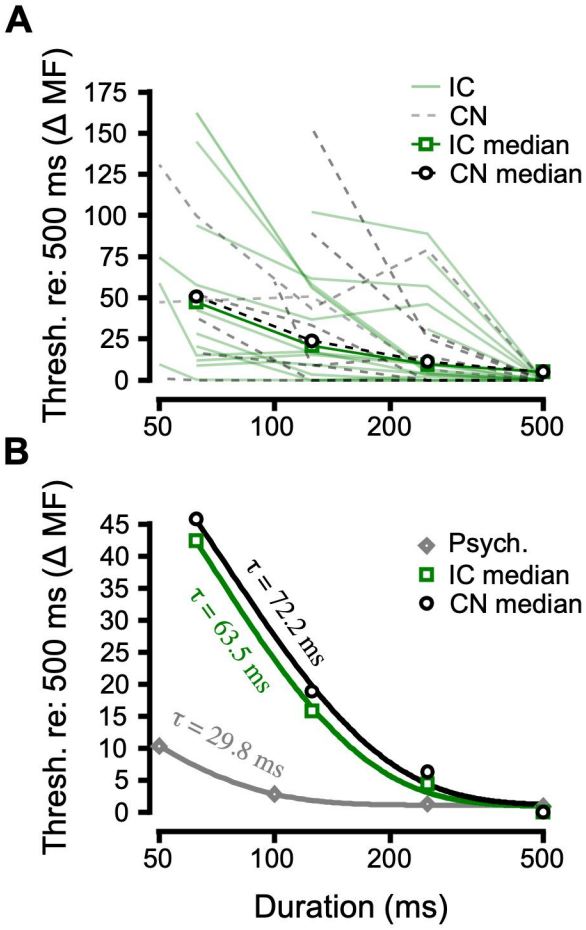

Figure 4.11 – Single neuron thresholds as a function of duration. A. All neurometric thresholds plotted as a function of stimulus duration (see Methods) for the IC (green) and CN (black dashes). Thresholds generally increased as duration decreased, as evidenced by the change in the median thresholds (green and black dashes with symbols). **B.** Median IC (green), CN (black), and mean psychometric (grey) thresholds plotted as a function of stimulus duration, and fit with three term exponential functions. The time constant (τ) of each exponential function is listed near each trace.

The DDM has been used to formalize assumptions about the evidence accumulation and decision-making process across many different psychological paradigms (de Gee et al., 2020; Liu et al., 2015; Murray et al., 2020; Ratcliff and Murdock, 1976; Ratcliff et al., 2018; Tsunada et al., 2015, 2019), and psychoacoustic studies have modeled AM perception at the computational level (e.g. Dau et al., 1997), but connections have not been made between AM perception and the DDM. In this study, having characterized temporal integration using signal detection theory at the sensory evidence level (the IC and CN) we then sought to computationally characterize neural integration of that sensory evidence using a DDM (see Methods, Figure 4.12). Drift rate was allowed to vary with noise modulation frequency and duration (Figure 4.12A and B), which lead to predicted changes in accuracy that resembled empirical psychometric functions (solid lines vs. dashed lines Figure 4.12 C and D). Predicted

discrimination thresholds and empirical discrimination thresholds (Hit Rate = 0.5) were nearly identical (Figure 4.12E and F). The goodness of fit was quantified with a posterior predictive check (see Methods) confirming that the 95% confidence intervals around the model estimates overlapped with the behavioral data. Monkeys Is and Da exhibited notable individual differences in performance that the model reproduced. The model also accounted for changes in speed (Figure 4.12G and H) as a function of duration. Combined with the single-unit analysis, these results provide an account of AM perception at the computational and neurophysiological levels and constrain future neurophysiological studies of how acoustic evidence is integrated (see Discussion).

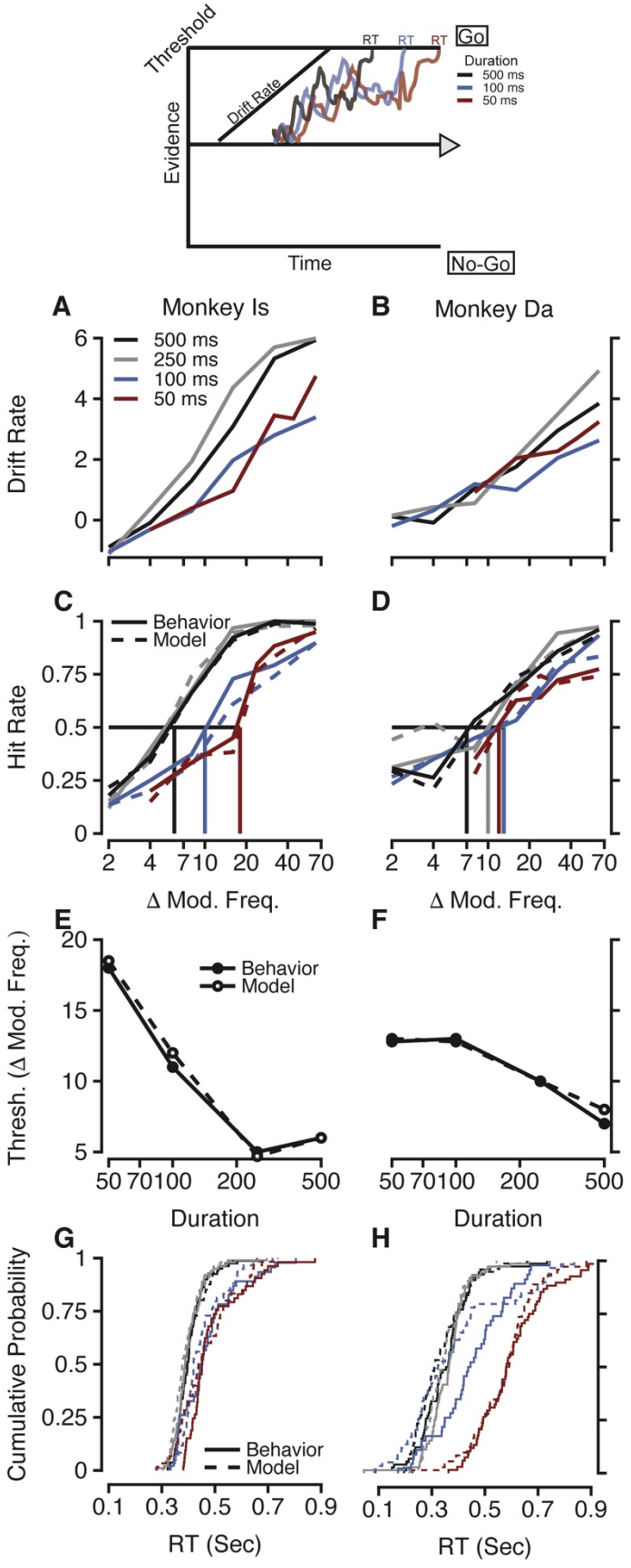

Figure 4.12– A hierarchical drift-diffusion model (DDM) of temporal discrimination performance. Top, an illustration of how manipulation of drift rate of a diffusion process can lead to predicted changes in reaction time in a Go/No-Go task. **A, B.** Drift rates for stimuli of different durations (shown as different colors), plotted as a function of modulation frequency, for monkeys Is (A) and Da (B). **C, D.** Empirical (solid) and simulated (dashed) psychometric functions produced by the DDM using drift rates shown in panels **A**, **B**. **E, F.** Empirical (solid) and simulated (dashed) discrimination thresholds functions produced by the DDM plotted as a function of duration using drift rates from panels **A**, **B**. **G, H.** Cumulative reaction time distributions from each monkey (solid) and from the DDM (dashed), with different durations represented by different colors, shown in panel A.

Interim summary: Having now characterized NHP AM processing at the behavioral, neurophysiological, and computational levels, we sought to understand how noise-induced hearing loss affects perception of AM in the MMR and AM discrimination tasks.

4.3.5 Effects of noise exposure on envelope processing

Noise exposure causing permanent threshold shift, hair cell, and synapse loss

The noise exposure (see General Methods) described below modeled permanent NIHL in that it caused permanent elevation of audiometric thresholds, and permanent cochlear damage measurable at the histological level (see Appendix). MMR was measured in these noise-exposed monkeys E, G, and L under the same conditions as normal-hearing monkeys. The results are shown in Figure 4.14. Figure 4.14A shows the detection performance of monkey L in the same format as Figure 1A. Note that the psychometric function showing detection of a 4 kHz tone in 150 Hz SAM noise (squares) overlapped with that obtained in 40 Hz modulated SAM noise (circles), and 10 Hz modulated noise (diamonds), which was very different from trends observed in NH animals (see Figure 4.3A). The lack of threshold change across masker modulation frequency, typically seen in controls (Figure 4.3), suggests a deficit in the ability to take advantage of the temporal cues afforded by amplitude modulation, even at slow temporal fluctuations.

The detection thresholds for monkey L as a function of modulation frequency for the 4 kHz tone are shown in Figure 4.14B. In contrast to the large (~10 dB) masking release shown in Figure 1B, there was little masking release, even through the noise did mask the tone. However, it was possible that there was not sufficient masking by the 30 dB SPL spectrum level masker (76 dB overall level), making the lack of MMR simply an issue of audibility. To rule this out as a potential explanation, we also tested monkey E's MMR in 40 dB spectrum level masker at 1, 2.828, 8, and 16 kHz. Exemplary data from the 2.828 and 4 kHz condition are shown in Figure 4.14B (red squares). Even though the 40 dB SPL spectrum level masker caused increased thresholds relative to the 30 dB SPL spectrum level masker (suggesting that the noise was indeed audible and effective as a masker), the thresholds in unmodulated noise were similar to the thresholds obtained in 10 Hz and 20 Hz modulated noise, suggesting that there indeed was no

MMR. In cases such as these, the MMR threshold frequency was taken to be 10 Hz, the lowest modulation frequency tested, and the MMR amplitude was 0 dB. For other tone frequencies (e.g. 1 kHz) the MMR thresholds were closer to those of NH macaques.

Figure 4.14C shows MMR thresholds as a function of the tone frequency for noise-exposed monkeys G (triangles), L (boxes), E (circles and x-hairs represent detection in 76 and 86 dB SPL maskers, respectively) and the control monkeys (diamonds). Note that MMR thresholds for the noise-exposed monkeys show a very different trend relative to controls. The MMR thresholds in the noise-exposed macaques were close to normal at frequencies outside the frequency range that showed large audiometric shifts, and decreased at frequencies near and above that of the noise exposure (2 kHz). The MMR thresholds were almost equal to that of the control group at 8 and 16 kHz for Monkey L, but remained at 10 Hz (indicating a lack of MMR) at all frequencies above 2 kHz for monkeys G and E. The differences in MMR threshold between NH and noise-exposed groups was significant, as indicated by linear mixed-effects model analysis ($t = -7.5$, $p = 3.3*10^{-10}$, $df = 59$).

MMR amplitude was drastically reduced in a frequency specific manner in the noise-exposed monkeys, as can be seen in Figure 4.14D. At certain frequencies (e.g. 1 kHz in all three monkeys) MMR amplitude was sufficient (> 6dB) to qualify as significant masking release (see Methods), but at most frequencies tested, MMR amplitude was zero. The differences in MMR amplitude between each control monkey and each noise-exposed monkey was significant, ($t = -4.19$, $p = 9.5*10^{-5}$, $df = 59$). However, the noise level (76 dB SPL) may have been so much higher than threshold in the normal hearing monkeys that the comparison between the two groups (NH and HL) did not account for the masker sensation level. A lower noise level for the control group could, theoretically, evoke less MMR, and reduce the contrast between the two groups. However, this is not the case. MMR with such a lower level masker (44 dB SPL) was published in Dylla et al., (2013) and the threshold shift values (typically the MMR amplitude) were similar to those reported here (10-15 dB). The average MMR from Dylla et al. (2013), measured as threshold shift, are shown inset, in grey, in Figure 4.14D, and as can be seen were not different from NH subjects, but very different from the HI animals.

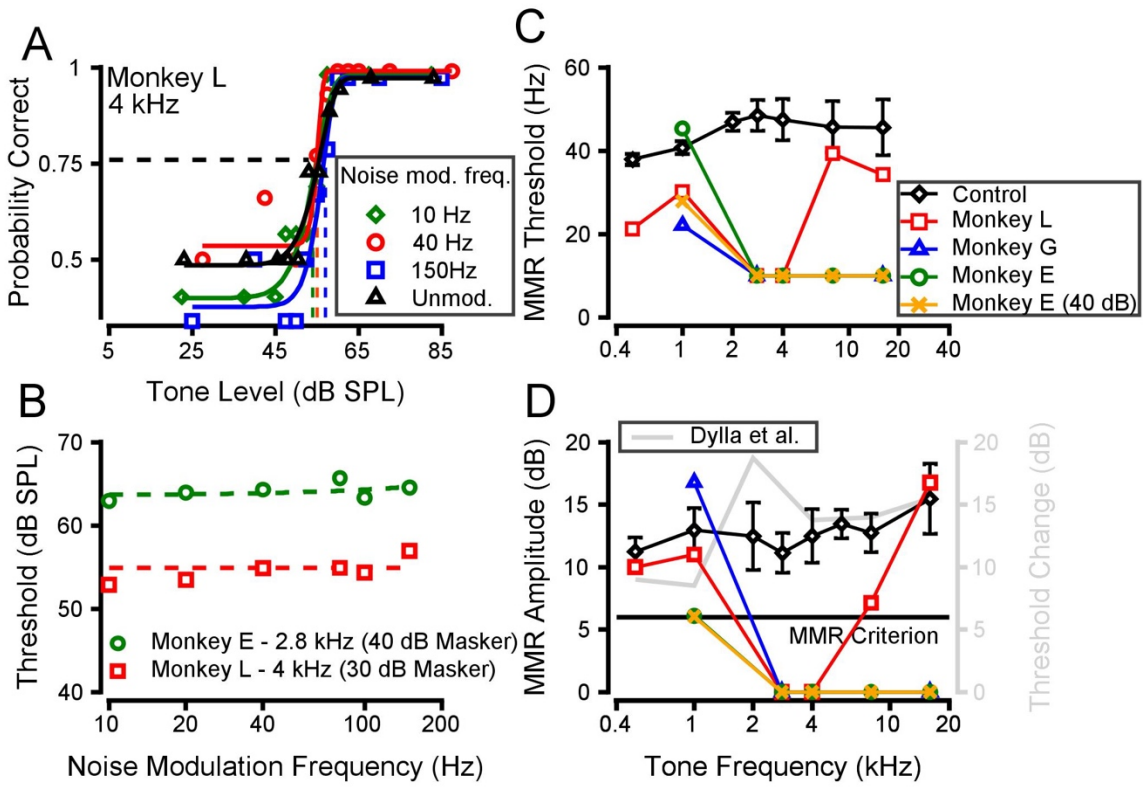

FIGURE 4.13 – MMR in noise-exposed macaques. A. Exemplar psychometric functions showing probability correct as a function of tone level for Monkey L, detecting 4 kHz tones embedded in noise, amplitude modulated at 10 (◇), 40 (○) or 150 Hz (□). B. Examples of the lack of MMR at any noise modulation frequency at frequencies showing pronounced cochlear damage in monkey E (○) and monkey L (□), where MMR threshold was taken to be 10 Hz, the lowest modulation frequency tested, and MMR amplitude was zero. C. MMR threshold in noise exposed macaques, compared to a group of non-noise-exposed monkeys (◇). D. MMR amplitude in noise-exposed macaques, compared to unexposed monkeys. MMR previously published in Dylla et al. (2013), estimated by threshold shift in 10 Hz AM noise relative to unmodulated noise shown inset, in grey. Conventions follow legend in part C. The format is similar to Figure 4.2. *Monkeys are Li, Gat, and Ec.*

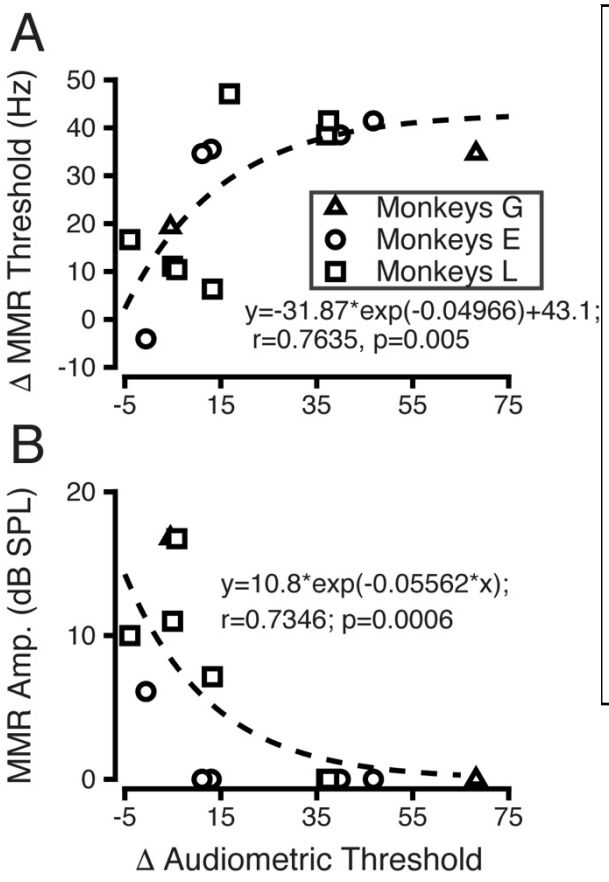

FIGURE 4.14 – Correlation of MMR with audiometric shift. A. Between group difference in MMR threshold as a function of change in audiometric threshold for the noise exposed monkeys G (△), E (○), and L (□). The dashed line represents the best fitting exponential function, with significance determined by non-linear regression. B. Modulation masking release amplitude as a function of audiometric shift. Symbols and lines follow the conventions in panel A. Symbols follow conventions in A. *Monkeys are Gat, Ec and Li.*

Correlation of MMR with audiometric shift

To examine the relationship between the audiometric consequences of noise exposure and the more complex consequences that may be related to hearing in noisy, realistic environments, correlations between MMR metrics with audiometric shift are shown in Figure 4.14. Monkeys L and E's MMR and SRM data were correlated with the initial audiometric shift, while Monkey G's data were correlated with the secondary audiometric shift (see section 3.3 for explanation). Since pre-exposure data was not available for all noise-exposed macaques, control MMR thresholds were averaged to provide normative values. The deficit (Δ MMR threshold) was calculated as the difference between these normative values and the MMR threshold for each noise-exposed monkey. Figure 6A shows that ΔMMR threshold increased exponentially with increases in audiometric threshold ($R = 0.7635$, $p = 0.005$). The second measure of

temporal processing used in this study, MMR amplitude also correlated with audiometric shift, decreasing exponentially as the audiometric shift increased (Figure 6B; non-linear regression, R = 0.7346, p = 0.0006). ΔMMR amplitude (the change in MMR amplitude, calculated as the difference between the mean amplitude of the control group and the MMR amplitude for each of the HI subjects) also correlated with audiometric shift (R = 0.76, p = 0.0095; not shown).

Correlation between MMR and sensory receptor survival in the cochlea

One goal of this project was to assess the relationship between temporal processing deficits and cochlear histopathology. The cochlear histology for the 141/146 dB SPL PTS noise exposure is shown in the Appendix. Δ MMR thresholds (Figure 4.15A) were lower where more OHCs survived and higher where fewer OHCs survived (Pearson's correlation coefficient, R = -0.6205, p=0.0179). Δ MMR threshold was also significantly correlated with survival of IHC synapses (Figure 4.15B, R = -0.295, p = 0.00013). MMR amplitudes (Figure 4.15C, D) were correlated with OHC survival (Figure 4.15C; non-linear regression, R = 0.601 p=0.00405) and with IHC synapse survival (Figure 4.15D; non-linear regression, R = 0.3937, p=0.0214). Δ MMR amplitude between groups also correlated with OHC loss and IHC synapse survival (OHC: non-linear regression, R = 0.489, p = 0.00039; SYN: R = 0.489, p = 0.00095). IHC survival did not correlate with Δ MMR threshold (R = 0.0498, p = 0.9), MMR amplitude (R = 0.0728, p = 0.057), or Δ MMR amplitude (R = 0.0507, p = 0.9).

Although the correlations with MMR suggest a relationship between temporal processing and loss of OHCs and IHC synapses, these histopathological metrics are also correlated with themselves. To address this, a mixed effects model was constructed with frequency, IHC, OHC, and synapse survival (SYN) as predictor variables, and each behavioral measure (ΔMMR threshold, MMR amplitude) as the dependent variable. In a stepwise fashion, interactions that were not statistically significant were removed until only significant ones remained (See Methods section 2.6.5). For Δ MMR threshold, the final model contained only OHC and IHC survival: Δ MMR threshold ~ IHC + OHC (R = 0.7893, p = 0.005), but this model's BIC value was higher than the simple linear regression against OHC loss shown in Figure 4.15A (109.48 vs. 106.01). The final model for MMR amplitude included quadratic terms (see Methods 2.6.5), interactions between

frequency and synapse survival, IHC and OHC survival, OHC and synapse survival, and main effects of IHC and synapse survival: MMR amplitude ~ 1 + Freq*IHC + Freq*SYN + OHC*IHC + OHC*SYN + $Freq^2$ + IHC^2 + SYN^2 (R = 0.999, p = 0.0006). This model had a much lower BIC value (-4.23) than the exponential models in Figure 4.15C and 8D.

The histopathological metrics above are all means from the two ears of each monkey. Although there were principled reasons for this binaural averaging (Heil, 2014), it was also of interest to see whether the behavioral results were driven by the better or the worse ear. Thus, for each analysis in Figures 8 and 9, we evaluated two models: one for the lower survival at each frequency in each animal, and a separate model for the better survival. We found no significant correlations between behavioral measures and unilateral histological damage, except for Δ MMR threshold, which correlated with OHC survival in the worse ear (linear regression; R = -0.56, p = 0.043), a notably weaker relationship than with average OHC survival across the two ears (R = -0.6205, p = 0.0179).

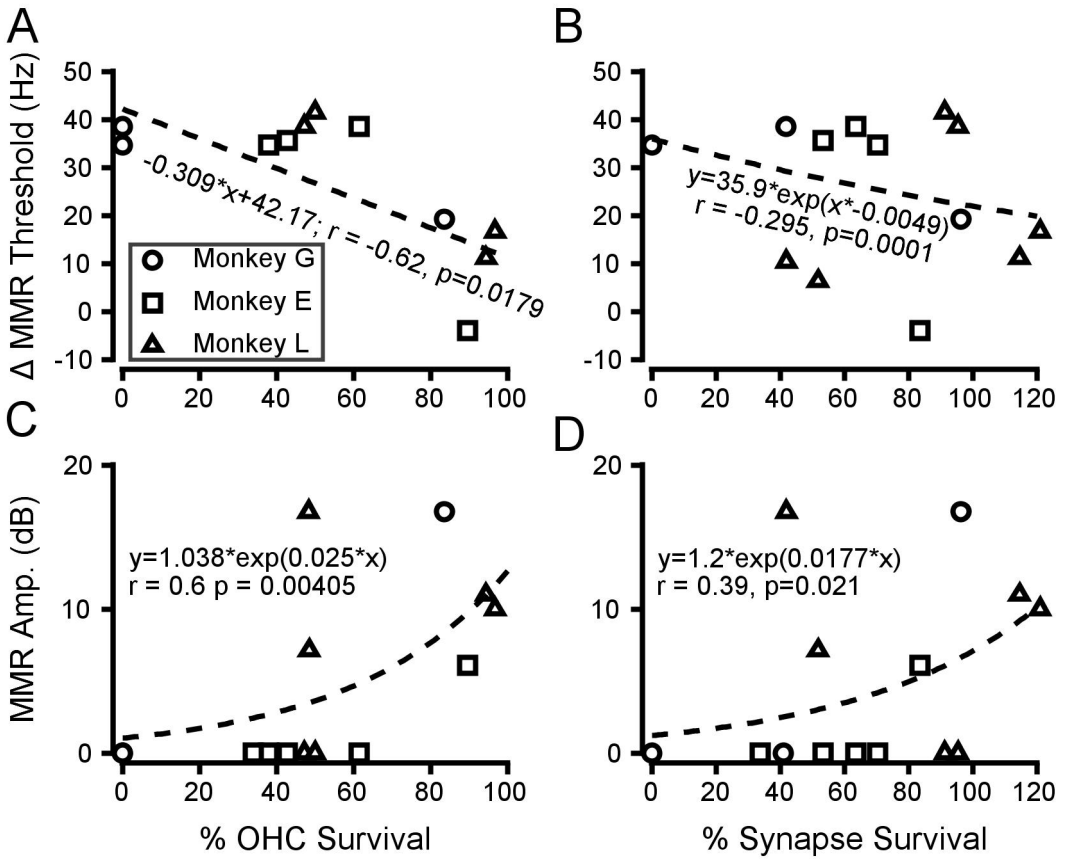

FIGURE 4.15 – Correlation of modulation masking release with histological changes. (Color available online). A. Between group differences in MMR threshold as a function of outer hair cell survival. B. Between group differences in MMR threshold as a function of ribbons synapse survival. C. MMR amplitude as a function of OHC survival. D. MMR amplitude as a function of ribbon synapse survival. The dashed lines represent the best fitting line as assessed by linear or non-linear regression. The percentage survival exceeded 100 in some cases due to variability in the mean numbers of ribbon synapses per inner hair cell in control animals. *Monkeys are Gat, Ec, and Li.*

Noise exposure causing temporary threshold shift, synaptic loss and dysfunction

Having established that MMR is compromised by the PTS-causing noise exposure, it was then of interest to assess the effects of synaptopathy on MMR. The 120 dB SPL noise exposure described in General Methods was designed to do this. This exposure modeled hidden hearing loss in that audiometric threshold (i.e. detection of 200 ms tones) was elevated for only a few days post noise exposure (i.e. a temporary threshold shift, in contrast to the PTS noise exposure; see Appendix) and was designed to cause inner hair cell cochlear synaptopathy. However, thus far in the histological analysis it appears that the synapse loss is present at 2 months post exposure but recovers by 10 months post exposure; however, an increase in synapse volume is sustained at least to 10 months post exposure, at the 2kHz and 5.6kHz places in the cochlea (see Appendix). It was hypothesized that insofar as this noise exposure causes synaptic dysfunction it should cause deficits in MMR, due to the correlation with synapse loss observed in the PTS monkeys, and based on neurophysiological, behavioral, and modeling studies (see General Introduction). Figure 4.16 shows examples of how modulation masking release was reduced following noise exposure.

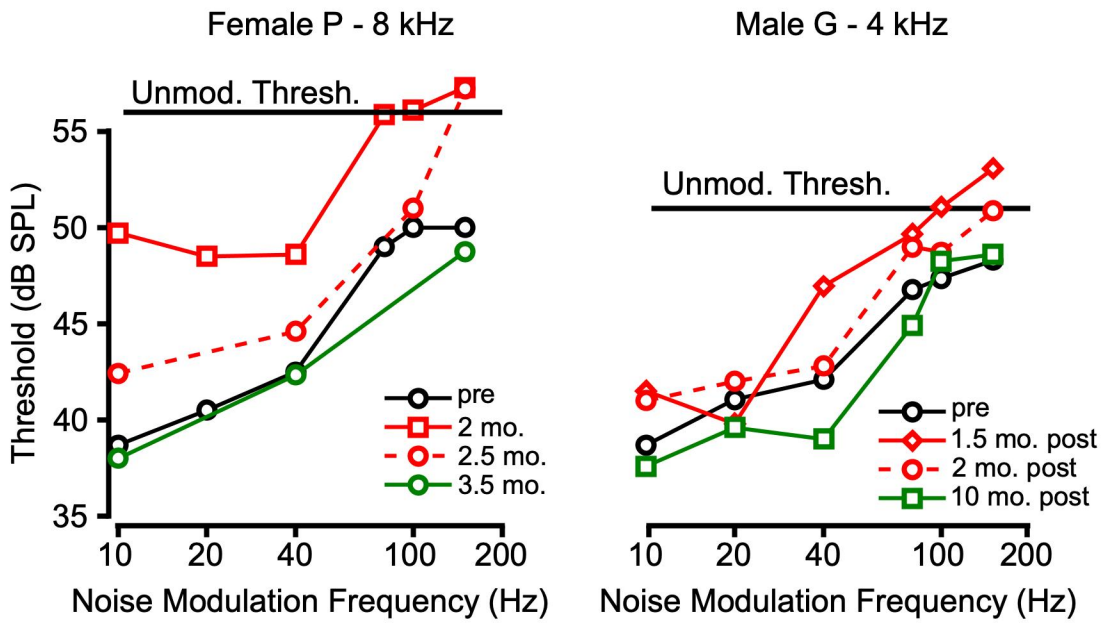

Figure 4.16. Examples of modulation masking release before and after noise exposure causing transient synaptopathy. **Left**, 8 kHz tone detection thresholds as a function of noise modulation frequency for monkey Pi. Only a few select time-points post noise exposure are shown, for visibility. Time-points exhibiting threshold shifts greater than 6 dB are shown in red, while thresholds from later time points, where shifts were less than 6 dB, are shown in green. **Right**, same as left panel, except showing 4 kHz data from Monkey Gan. Detection threshold in unmodulated noise is shown as a black line.

Notably, at baseline, female monkeys exhibited larger masking release in the 150 Hz condition than male monkeys, who often exhibited little to no release (Figure 4.16). Figure 4.16's left panel shows example data from female monkey P, who exhibited large threshold shifts after noise exposure across different modulation frequencies at 2 and 2.5 months post noise exposure. Similarly, on the right, male monkey G exhibited threshold shifts at similar time-points (1.5-2 months). These transient deficits were consistent across five out of seven monkeys (three male, two female) in the joint male/female cohort, as can be seen in Figure 4.17. The top panel of Figure 4.17 shows threshold in a select condition (usually the 40 Hz noise condition) across time relative to noise exposure, and the bottom panel shows threshold change (relative to pre-exposure) across time. Most monkeys exhibited threshold changes greater than 6dB that relaxed to pre-exposure values by 3 months post exposure. The effect of time post noise exposure

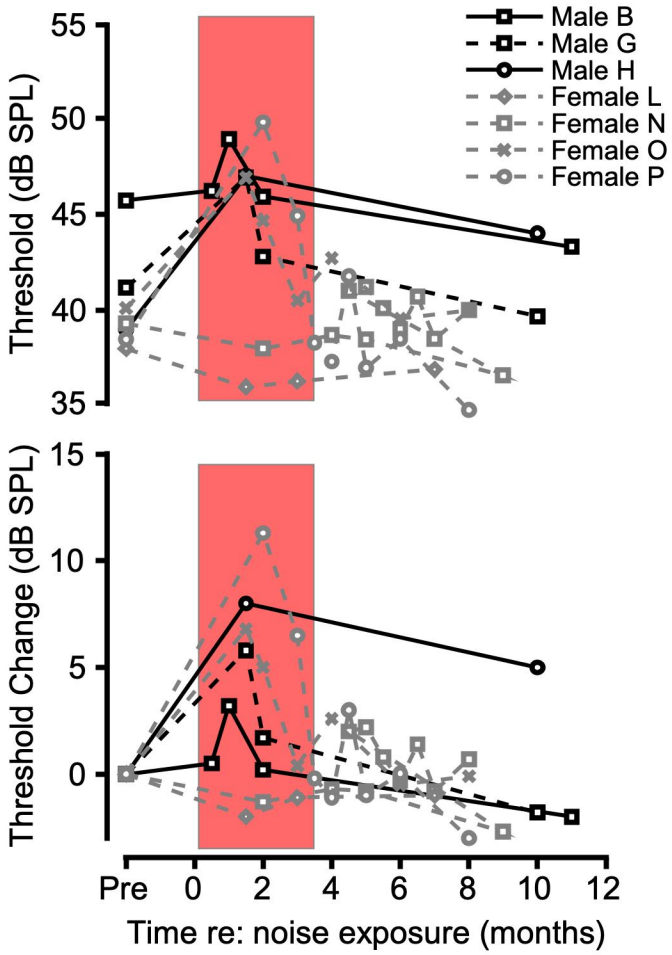

Figure 4.17. Change in modulation masking release over time following noise exposure causing transient synaptopathy. **Top,** detection threshold in a select condition as a function of time post noise exposure for all monkeys. Male monkeys are shown in black, female monkeys in grey. Putative period of synapse loss is shown as a red rectangle, spanning the 0-3 month period post noise exposure. **Bottom,** Threshold (normalized to pre-exposure values) as a function of time. *Monkeys are Bi, Gan, Ha, Lu, Ne, Op, and Pi.*

on threshold change (Figure 4.17) was significant in a mixed effects model that took the form *Threshold Change ~ Sex + Time^2 + (1|Monkey)*. This model was selected based on goodness of fit (Bayesian Information Criterion) compared to models with all other possible combinations of independent variables (e.g. models with sex by time interactions, which were not significant), and models with a linear effect of time (which, qualitatively, were not plausible as indicated by the nonlinearity in Figure 4.17). The effect of time (*t =-2.5, df = 40, p = 0.01)* indicates a transient deficit in temporal processing as measured by MMR. This transient deficit followed the time-course of the transient cochlear synaptopathy (this analysis is preliminary, see Appendix), shown as a red rectangle in figure 4.17.

Effect of noise exposure causing synaptic loss and dysfunction on temporal discrimination

Having established that MMR is sensitive to both noise exposures, we hypothesized that sound envelope processing as measured by temporal discrimination (as opposed to detection) would exhibit larger, sustained (as opposed to temporary) deficits due to the different informational demands posed by discrimination paradigms (Lentz and Valentine, 2015; Moody, 1994; Wakefield and Viemeister, 1990). However, this was not the case in our admittedly small sample size (Monkeys Is and Da). Figure 4.18 shows example psychometric functions from Monkey Is in several conditions hypothesized to substantially task the auditory system's temporal precision. Noise bandwidth was manipulated to target places along the cochlear length exhibiting synaptic enlargement/dysfunction: broadband (BBN) vs. third-octave narrowband noise around 4 kHz (NBN); noise duration was manipulated: 500 ms vs. 50 ms; and finally, noise modulation frequency was manipulated: 20 Hz vs. 120 Hz. It was hypothesized that short duration, narrowband, high MF signals would task the auditory system the most. However, as can be seen, the only changes that occurred were those indicating improved performance as assessed by threshold, psychometric function slope, and reaction times (not shown). Figure 4.19 shows Monkey Is and Da discrimination thresholds over time relative to noise exposure, indicating that these effects were relatively stable over time, with the only notable change being that Monkey Is improved.

Explanations for this lack of effect despite the substantial literature predicting it will be addressed in the discussion section.

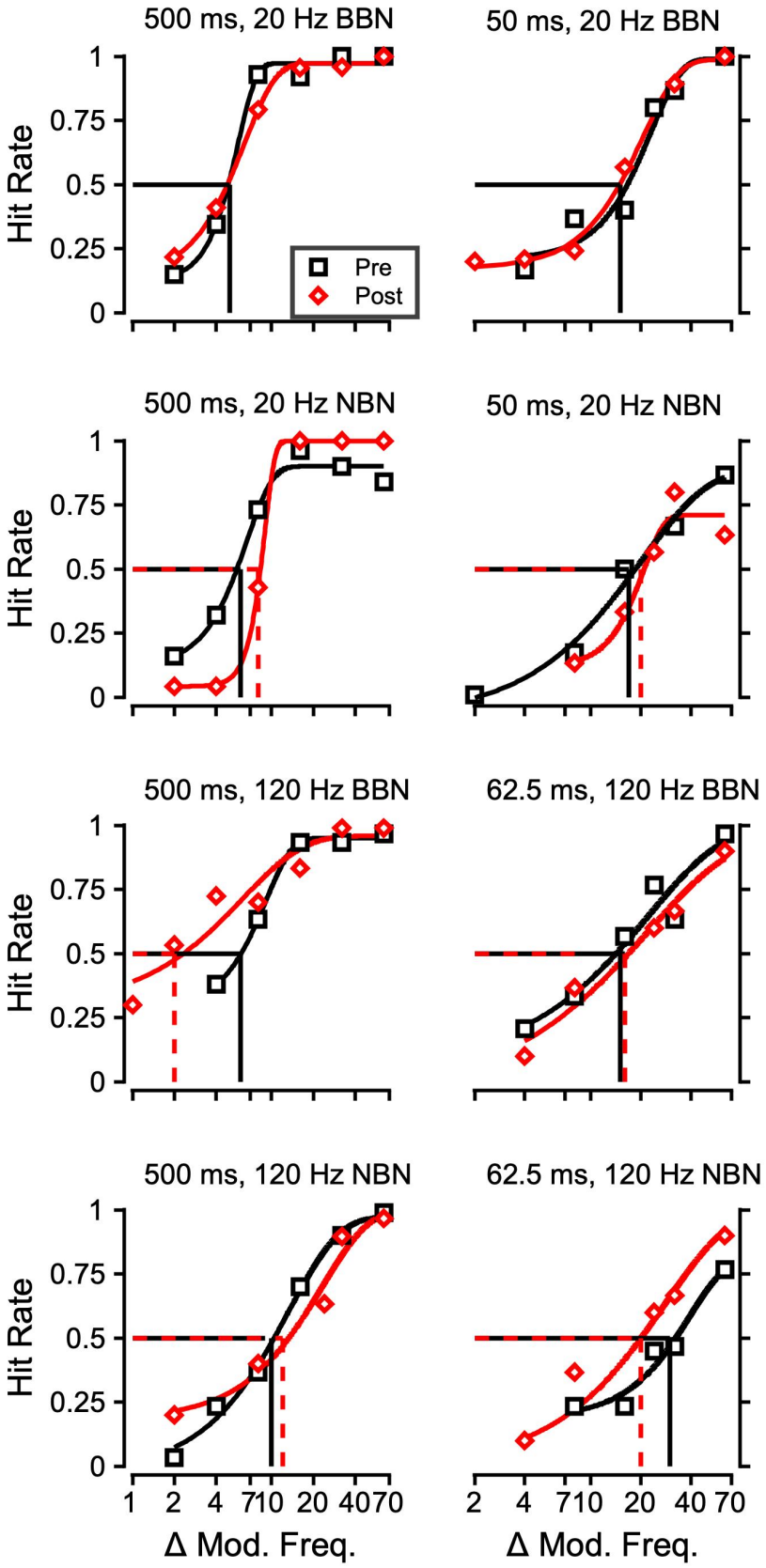
500 ms, 20 Hz BBN
50 ms, 20 Hz BBN
500 ms, 20 Hz NBN
50 ms, 20 Hz NBN
500 ms, 120 Hz BBN
62.5 ms, 120 Hz BBN
500 ms, 120 Hz NBN
62.5 ms, 120 Hz NBN
Hit Rate
1
0.75
0.5
0.25
0
Pre
Post
1 2 4 710 20 4070
2 4 710 20 40 70
Δ Mod. Freq.

Figure 4.18. Psychometric functions from Monkey Is before (black squares) and after (red diamonds) noise exposure causing synaptic loss and dysfunction. Noise stimulus characteristics are written above each panel. Noise could be broadband (BBN), third-octave narrowband (NBN) around 4 kHz, and long (500ms) or short (50 ms) in duration.

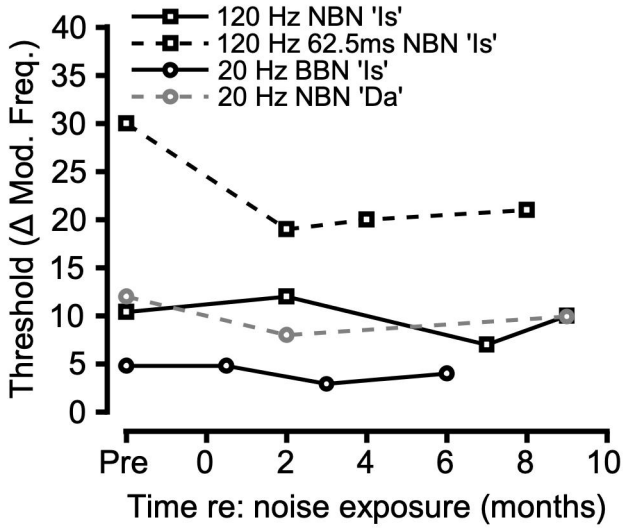

Figure 4.19. Temporal discrimination thresholds vs. time following noise exposure causing synaptic loss and dysfunction.

4.3.6 Discussion

These results suggest subcortical spiking activity and a temporal integration model can account for sound envelope discrimination performance and suggest a new potential behavioral correlate of cochlear synaptic dysfunction. The implications of these findings for specific ideas in the literature are detailed below.

The neural basis of sound envelope processing

The single-unit results confirm that there is an increased prevalence of rate-coding of AM as the primate auditory neuraxis is ascended, which may support sound envelope processing. However, a few of the results may indicate need for reconsideration of the existing literature on how the primate auditory system processes AM. This partially stems from the fact that, to the authors' knowledge, there is only a single study on how the neurons in the primate CN encode AM, and no such studies of the primate IC. The CN study used an anesthetized preparation, and found that there was no rate encoding of AM (e.g. all-pass rate MTFs) in the cochlear nucleus (CN) of multiple primate species (Rhode et al., 2010). This differs from the present results, where rate-tuning was encountered despite the small sample size. The simplest explanation for this difference seems to be the use of anesthesia, which is known to impact sound encoding (Noda and Takahashi, 2015; Ramachandran et al., 1999; Schumacher et al., 2011). However, rate-tuned CN neurons have been found in other species, even under anesthesia; these neurons generally display onset-chopper PSTHs in non-primate species (Joris et al., 2004). In our admittedly small sample, we did not encounter onset-choppers, despite encountering rate-tuning. It seems unlikely that this is sampling bias, as few onset-choppers were found in a larger sample (92 neurons) from this lab (Mackey et al., 2022; Ramachandran, 2018). This difference could be due to the use of an awake experimental preparation, the fact that the macaques had experience in AM processing tasks, or a unique aspect of primate CN neurophysiology. The last conclusion is supported by anatomical studies of primate CN anatomy (Adams, 1986; Kavanagh Moore, 1980b; Moore et al., 1996; but see Rubio et al., 2008).
The CN results presented here also differ with respect to how they relate to perception. The finding that average cochlear nucleus (CN) neuronal spike-timing is not as sensitive as behavior (see Results), contrasts a previous study in anesthetized chinchilla CN--the

only study where comparable neurometric analyses were done using CN data (Sayles et al., 2013). Sayles et al. found that CN spike-timing, on average, was as sensitive as chinchilla behavior, and they thoroughly addressed necessary methodological caveats in their discussion (e.g., anesthesia). It's possible that the use of anesthesia is responsible for the differences between their data and the present data. This difference could also represent a species difference, as chinchillas and primates display perceptual differences in temporal discrimination (See Figure 4.4; Moody, 1994).

Many studies have addressed questions about what neural code in the IC supports envelope processing (Henry et al., 2016, 2017; Lorenzi et al., 1995; Nelson and Carney, 2004, 2007). Two studies that are very comparable to the present results have suggested rate responses, even optimally pooled across a large sample, are insufficient to explain AM detection and depth discrimination performance (Henry et al., 2016; Nelson and Carney, 2007). Given this, it is surprising to consider that both spike rate and timing measures in the IC provided a close match to macaque and human AM discrimination performance in the present analysis. Similar hierarchies in temporal encoding have been found in a study of IC, medial geniculate body, and primary auditory cortex (Asokan et al., 2021), which characterized how progressively longer timescales are encoded in these regions. These results here are consistent with such a hierarchy, and build on our previous finding that IC responses provide more reliable estimates of psychometric threshold and slope, compared to CN responses, and that IC neurons exhibit significant choice-probabilities (Mackey et al., 2022). This neurometric-psychometric correlation supports the notion that the greater prevalence of band-enhanced and band-suppressed rate profiles in the midbrain may have significance for perception that was previously unclear due to the greater sensitivity of spike-timing found in Henry et al. (2016) and Nelson and Carney (2007). This conclusion is consistent with previous IC model comparisons to human AM detection (Lorenzi et al., 1995).

The results presented here are also interesting in the context of previous AM studies in macaques, which have exclusively focused on the cortex. A previous study in A1 found that single neuron rate or timing, on average, were less sensitive than macaque AM detection behavior; consistent with the lower-envelope principle (Johnson et al., 2012). This is surprising given that the present results suggest nearly half the single

neuron sample recorded in the IC matched behavior in rate and vector strength. The finding that average single neuron sensitivity could not explain behavior, led Johnson et al. to pool responses in the same way as the present study. Their analysis suggested 25 neurons' rate responses were sufficient to account for behavior. This was the case particularly for low modulation frequencies (10-20 Hz) where vector strength (single neurons or pooled responses) was insufficient to explain AM detection. Sensory evidence necessary for the *discrimination* (as opposed to detection) of such low ("flutter") frequencies has been suggested to reside in A1 in the form of a rate code (based on macaque data: Lemus et al., 2009b). However, the results presented here suggest a substantial degree of perceptual AM sensitivity could be inherited from subcortical stations in the form of a rate or spike-timing code.

These differences from previous CN and IC studies must be taken with a caveat: the onset response has been excluded in many previous studies (Beitel et al., 2003; Henry et al., 2016; Johnson et al., 2012; Sayles et al., 2013), though, interestingly, Johnson et al. (2012) report that "including the onset response did not substantially alter the results." Some more recent studies of primate auditory cortex have included the onset response, which facilitates comparison to the current results. These studies also used a modulation frequency decoding framework, further aiding comparison to the present results (Downer et al., 2021; Hoglen et al., 2018). Hoglen et al. (2018) report that decoding of modulation frequency exhibited similar patterns across 0-750 ms and 250-1000 ms time-windows, which may indicate that the onset response does not alter results in the present report, and is consistent with the remarks in Johnson et al. (2012). In this report, the onset response was included to facilitate comparison with these previous publications and with the behavioral experiments, where presumably the macaques may use the onset response. This also enabled us to make comparisons to experiments where the duration of the stimulus was reduced to 50 ms, where presumably only some form of onset response is available. Psychometric thresholds at short durations were substantially lower than most neurometric thresholds, suggesting that macaques can use information present in the onset response. The present results are not the first to suggest this, as a previous study provides strong evidence that the onset response in the IC is of great utility for localization performance in reverberant environments (Devore et al., 2009).

The effects of duration in this study extend work on auditory temporal integration to an AM discrimination paradigm, as opposed to more common tone detection paradigms (Costalupes, 1983; Heil et al., 2017; Mackey et al., 2021a; O'Connor et al., 1999; Plomp and Bouman, 1959). Temporal integration of AM stimuli has been explored almost exclusively at the psychophysical level, and mostly in humans (Dau et al., 1997; Lee, 1994; O'Connor et al., 2011; Sheft and Yost, 1990), though one group has reported causal evidence that parietal cortex is involved (Yao and Sanes, 2022; Yao et al., 2020). Yao et al. (2020) used a gerbil model, which permits the use of powerful genetic techniques. However, our previous work found that macaques and budgerigars exhibit unique similarity to humans in auditory temporal integration (Mackey et al., 2021a; also see Figure 4.4), which highlights the value of exploring these questions in a variety of animal models. The behavioral time constant reported here (30 ms) is almost identical to our previous report (Mackey et al., 2021a), and is much lower than the IC and CN, which suggests IC and CN integrate AM more slowly than macaques. A related question is how downstream regions of the brain integrate sensory evidence. Posterior parietal cortex (PPC) is one candidate integrator of acoustic evidence (Yao et al., 2020), and sensory evidence more generally (e.g. Cohen et al., 2004; Huk and Shadlen, 2005). Alternatively, the superior colliculus (SC) could serve this role, as multiple studies of spatial processing have found (Jay and Sparks, 1987; Rajala et al., 2017; Wallace et al., 1996), and there is causal evidence for its role in evidence accumulation in the visual domain (Jun et al., 2021). In the absence of neural data from one of these regions in this study, a DDM was used to characterize the integration process at the computational level, providing constraints on future neurophysiological studies in regions like PPC or SC. Specifically, the model results suggest that the effects of modulation frequency on the rate of integration decrease as duration decreases. This is indicated by the slope of the drift rate functions in Figures 4.11A and B, which increase as duration decreases. Candidate neural sites of integration should display this key aspect of auditory temporal integration.

Effects of noise-induced hearing loss on temporal sound envelope processing

The permanent deficits in MMR after high level noise exposure are consistent with previous studies in hearing impaired human MMR (Bacon et al., 1998; Dubno et

al., 2002; Festen and Plomp, 1990; Füllgrabe et al., 2006) and gerbils (Ihlefeld et al., 2016). The finding that changes in MMR correlated with OHC and synapse loss are, to the best of the authors' knowledge, the first in an animal model that correlate with behavioral measures of hearing in complex environments, and contribute to the literature on the relationship between noise-induced cochlear histopathology and behavior (Landegger et al., 2016; Moody et al., 1978; Ward and Duvall, 1971). The current findings also extend these findings by testing the relative explanatory power of multiple statistical models that incorporate interactions between IHC, OHC and synapse loss. The better fit of the multivariate model indicates additional explanatory power from interactions among the individual components of the cochlear damage, and unsurprisingly suggests that, despite the two being correlated with MMR amplitude, this perceptual deficit is not a simple product of OHC or IHC synapse loss alone. A similar conclusion was made in a human temporal bone study (Wu et al., 2020, 2021), and the increased experimental control in the NHP model serves to corroborate this finding.

The temporary deficits in MMR after noise exposure corroborate longitudinal reports of plasticity following hearing loss (e.g. Burke et al., 2022; Han et al., 2021), and, more generally, findings of plasticity in representations of sound envelope (Beitel et al., 2003, 2020). Such deficits may be overlooked by typical approaches that measure changes following noise exposure at a single time point (e.g. Furman et al., 2013; Kujawa and Liberman, 2009). Reports of the dynamic nature of synaptopathy also support a more longitudinal approach (Hickman et al., 2020a, 2021; Liberman and Liberman, 2015; Liu et al., 2012; Song et al., 2016). These studies measured auditory nerve responses at the single-unit level, or via the auditory brainstem response, and thus left open the question of how complex stimuli may be encoded differently over the course of a dynamic synaptopathy. The results in this chapter suggest temporal processing deficits may be temporarily compromised following such noise exposures, given that the time-course of the MMR deficits reported here roughly track with the time-course of synapse loss (see Appendix). The transient nature of these deficits may also shed light on the equivocal nature of the human literature (Bramhall et al., 2019; DiNino et al., 2021), with some groups reporting correlates of hidden hearing loss (Bharadwaj et al., 2015; Bramhall et al., 2019, 2020; Parthasarathy et al., 2020a; Ruggles et al., 2011), while others conclude there is a lack of evidence (Grose et al., 2019;

Guest et al., 2017, 2018). DiNino et al. (2021) thoroughly addressed potential stimulus characteristics that could explain such discrepancies in the literature. The MMR results here add to this, suggesting the time of measurement following noise exposure may also be a confound between studies. It should also be noted that, by design, these analyses cannot tease out the contribution of learning to performance after noise exposure. It may be fruitful for future studies of hidden hearing loss to consider the degree to which listeners adapt to noise-induced deficits.

Finally, it is surprising that the discrimination of AM noise presented here showed no signs of impairment during or after the time period when synaptopathy was suspected based on histological analyses (see Appendix). Deficits were predicted based on a substantial literature suggesting that AM processing should be compromised by synaptopathy, and based on the MMR results. This literature consists of computational models (Paul et al., 2017; Verhulst et al., 2018), human behavioral studies (e.g. Bharadwaj et al., 2015, discussed above), and neurophysiological studies detailing the impact of synaptopathy on the encoding of AM (e.g. Shaheen et al., 2015) and speech (Monaghan et al., 2020). Moreover, recent work has demonstrated how enhancing the neural encoding of AM with specific hearing-aid algorithms can improve AM detection in patients with the hidden hearing loss profile (Drakopoulos et al., 2022). The contrast with MMR may offer some insight; it may be that the encoding of AM in the presence of a competing signal (e.g. a tone in noise) is required for such deficits to emerge, in contrast to the AM noise used in the discrimination experiments, which was not masked.

CHAPTER 5 – SPATIAL PROCESSING

Sections of this chapter appear in:

Mackey, C. A., McCrate, J., MacDonald, K. S., Feller, J., Liberman, L., Liberman, M. C., Hackett T.A. & Ramachandran, R. (2021). Correlations between cochlear pathophysiology and behavioral measures of temporal and spatial processing in noise exposed macaques. *Hearing Research*, *401*, 108156.

5.1 INTRODUCTION

Sensory systems have evolved to enable organisms to successfully navigate environments using spatial information (Heffner and Heffner, 2018, 1992; Lamb et al., 2007). The auditory system is no exception to this: how the brain encodes sound localization cues, and how this process is disrupted by hearing loss are key questions in auditory neuroscience (see General Introduction). This chapter is focused on experiments testing assays of spatial processing in a nonhuman primate model of noise-induced hearing loss (NIHL), with the goal of establishing behavioral correlates of **1)** NIHL associated with hair cell and hair cell synapse loss, and **2)** NIHL associated with selective inner hair cell synaptic pathophysiology. Motivation for 1 stems from the finding that irrelevant signals (noise) at a spatial location that is different from the relevant signal (target) location show reduced masking/distracting effects, such that the detection or recognition threshold for a target masked by a spatially disparate masker is lower than for a target co-localized with the same masker/distractor (spatial release from masking, SRM; Best et al., 2012; Carhart et al., 1968; Freyman et al., 2001; Greene et al., 2018; Rocchi et al., 2017; Saberi et al., 1991) and that SRM is reduced in hearing impaired subjects (Arbogast et al., 2005; Best et al., 2017; Gelfand et al., 1988). However, the underlying cochlear pathophysiology in these studies is unclear because they have generally been conducted in humans. Animal models of NIHL permit post-mortem cochlear histological measures, but rarely test spatial hearing. This motivated the assessment of SRM in a nonhuman primate model of NIHL in this chapter.

Motivation for 2 stems from the fact that many normal-hearing listeners experience difficulty hearing in noise, despite having normal audiometric thresholds (e.g. Cooper and Gates, 1991; Parthasarathy et al., 2020b; Tremblay et al., 2015). Studies in rodents suggest cochlear synaptopathy (CS) as a candidate explanation, with compelling neurophysiological evidence suggesting CS alters the excitatory-inhibitory balance necessary to encode spatial and temporal sound features (Shaheen and

Liberman, 2018; Shaheen et al., 2015; for full discussion of the literature see General Introduction on hidden hearing loss). This suggests CS could cause spatial hearing deficits, but this has yet to be demonstrated in an animal model permitting invasive cochlear histology. Beyond finding measures that are sensitive to CS, there is substantial motivation in translational research to establish measures that can be used in a clinical setting where time is limited (Bharadwaj et al., 2019). This has motivated the development of rapid measures of SRM for clinical use (Jakien et al., 2017). The second measure of interest here is the binaural interaction component of the auditory brainstem response (BIC of the ABR). The BIC refers to the fact that ABR Wave IV/V is smaller in response to binaural stimulation than the sum of Wave IV/V responses to left and right ear stimulation, indicating inhibition measurable at the population level. The BIC likely depends on subcortical E/I balance (Benichoux et al., 2018), the very signaling compromised by CS (Asokan et al., 2018; Bakay et al., 2018; Shaheen and Liberman, 2018). Moreover, BIC amplitude correlates with spatial hearing abilities in hearing impaired and normal hearing subjects (Delb et al., 2003; Gopal and Pierel, 1999; Laumen et al., 2016). Importantly, some of these subjects had the hidden hearing loss profile - normal hearing thresholds in the presence of suprathreshold processing deficits. Here we knit together these lines of evidence by conducting a longitudinal study of the effects of synaptopathic noise exposure on the BIC and spatial hearing in macaque monkeys.

5.2 METHODS

5.2.1 Subjects

General subject information (e.g. institutional water requirements, surgical procedures, food, environmental conditions etc.) is provided in General Methods.

141/146 dB noise exposure. Experiments were performed on normal-hearing male macaques (*Macaca mulatta*, n=7), noise-exposed male macaques (Monkey Li, *Macaca mulatta*, n=1), and one macaque before and after noise exposure (Monkey Ec, *Macaca radiata,* n=1). Body weights ranged from 10-12 kg. For noise exposed monkeys, ages at the time of noise exposure were as follows: 10 years (Monkey Li), and 11 years (Monkey Ec). Normal-hearing monkeys presented for comparison to Li and Ec were from male Monkeys aged 5-9 years old.

120 dB noise exposure. Data will also be presented from monkeys exposed to a lower-level noise than the one to which L, G, and E were exposed. These monkeys participated in the experiments before and after noise exposure, and did not overlap with the noise exposed group described above. Male monkeys Bi, Ga, Ha were 10-12 kg, female monkeys Lu, Ne, Op, and Pi were 5.5-7 kg. All monkeys (male and female) in this group were 6-8 years old at the time data collection began, and at the time of noise exposure.

Names in the figures are often restricted to a single letter, but in this section and in figure captions more letters will be used to enable readers to know monkey identity across chapters in this dissertation.

5.2.2 Experimental procedures

General information about experimental procedures (e.g. the detection task, noise exposure, cochlear histology) are provided in the General Methods.

Spatial release from masking task

For the spatial experiments, speakers were placed at different angles on the azimuthal plane. Tones and 76 dB SPL (30 dB spectrum level) broadband noise were presented from different speakers for the 22.5, 45, 67.5, and 90-degree conditions of the spatial release of masking experiments. In some conditions the noise was 40 dB spectrum level (86 dB SPL) to guard against the possibility that the monkeys with

permanent threshold shifts required a higher noise level to induce masking release. The speakers were calibrated with a ¼ inch microphone (378C01, PCB Piezotronics) that was located just outside the monkey's ear canal. Care was taken to make sure that the speaker outputs were within 3 dB across all frequencies to ensure that that there were not speaker specific cues. Calibrations were also performed at the different speaker locations used in the spatial experiment to ensure that the sound level at the entry to the ear canal was as specified.

Binaural interaction component recordings

Methods used for recording the BIC were recently reported in macaques by the authors (Peacock et al., 2021), and mirror previous publications by the Tollin lab (Benichoux et al., 2018; Sammeth et al., 2020), with the exception that the data presented here were recorded using gas isoflurane anesthesia (1.5-2%). Briefly, steel subdermal needle electrodes (Grass Technologies) were placed at the apex along the interaural axis between the ears, with a reference electrode at the nape of the neck, and a ground electrode on the monkey's shoulder. Stimuli were generated and evoked potentials recorded via an RME Fireface UCX soundcard (RME audio) and a World Precision Instruments (WPI) ISO-80 biological amplifier. Custom eartips were used to deliver click stimuli with variable interaural time differences via MATLAB. Clicks were 90 dB SPL presented at an average rate of 33 Hz via Tucker Davis Technology MF-1 speakers, which were calibrated with a Bruel and Kjær type 4182 microphone. ITDs were -1500 to 1500 μs in steps of 500 μs. Monaural and binaural clicks with varying ITDs were interleaved, and presented 3000 times each.

5.2.3 Data analysis

Spatial release from masking

Psychometric functions were plotted and thresholds calculated for each tone frequency, and for each noise location. The decrease in threshold due to the spatial separation of signal (tone) and noise was quantified as the spatial release from masking, and was calculated as $SRM(\theta, f) = threshold(f)^{signal\ @\ 0°}_{masker\ @\theta\ °} - threshold(f)^{signal\ @\ 0°}_{masker\ @\ 0°}$, where θ was the spatial separation between signal and masker. Thus, negative values represent spatial release from masking (a reduction in threshold in the spatially

separated condition vs. colocalized condition), and values close to zero represent a lack thereof. Positive values, though rare, suggest masking greater in the separated condition than in the colocalized condition.

Calculation of binaural interaction component

The BIC is calculated by averaging the auditory brainstem response (ABR) signal in each condition with filter cutoffs of 30 Hz and 3 kHz. Each monaural trace was shifted by ITD/2 to compensate for the delay in the ITD conditions. The BIC was calculated as the difference between the binaural stimulation condition and the algebraic sum of the monaural conditions.

Histological-behavioral correlations

Correlations between SRM with audiometric shift and histological data were calculated using the "corrcoef" function in MATLAB (2018a), which gives Pearson's correlation coefficient, R and significance value. Additionally, "fitlm" and "fitnlm" were used to assess goodness of fit of each linear or non-linear fit, respectively. Choice of model was always validated using the "fitlm" and "fitnlm" functions, which gives Bayesian Information Criteria (BIC). Statistical analysis of the differences between noise-exposed and control data were conducted using linear mixed effects models ("fitlme") in MATLAB 2018a. These models accommodate datasets with missing points. This reason, among others, has motivated many researchers to opt for mixed effects models over repeated measures ANOVA (Krueger & Tian, 2004). The dependent variable in each model was SRM. Noise exposure status, tone frequency, and an interaction term between the two were entered as fixed effects into the model, while intercepts for individual macaques were entered as random effects. P-values were obtained by likelihood ratio testing of the model with the effect in question against the model without the effect in question.

The histological-behavioral models that incorporated frequency (tone frequency and frequency place of the cochlea), inner hair cell survival, synapse survival, outer hair cell survival, and behavioral performance were constructed using "stepwiselm" in MATLAB, which starts with a model that contains all of the data, and systematically removes factors and interaction terms that do not add significant ($p < 0.05$) explanatory power to the model. In all cases the residuals (the error of the model) were compared

against the fitted values of the model, and linear regression was only used if the residuals were randomly distributed.

General statistical analysis

In all cases, curve fits attained via non-linear least squares method implemented in MATLAB. Statistical effects reported were assessed by using linear mixed effects models ("fitlme") in MATLAB 2018a. P-values were obtained by likelihood ratio testing of the model with the effect in question against the model without the effect in question.

5.3 RESULTS

5.3.1 SRM in normal-hearing macaque monkeys

Figure 5.1A shows exemplar psychometric functions for NH Monkey B. The psychometric function for the colocalized tone and masker condition is shown in blue (circles), while the psychometric functions when the masker was separated by 45˚ and 90˚ in azimuth are shown in red diamonds and green triangles respectively. The dynamic ranges and detection thresholds for these conditions were shifted to lower SPLs relative to the co-localized masker condition, indicating a release from masking proportional with the degree of spatial separation between the signal and noise. Figures 5.1B and 5.1C show the spatial metric, spatial release from masking (SRM(θ, f)), calculated as the difference between detection thresholds when the masker was at 45º or 90˚ azimuth, compared to 0˚ azimuth as a function of the tone frequency. SRM at 45º (Figure 2B) was between 2 and 18 dB, and appeared to increase slightly as a function of tone frequency. For the masker at 90º (Figure 5.1C), the SRM was larger (7-28 dB), as expected, compared to the SRM at 45º. The SRM increased as a function of frequency, and was consistent across the six NH monkeys tested.

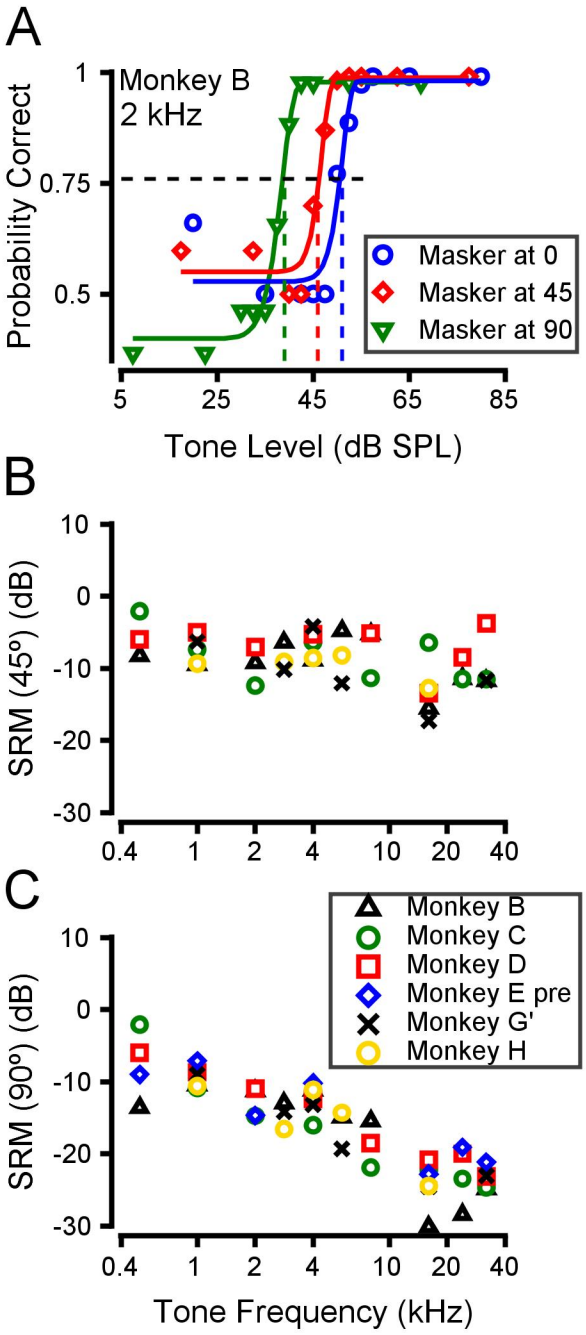

FIGURE 5.1 – Spatial release of masking (SRM) in normal-hearing macaques. A. Exemplar psychometric functions showing SRM, the difference between thresholds (*pc*=0.76) when the noise masker was at 45° (◇) or 90° (△) and 0° (○) along the azimuthal plane. B. SRM at 45° for each monkey at each tone frequency measured. C. SRM at 90° for each monkey at each tone frequency measured. *Monkeys are Bi, Ch, De, Ec, Gan, and Ha.*

5.3.2 SRM after noise exposure causing permanent threshold shift, hair cell loss, and synapse loss

Effects of noise exposure on SRM

Figure 5.2 shows the effect of NIHL on SRM in monkeys E and L. The psychometric functions obtained with a 2 kHz tone are shown in Figure 5.2A, using the same format as Figure 5.1A. The dynamic ranges for the cases when the noise and the tone were spatially separated (diamonds and triangles) were not shifted to lower levels in these subjects, in contrast to the normal-hearing macaques. Thus, the SRM found in the normal hearing subjects was absent in the noise-exposed animals at every tone frequency tested, and confirmed by mixed model analysis ($t = -3.01$, $p = 2.9*10^{-5}$, $df = 43$). These observations are expanded in Figures 5.2B and 5.2C, which plot SRM as a function of tone frequency when masker azimuth was at 45˚ (Figure 5.2B), and 90˚ (Figure 5.2C). These data show that rather than a masking release, there was additional masking at some of the frequencies, indicated by SRM being positive. The 40 dB masking condition was included in the event that the permanent threshold shifts (PTS) exhibited by monkeys L and E rendered the comparison between control and exposed monkeys inappropriate due to the fact that the masking noise would be less audible, and would evoke less SRM. The fact that the 40 dB condition also showed no SRM across frequencies indicates that the deficits were not due to a low masker level.

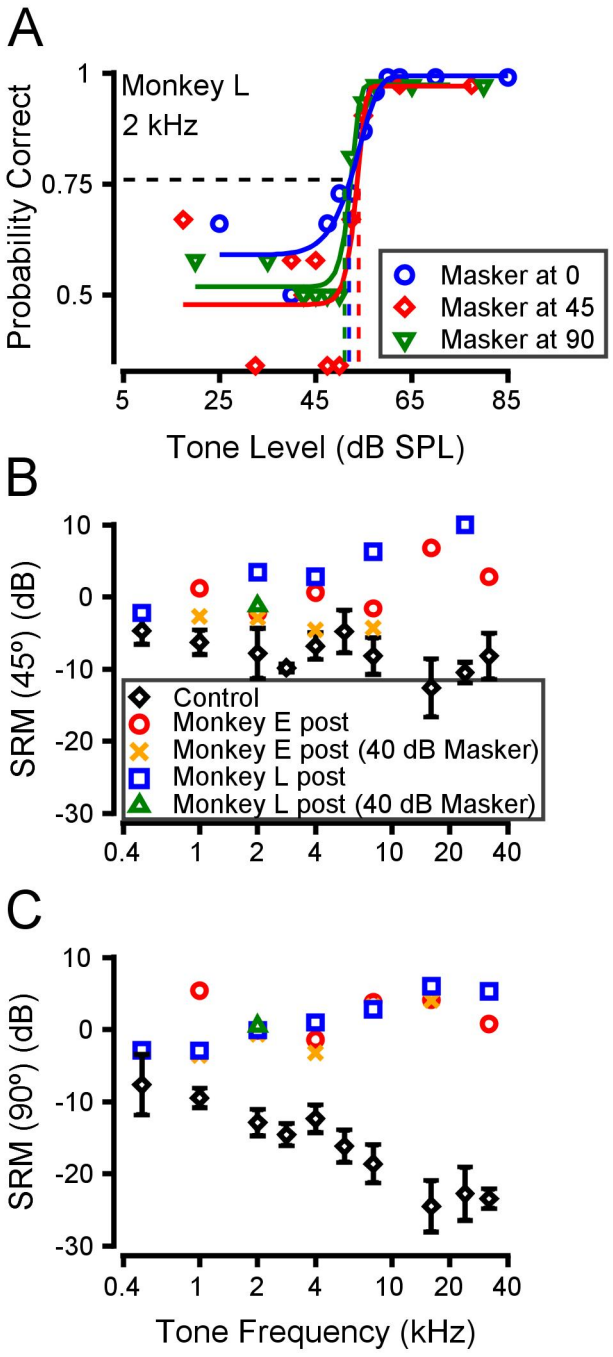

FIGURE 5.2 – Spatial release of masking in noise-exposed macaques
A. Exemplar psychometric functions showing lack of SRM when the noise masker was at 45° (◇) or 90° (△) and 0° (○) along the azimuthal plane. B, C. SRM at 45° and 90° for each monkey at each tone frequency measured, compared to unexposed monkeys (◇). *Monkeys are Li and Ec.*

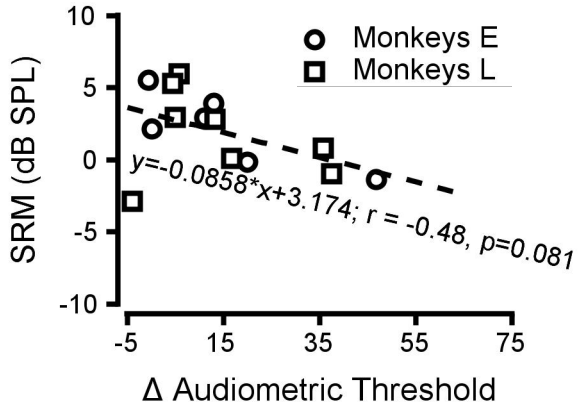

FIGURE 5.3 – No correlation of SRM with audiometric shift. The dashed line represents the best fitting linear regression. *Monkeys are Ec and Li.*

Correlation with audiometric shift and cochlear pathophysiology

To examine the relationship between the audiometric consequences of noise exposure and the more complex consequences that may be related to hearing in noisy, realistic environments, and SRM with audiometric shift are shown in Figure 5.3 (also see audiometric shifts in the Appendix). The goal was to acquire the best estimate of *change* in spatial sensitivity as a result of noise exposure, the difference between control and noise-exposed monkeys did not seem suitable for this analysis, because the trend in Δ SRM is almost completely driven by the control data. This is illustrated in figure 5.2. The noise-exposed subjects show a flat trend, while control subjects' SRM increased with tone frequency, making any correlation we attempted to establish using Δ SRM, in reality, a correlation with the control data. To avoid these issues, we used SRM at 90° to correlate spatial-processing with audiometric change, and histological changes. Figure 5.3 shows a scatter between the SRM at 90° and the audiometric change for each tone frequency for monkeys E and L. The lack of correlation between the two quantities was confirmed by a Pearson correlation coefficient value of -0.4824 (p = 0.081). SRM also did not correlate with OHC survival (Figure 5.4A; Pearson's correlation coefficient: R = -0.139, p=0.63), with IHC synapse survival (Figure 5.4B; R = -0.39, p=0.16), or with IHC survival (data not shown; R = -0.41, p = 0.148). The implications of this lack of correlation are detailed in the discussion section.

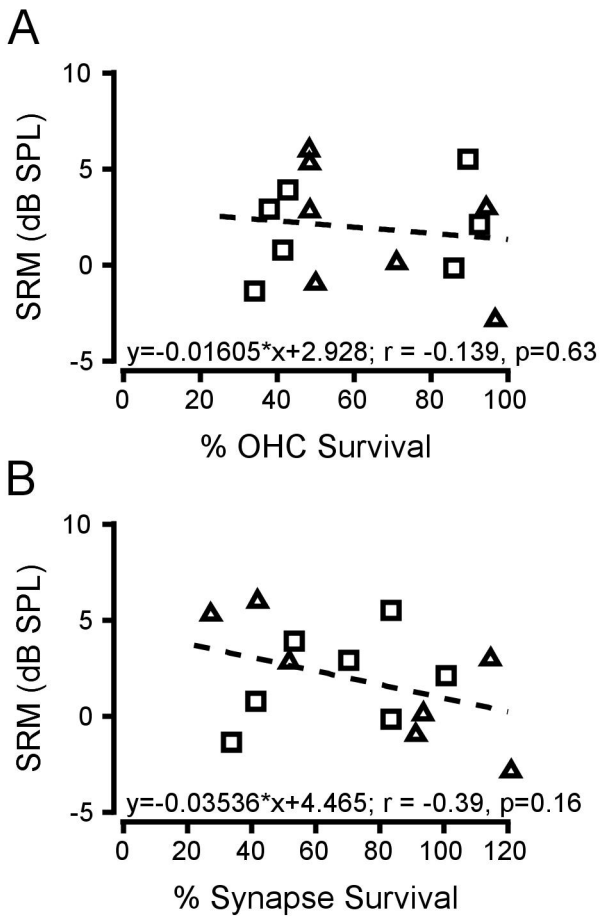

FIGURE 5.4 – Correlation of spatial release of masking with histological changes. A. Maximal SRM (90°) as a function of outer hair cell survival for noise-exposed monkeys E (circles) and L (squares). B. Maximal SRM as a function of ribbon synapse survival.

5.3.3 SRM after noise exposure causing temporary threshold shift, synaptic loss and dysfunction

SRM in male macaques

To understand why listeners with normal audiometric thresholds display spatial hearing deficits, spatial hearing was evaluated in a cohort of monkeys exposed to a 120 dB SPL noise designed to cause cochlear synaptopathy (see Methods and Appendix). This was done in a similar fashion to the previous section on monkeys with permanent threshold shifts but a few improvements in SRM measurement were implemented. SRM was measured at more locations (22.5, 45, 67.5, 90 degrees), at multiple time-points to address the dynamic nature of cochlear synaptopathy (see Introduction and Chapter 4; Hickman et al., 2020b; Liberman and Liberman, 2015; Liu et al., 2012; Shi et al., 2013), and in both sexes. In male monkeys, SRM to 5.6 kHz tones was impaired across locations; Figure 5.5 A-C shows that this effect was consistent across monkeys. SRM

values at different spatial separations were fit with lines to estimate slope and intercept, providing a summary measure of SRM that could be displayed across different tone frequencies (Figure 5.5 D-E). Deficits due to noise exposure could manifest as slope decrease or intercept increase. SRM slope for 5.6 kHz tones decreased after noise exposure for monkeys Bi and Ha, while SRM intercept at 5.6 kHz increased in Monkey Ga. The effect of noise exposure and its frequency specificity were confirmed using mixed effects model analysis that explicitly accounts for individual animal differences. The model took the form "SRM ~ Noise Location + Tone Frequency*Noise Exposure Status + (1|Monkey)" and the interaction between noise exposure and tone frequency was significant ($t = 4.11$, $df = 192$, $p = 5*10^{-5}$). SRM was reassessed 10-11 months post noise exposure, and still indicated a deficit (pink data points). In Monkeys Bi and Ha, the deficit appeared to increase slightly over time. Efforts to quantify and statistically confirm the effect of time are discussed in the following section.

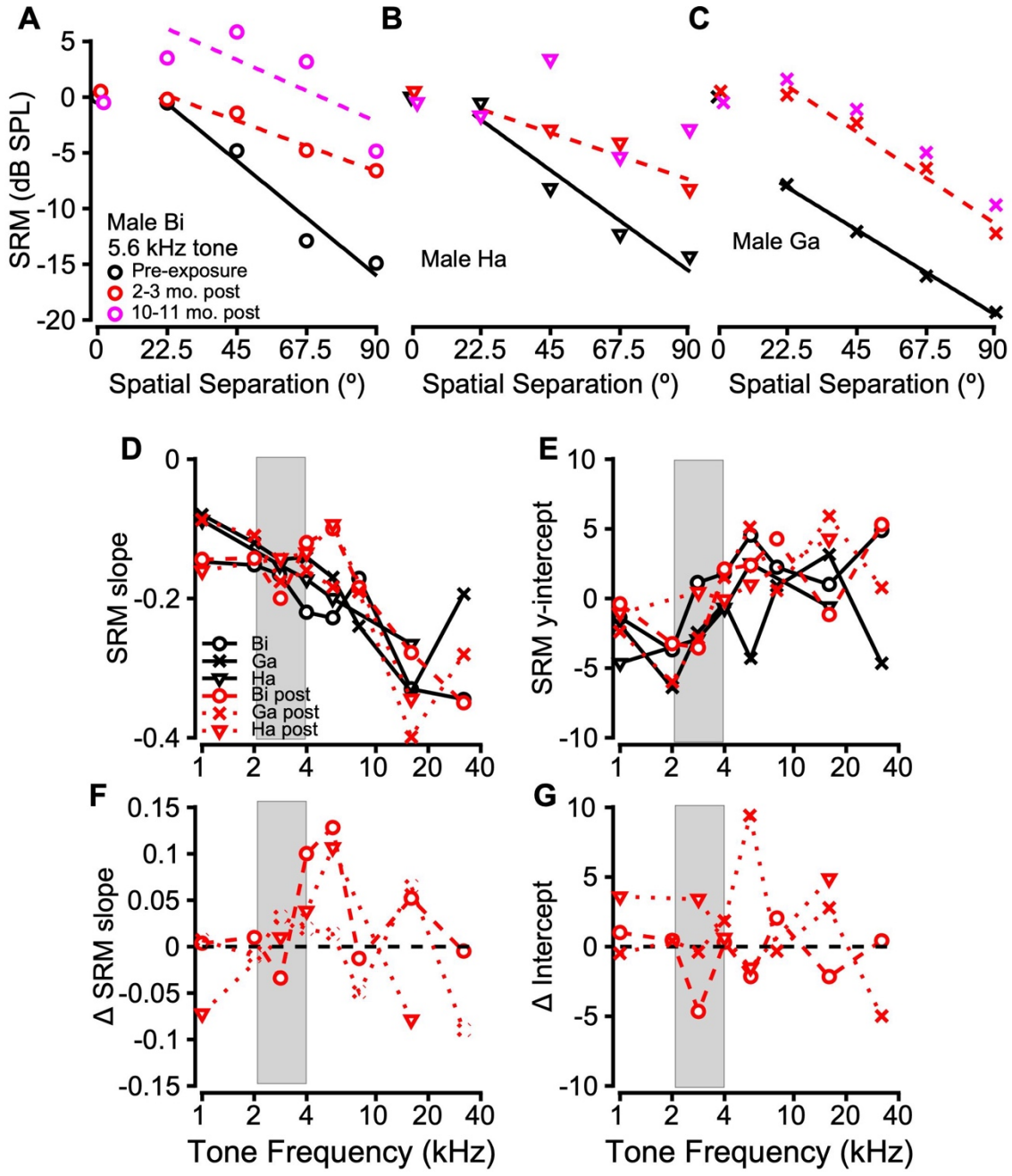

FIGURE 5.5 – Effects of noise exposure on male macaque spatial release of masking. A-C. SRM as a function of spatial separation before and after noise exposure. Lines are linear regressions fit to SRM to estimate slope and intercept. D-E. Slopes and intercepts as a function of tone frequency before and after noise exposure. F-G. Change in slopes and intercepts before and after noise exposure. *Monkey Ga = Gan.*

SRM in female macaques

Noise exposure also impaired SRM in a female macaque cohort (n=4). The effect occurred at a wider range of frequencies than in the male cohort, but the impaired frequencies were still at or above the exposure noise band (2.8-5.6 kHz). As with male macaques, this difference was quantified using SRM slope and intercept (Figure 5.6). All four monkeys displayed slope reductions at least one frequency in the 2.8-5.6 kHz range.

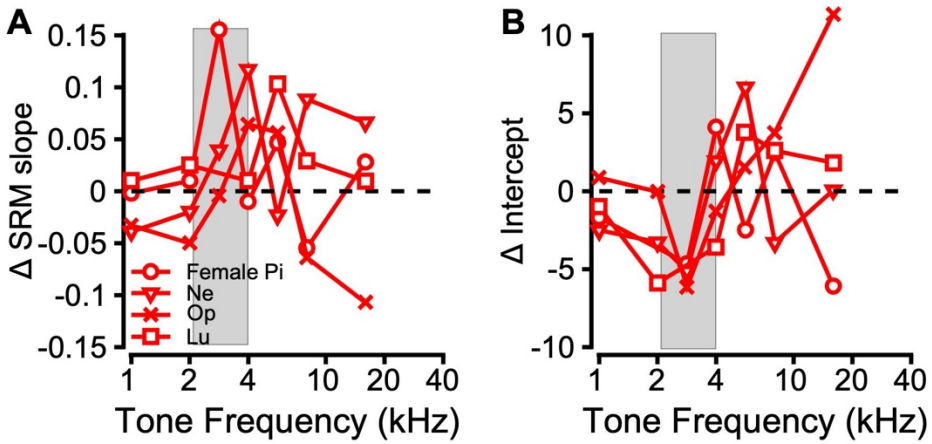

FIGURE 5.6 – SRM slope and intercept in female monkeys. A. Change in SRM slope as a function of tone frequency in female monkeys Lu, Ne, Op and Pi. B. Change in SRM intercept as a function of tone frequency.

The similarity in noise induced deficit between the sexes was formalized in mixed effects models (Table 5.1) that took the form "SRM ~ Noise Exposure*Sex + Frequency*Location + (1|Monkey)" (Effect of sex: t = 0.49, df = 405, p = 0.6; interaction of noise-exposure and sex: t = -0.77, df = 405, p = 0.4). The testing of interactions of sex with noise exposure is crucially different than simply comparing the effects of noise exposure between the cohorts, which is a common mistake when investigating sex-differences (Garcia-Sifuentes and Maney, 2021). The effect of noise exposure on SRM in the female cohort was significant, as with the male cohort (t = 3.7, df = 209, p = 0.0002), and the effect of noise exposure on SRM in the dataset with both sexes was significant ($p = 1.9*10^{-6}$; Table 5.1).

Female macaques displayed greater variability than male macaques in that the frequency specificity of SRM deficits changed over time. Data from two post exposure time-points are shown in Figure 5.7. For example, Monkey Lu (Figure 5.7, top row) exhibited an initial deficit at 5.6 kHz, consistent with male macaques, but at 2.8 kHz a deficit emerged at 9 months that was not present at the 3-month time-point. In contrast, Monkey Pi (Figure 5.7, bottom row) displayed no deficit at 5.6 kHz at 3 months, but at 9 months SRM decreased as several spatial separations. Efforts were made to statistically formalize this interaction of sex with time-point, but no significant effect was found, likely due to the variability across animals, frequency, time, and sex.

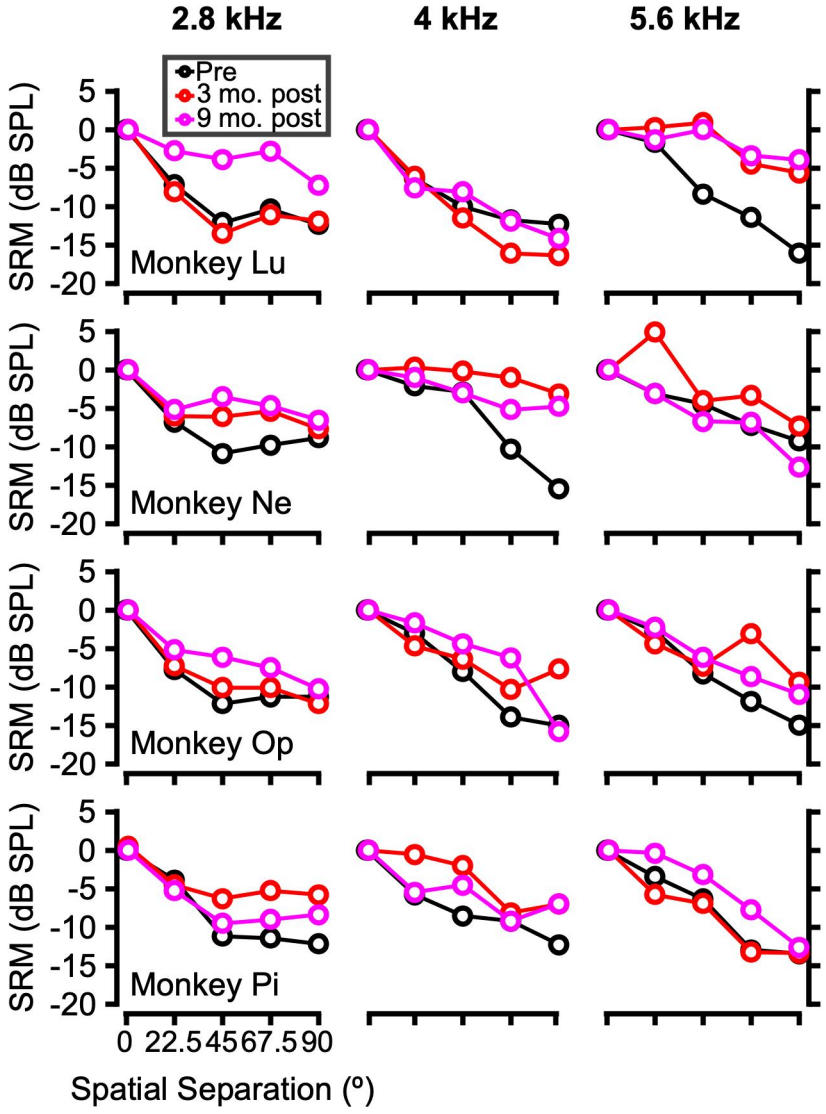

FIGURE 5.7 – SRM over time in female macaques. SRM as a function of spatial separation is shown at three frequencies (different columns) for each monkey (different rows) at the pre exposure (black), 3 month post (red), and 9 month post time-points.

Table 5.1 – Mixed effects model analysis of the effects of noise exposure and sex on SRM

MODEL	Effect of noise exposure (t-stat, *p-value)*	Effects of sex (t-stat, *p-value)*
Male cohort SRM ~ Noise Location + Tone Frequency*Noise Exposure Status + (1|Monkey)	Noise Exp*Freq: t = 4.11, $p = 5*10^{-5}$	N/A
Female cohort SRM ~ Noise Location* Tone Frequency + Noise Exposure Status + (1|Monkey)	Noise exposure: t = 3.7, $p = 2*10^{-4}$	N/A
Male/Female SRM ~ Noise Exposure*Sex + Frequency*Location + (1|Monkey)	Noise exposure: t = 2.86, $p = 0.018$	• Sex: t = 0.49, $p = 0.6$ • Noise exposure*Sex: t = -0.77, $p = 0.44$
SRM ~ Noise Exposure + Location + Sex*Frequency + (1|Monkey)	Noise exposure: t = 4.83, $p = 1.9*10^{-6}$	• Sex: t = 1.5, p = 0.12 • Sex*Frequency: t = -2.2, $p = 0.026$

Reaction-times and psychometric function slope

A goal of the present work was to characterize synaptopathy's effects on measures other than threshold, such as reaction times (RTs). Previous work has characterized how RTs change with sound level, and signal-to-noise ratio (Dylla et al., 2013; Kemp, 1984). Namely, RTs decrease as sound level increases, and conversely RTs increase as SNR

decreases. These effects have been quantified using a linear fit to RT as a function of tone level (Dylla et al., 2013). The two parameters of the RT vs. level function (slope and intercept) were used in the present analysis to assess two potential effects of synaptopathy on RTs: a change in the growth of loudness (slope change), or an overall change in the speed of auditory processing (intercept change). To test these hypotheses, the slope and intercept of each RT vs. level fit were calculated for each monkey, at each tone frequency (1-16 kHz) and spatial separation (0-90 degrees). RT intercept slightly decreased (by ~25 ms on average) after noise exposure in a model that took the form "RT intercept ~ Frequency + Noise Exposure Status*Noise Location + (1|Monkey)", (Coefficient estimate: -26 ms; t = -2.4, df = 364, p = 0.018), possibly an effect of training. This training effect interpretation is corroborated by the interaction between noise exposure and noise location not being significant, and other models incorporating an interaction between frequency and noise exposure exhibited no significant effect. RT slope changed after noise exposure, which could be modeled as an interaction between noise location and noise exposure status (t = 2.29, df = 364, p = 0.023). The interaction indicates that before noise exposure RT slope did not change as a function of noise location, but following noise exposure RT slope decreased as a function of location. This decrease indicates a reduction in the faciliatory effects of tone level on detection speed. However, the magnitude of the change was small: the maximal effect (0.4 ms/dB decrease in RT slope at 90 degrees) amounted to a 12 ms change in RT.

The slope of the psychometric function serves as a third measure of auditory processing that could theoretically be sensitive to synaptopathy. Previous work has documented effects of various stimulus features on the slope of the psychometric function (Mackey et al., 2021a; Rocchi and Ramachandran, 2018), which can be quantified using the psychometric dynamic range (DR; e.g. the tone levels spanned by the sloping portion of the function). DR slightly increased following noise exposure (Coefficient estimate: 1 dB; t = 2.6, df = 365, p = 0.01). The effect was significant in the best fitting mixed effects model, however, an interaction between noise location and noise exposure was significant in a worse-fitting model (t = 2.39, df = 364, p = 0.017).

5.3.4 Binaural interaction after noise exposure causing temporary threshold shift, synaptic loss and dysfunction

The finding that noise exposure impairs spatial hearing suggests the encoding of localization cues is compromised. This positions the binaural interaction component (BIC) of the ABR as a promising noninvasive measure of cochlear synaptic integrity (see Introduction). To capitalize on this opportunity, the BIC of the ABR was measured in male and female macaques before and after noise exposure. The BIC is a derived measure of the click-evoked ABR, calculated by subtracting the algebraic sum of monaural ABRs from the binaural ABR. Example evoked potentials and calculation of the BIC are shown in Figure 5.8. Data are from female monkey Pi. Figure 5.8 A and B show monaural ABRs in response to clicks, which are summed to give the dashed trace in Figure 5.8C. The BIC is calculated as the difference between the summed trace and the binaural trace (evoked response to simultaneous clicks to both ears) which is shown as a solid trace in Figure 5.8C. Figure 5.8D shows the BIC trace, exhibiting a stereotypical negativity around four milliseconds, which, after the sign is inverted, will be referred to as the BIC amplitude. Figure 5.8E shows monkey Pi's BIC traces before and after noise exposure. Noise exposure reduced BIC amplitude from 465 nanovolts to 231 nanovolts. This halving of the response was not uncommon. It is notable that monkey Pi exhibited an increase in the positivity just before the BIC's negativity, which could be further evidence of altered E/I balance (e.g. increased excitability). However, to provide comparison to other BIC studies, the negativity of the BIC (also known as DN1) was used for analysis. Anecdotally, the increase in positivity before the DN1 was observed frequently.

Across subjects, the BIC at 0 ITD was reduced from about 400 to about 100 nV. The group data are displayed in Figure 5.9. BIC amplitudes at zero ITD are plotted for each monkey individually in Figure 5.9A, and BIC latencies are plotted in 5.9B. All BIC amplitudes are plotted as a function of interaural time difference (ITD) in figure 5.9C. Data were statistically analyzed using mixed effects model analysis. The best fitting model, as defined by having the lowest Bayesian information criterion value, took the form $BIC \sim ITD + Noise\ Exposure + ITD^2 + ITD^2 * Noise\ Exposure + (1|Monkey)$. Noise exposure caused a significant reduction in BIC amplitude ($t = -9.02$, $df = 77$, $p = 1*10^{-13}$), and interacted with ITD ($t = 2.48$, $df = 77$, $p = 0.015$). The positive t-statistic indicates that the effect of noise exposure was to reduce the effect of ITD (i.e. BIC vs. ITD trends were shallower following noise exposure). To visualize this statistical analysis, linear

regressions taking the same form as the mixed effects model are plotted in Figure 5.9C, demonstrating that the 95% confidence intervals of the groups (black and red error bands) do not overlap between -500 and 500 ITD, and that at a group level the effect of ITD was reduced post noise exposure (red regression is shallower). There were no main effects of sex, or interactions of sex with ITD or noise exposure. BIC latencies also showed no effects of sex, effects of noise exposure, or interactions of sex and noise exposure. A preliminary analysis of the correlation between maximum BIC reduction and maximum SRM reduction did not yield significant results (Spearman correlation, $p = 0.53$). However, this was likely partially due to the sample size, as there were only six monkeys with both SRM and BIC data, and to our knowledge there is no clear way to correlate different conditions (e.g. location vs. ITD, tone frequency, etc.). However it is a strength of this finding that every monkey with SRM deficits also exhibited BIC reduction. When possible, BIC was measured at multiple time-points after noise exposure to account for the dynamic nature of synaptic damage observed in our data and in other studies. BIC reduction was consistent across time following noise exposure in all cases, though it was admittedly not systematically measured across time in all animals. Taken together these data suggest that this noise exposure, which does not elevate audiometric threshold, and preferentially targets cochlear synapses, degrades processing in the binaural brainstem circuitry involved in spatial hearing.

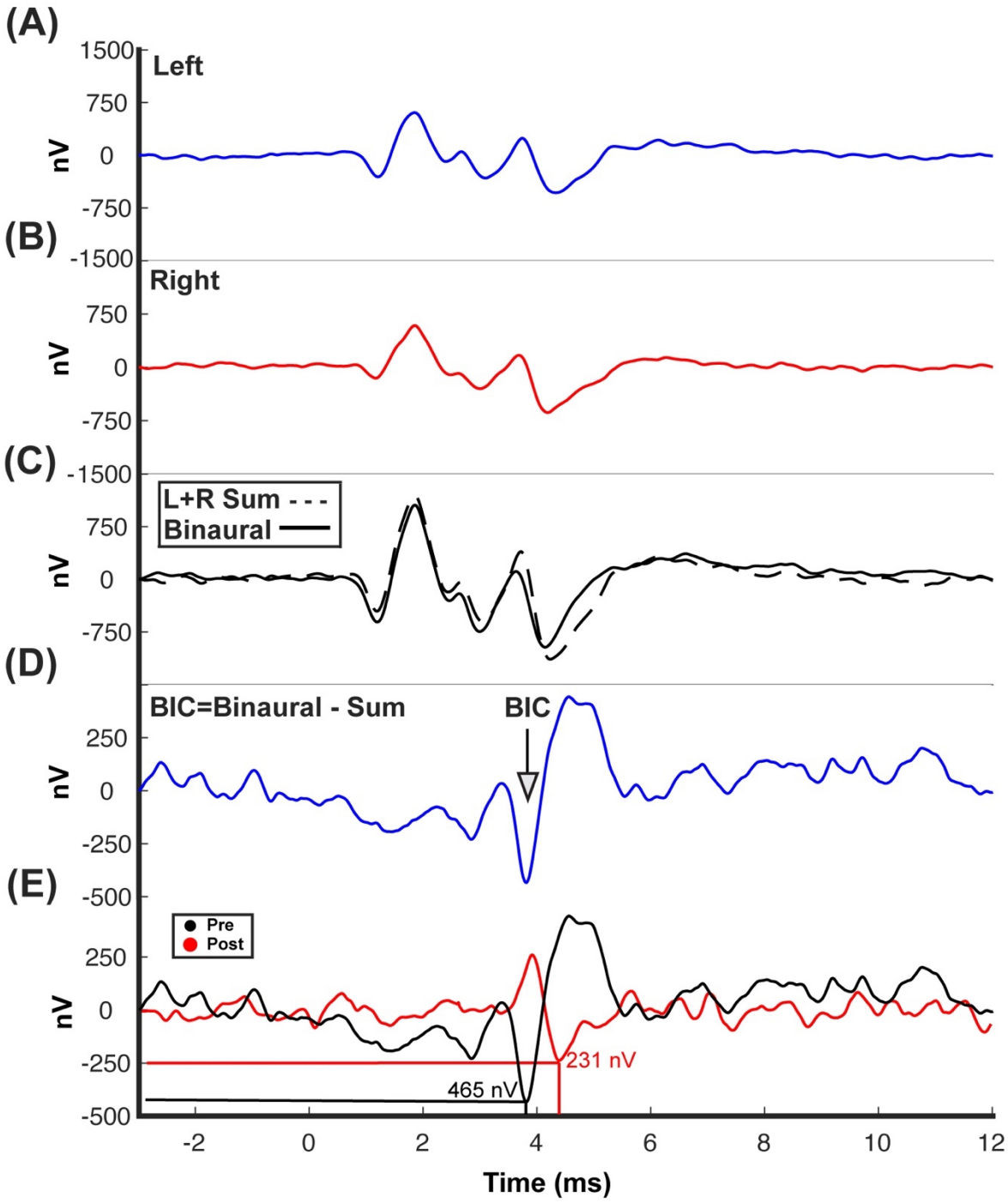

Figure 5.8. Example binaural interaction component of the auditory brainstem response from monkey Pi before and after noise exposure. **A, B.** Monaural ABRs in response to clicks presented to the left (A) and right (B) ears. **C.** Monaural sum (dashed line) and binaural response (solid black trace) used for the calculation of the BIC. **D.** BIC trace, with arrow pointing to the negativity, called DN1 or BIC amplitude. **E.** BIC traces before (black) and after (red) noise exposure, with lines pointing to the DN1/BIC amplitude.

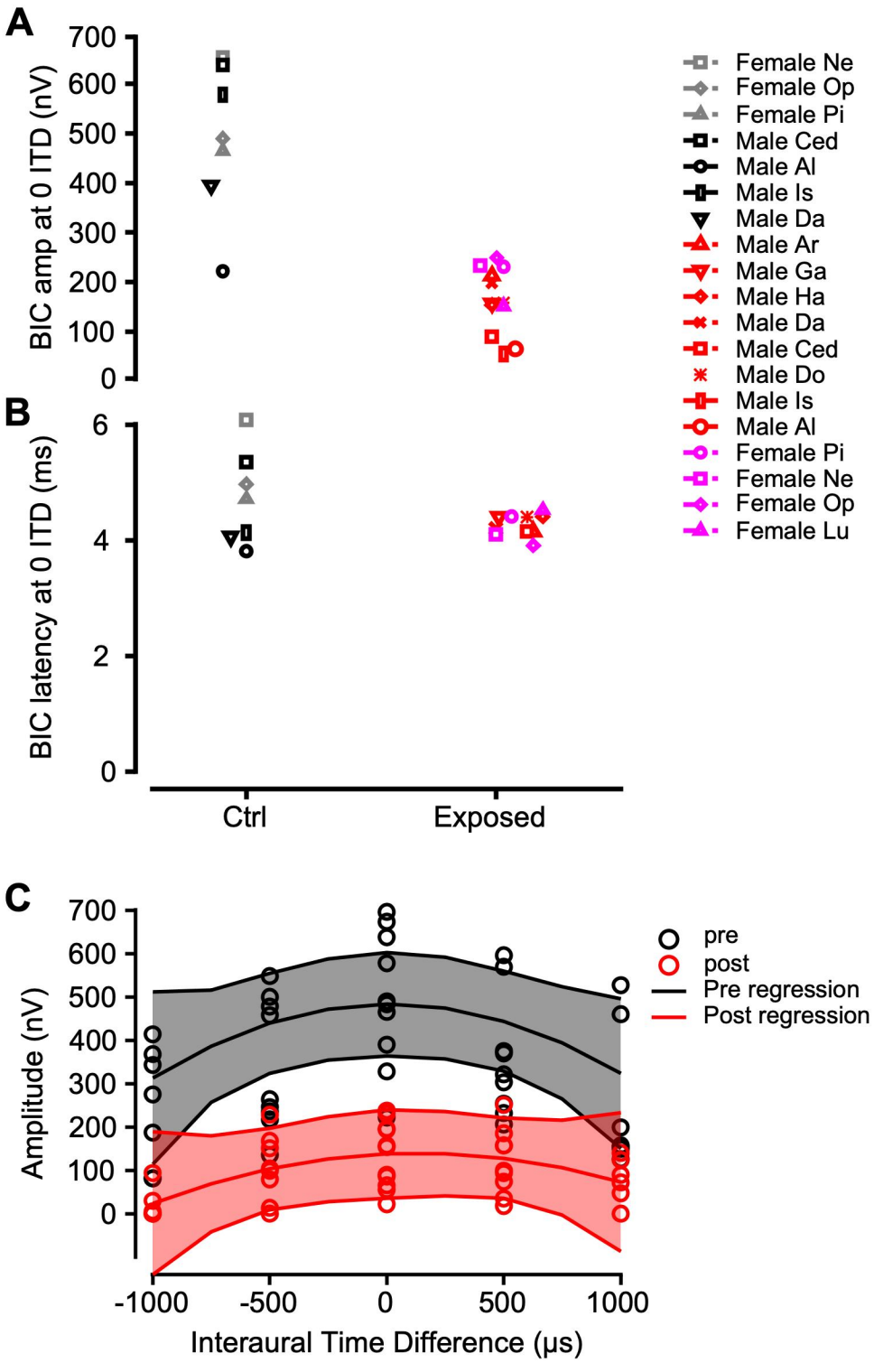
A
BIC amp at 0 ITD (nV)
700
600
500
400
300
200
100
0
B
BIC latency at 0 ITD (ms)
6
4
2
0
Ctrl
Exposed
Female Ne
Female Op
Female Pi
Male Ced
Male Al
Male Is
Male Da
Male Ar
Male Ga
Male Ha
Male Da
Male Ced
Male Do
Male Is
Male Al
Female Pi
Female Ne
Female Op
Female Lu
C
Amplitude (nV)
700
600
500
400
300
200
100
0
-1000
-500
0
500
1000
Interaural Time Difference (µs)
pre
post
Pre regression
Post regression

Figure 5.9. Group BIC data. **A.** BIC amplitudes of individual monkeys shown as different symbols before (black and grey) and post (red and pink) noise exposure. Male data are shown in black (pre) and red (post). Female data are shown in grey (pre) and pink (post). **B.** BIC latencies shown in the same format as A. **C.** BIC amplitudes plotted as a function of interaural time difference pre (black) and post (red) noise exposure. Data are shown as circles. Lines are multivariate linear regressions of the form *BIC ~ ITD + Noise Exposure + ITD^2 + ITD^2*Noise Exposure*. The shaded error-bands show the 95% confidence intervals around the regression. *Monkey Ga is monkey Gan*.

5.4 DISCUSSION

These results provide some of the first links between cochlear pathophysiology, binaural brainstem activity, and behavioral measures of spatial hearing in the context of a controlled noise exposure. They also represent an important advance in this lab's recent nonhuman primate model of noise-induced hearing loss.

Comparison to previous studies of SRM

The release of masking observed when signal and masker are spatially separated has been replicated in a number of studies. Freyman et al. (1999) used narrow-band noise as the target signal and found up to 13.8 dB masking release for certain narrowband noises when 60° separation was used. Although 60° separation was not tested in the present study, this value falls nicely between the maximal release reported here, at 45° and 90°. The masking release also increased as a function of narrowband noise center frequency, consistent with the present results in NH monkeys (Figure 2C). Arbogast et al. (2002) found up to 18.4 dB masking release at 90° separation, which is consistent with the maximal SRM shown here. However, the stimuli in their study were designed primarily to dissociate the effects of energetic and informational masking. The maximal masking release in that study was found when the target sentence was masked by noise generated by summing six bands of a masker sentence, whose spectrum was outside that of the target sentence. Thus, the masking release in that condition was mainly informational. In the energetic masking condition, more comparable to the results presented here, SRM was only ~7 dB. However, this difference could partially be

attributed to the use of a lower level masker (60 dB SPL in the earlier study, compared to the 76 dB SPL used here). Additional differences that could explain the differences in SRM magnitude include the differences in target stimuli (speech vs. pure tones). Bronkhorst and Plomp (1992) also measured SRM for speech and found that the maximum SRM for the NH group was 8 dB. Once again, differences in stimuli complicate the comparison with current results. For example, the masker was 65 dBA noise, modulated to match the envelope fluctuations of the target speech signal. These studies also found that SRM was reduced in hearing impaired subjects. Comparisons with hearing-impaired human subjects are limited by our noise exposure approach, which differs from the long-term exposures in humans with acquired hearing loss. Another concern in synthesizing the present data with the existing literature is the possibility that the spatial hearing deficits observed here were due to asymmetrical thresholds in each ear. As all behavioral data presented here were acquired in free-field, this question can be addressed using ABR threshold. Monkey G and L's ABR thresholds for each ear were published in Hauser et al., (2018), and displayed < 5 dB asymmetry at and above 2 kHz. However, these data were collected after the initial threshold shift, but before the secondary audiometric threshold shift (see Appendix). This secondary shift was presumably caused by progressive degeneration in the cochlea, some of which was asymmetric between the ears. The histological data for each ear are shown in Burton et al. (2020), and the asymmetries are discussed. A legitimate concern is whether the secondary shift and asymmetric cochlear damage undermine the correlations (and lack thereof) with behavior presented here. However, given that the deficits in SRM were not frequency specific, and the deficits in MMR were (see Chapter 4), changes in the magnitude or asymmetry of the cochlear histopathology (which was presumably always frequency-specific, see Appendix) would not be expected to change the histological-behavioral correlation presented here. Moreover, the SRM deficits were observed before the secondary threshold shift, when the damage to the ears was presumably symmetric (see ABR thresholds in Hauser et al., 2018).

Although few studies of SRM in non-human animals have been conducted, the findings complement available data. Studies in treefrogs have measured SRM using orientation to conspecific vocalizations (Bee, 2008; Nityananda and Bee, 2012). Maximum SRM with 1.3 and 2.6 kHz signals was 3 dB at 90^{0} separation. SRM in

pinnipeds better approximated the magnitude we report here (Figure 2C), with a group reporting 19 dB at 90° separation (Holt and Schusterman, 2007). Other species have been used to investigate SRM, such as budgerigars (Dent et al., 1997) and guinea pigs (Greene et al., 2018), but to the authors' knowledge, none have measured SRM after experimentally induced cochlear insult, adding novelty to the current results. Despite the methodological differences between studies, these results demonstrate the existence of SRM. And the human literature provides a strong basis for the claim that hearing loss degrades the auditory system's ability to use spatial cues to segregate auditory objects. The findings here appear to be the first to bridge the gap between human and non-human work.

Correlation with audiogram and cochlear pathophysiology

These results also highlight that the audiogram is not sufficient for predicting performance in realistic environments that provide spatial cues. The lack of correlation between SRM and audiometric threshold changes shown here contrasts with other work suggesting that SRM is inversely related to audiometric shift (Besser et al., 2015; Marrone et al., 2008). Furthermore, the results of from the TTS group exposed to the lower (120 dB) noise exposure also support similar conclusions, as SRM deficits were observed in the absence of audiometric threshold shifts (see Appendix). SRM also did not correlate with measures of cochlear histopathology (e.g. hair cell or synapse loss) in the PTS group, and, insofar as the TTS group did not exhibit synapse loss (see Appendix), there was apparently no relation between SRM deficits and synapse loss. This could be interpreted as being a consistent finding across groups, though the finding that noise exposure permanently enlarged IHC ribbon synapses complicates this interpretation (preliminary analysis in Appendix). The lack of relationship between audiogram and SRM, and between certain measures of cochlear damage and SRM may be due to the stimulus configuration used in the SRM task. Previous acoustic analysis has suggested SRM elicited by high frequency tones in broadband noise is largely due to spectral modulations introduced by the head and pinnae (Gilkey and Good, 1995). The bandwidth of such modulations is broad compared to tones, and may offer some explanation as to why there is no correlation with frequency-specific damage in the cochlea (Spezio et al., 2000), and no correlation with audiogram measured using tones.

NIHL-related changes in spatial processing are likely better correlated with altered processing in more central structures, as the BIC data presented here suggest, and will be elaborated upon in the General Discussion. NIHL-related central changes, such as central gain, have been documented in other species such as mice and cats (Chambers et al., 2017; Eggermont, 2017; Resnik and Polley, 2017, 2021; Willott and Lu, 1982), though not in all cases (Shaheen & Liberman, 2018). And, both age-related, as well as pharmacologically induced hearing loss cause central changes, and have been described in macaques (Juarez-Salinas et al., 2010; Ng and Recanzone, 2017; Schwaber et al., 1993). Such changes, and subsequent degraded sound localization cue encoding could explain the deficits in the high level noise exposure model presented here.

Significantly less is known about the central changes and associated perceptual deficits caused by noise exposures that only cause temporary threshold shifts, and which preferentially target inner hair cell synapses. Central neural correlates of temporary audiometric threshold shifts have been investigated in the nonhuman primate auditory pathway (i.e. simultaneous behavioral and neuronal shifts in the CN and IC; Lonsbury-Martin and Martin, 1981; Lonsbury-Martin et al., 1987), and such noise exposures are known to impact sound encoding in the auditory nerve and midbrain (Asokan et al., 2018; Shaheen and Liberman, 2018; Shaheen et al., 2015), but how these changes relate to the reports of hidden hearing loss in humans (e.g. Bharadwaj et al., 2015) was previously unclear. The data presented here demonstrate that such noise exposures can impact binaural brainstem circuitry and spatial hearing. This offers an explanation for hidden hearing loss, namely that moderate level noise exposures may cause cochlear synaptopathy, deafferentation, and subsequent changes in binaural brainstem circuitry that permanently disrupt spatial hearing; potential circuitry underlying these changes will be addressed in the General Discussion. Moreover, this relationship appears to translate to other species, as indicated by preliminary conference reports in a guinea pig model (Benson et al., 2020, 2022). This bodes well for the future diagnosis and treatment of hearing loss, as biomarkers and potential therapeutic targets continue to be established.

CHAPTER 6 – GENERAL DISCUSSION

The data presented here inform current models of the neural basis of hearing in noise, and its dysfunction, on many fronts; one of which concerns the range of species studied previously. These experiments described here provide knowledge of hearing in noise through the use of a macaque monkey model. In general, nonhuman primate research has provided invaluable knowledge of the brain, and unique aspects of primate (human and nonhuman) brain function have been noted across a wide range of studies, such as in the study of memory (Thome et al., 2017), Alzheimer's disease (Arnsten et al., 2019), cortical connectivity (Loomba et al., 2022), retinal processing (Bryman et al., 2020), and many others which are beyond the scope of this section to review. Previous studies such as these have demonstrated that NHPs form an essential translational bridge to humans, and the experiments discussed here provide some of the first demonstrations of this, specifically for the domains of auditory temporal integration, temporal sound envelope processing, and spatial processing. The temporal integration experiments form a theoretical foundation which can be applied to the other forms of auditory processing (temporal and spatial) due to the fact that processing of acoustic content requires integration of stimulus characteristics over time. The finding that macaques exhibit unique similarities to humans in temporal integration of simple tones in quiet environments suggests far-reaching similarities. The analyses of reaction-times and psychometric function slope that spans all chapters here also provides foundational knowledge for future studies, as previous studies in non-primate species have often noted null effects, or contradictory effects compared to the ones documented here, and in human studies (see Chapter 3).

These data also inform general knowledge of the functioning of the subcortical auditory system through the use of awake, and often behaving, experimental preparations, which have often been lacking in studies of the cochlear nucleus and inferior colliculus (Chapters 3 and 4). A goal of these projects was to provide this foundational knowledge for future investigators to capitalize on, and to remove methodological barriers in the comparison to studies of the auditory forebrain, where awake preparations are more typical.

Another aspect in which these data advance current knowledge is through the use of similar experimental design and data analysis across multiple acoustic features. This will hopefully aid in the comparison to other work within the macaque model, where different sound features have been explored (e.g. Burton et al., 2018), and synthesis across such studies can provide a comprehensive picture of NHP auditory perception.

These basic advances to the study of hearing formed an experimental foundation for the study of noise-induced hearing loss in the macaque model. The results presented here suggest that some measures of temporal processing relate strongly to outer hair cell and IHC synaptic function, while measures of spatial processing, unsurprisingly, relate to changes to binaural circuitry in the auditory pathway. In this section an attempt will be made to speculatively synthesize these findings. Taken together, the results from chapters 3-5 are consistent with an account of NIHL whereby cochlear insults cause deafferentation of ANFs, which decreases temporal integration at the periphery (Lopez-Poveda and Barrios, 2013), and, downstream of the ANF, reduces binaural interaction, either by increased spike jitter, or simply through the reduction in ANF input to binaural circuitry (Benichoux et al., 2018; Brown and Tollin, 2016), following which plasticity permits the system to decrease inhibitory tone (Caspary et al., 2008), and, consequently, temporal and spatial encoding are disrupted (Asokan et al., 2018; Bharadwaj et al., 2014, 2015; Shaheen and Liberman, 2018; Shaheen et al., 2015). The MMR results and cochlear histological analysis here suggest that this process is dynamic, which provides the first corroboration (at the behavioral level) of previous dynamic histological results (e.g. Hickman et al. 2021; see chapter 4). And, while previous studies have provided support for components of this account, rarely is this evidence presented in the context of a single experimental model.

This account of NIHL and hidden hearing loss can form the basis for future translational work in humans, which is already ongoing. Rapid tests of SRM have been published for clinical purposes, which may serve this function (Jakien et al., 2017), along with the binaural interaction component of the ABR, which has been established in humans and macaques (Delb et al., 2003; Kelly-Ballweber and Dobie, 1984; Peacock et al., 2021; Sammeth et al., 2020). Future studies can link measures such as these, and, using the knowledge established here, further the study of the neural basis of NIHL, laying the groundwork for the development of more sensitive diagnostic tests and

therapeutic targets along the auditory pathway. These efforts will hopefully lessen the global burdens NIHL presents (Davis and Hoffman, 2019; World Health Organization, 2018), and demonstrate the utility of basic studies of the auditory pathway.

Appendix

These analyses previously appeared in Dr. Jane Mondul's dissertation, and figures A1 and A7 previously appeared in Mackey et al. (2021, *Hearing Research).*

METHODS

Subjects

Noise exposure causing hair cell loss and synaptopathy. Macaques Gat and Ec were exposed to 146 dB SPL noise, and Li was exposed to 141 dB SPL noise described in the General methods. They will be referred to as G, E, and L in the figure here.

Noise exposure designed to cause synaptopathy. Cochlear tissue was obtained from sixteen adult rhesus macaques (*Macaca mulatta*, 7-10 years old, 1 female). As described in the General Methods, subjects comprised three groups: unexposed controls (n = 10), short-term post-exposure survival (2 months; n = 2), and long-term post-exposure survival (10 months; n = 4). Noise was 120 dB SPL (see General Methods)

Statistical analyses

Statistical analyses were conducted using linear mixed effects models ("fitlme" in MATLAB 2018a). The dependent variable in the models was hair cell count, ribbon count, ribbon size, or efferent terminal density. Ear laterality, frequency, noise exposure status, and post-exposure survival time were entered as fixed effects into the model, while intercepts for individual subjects were entered as random effects. In all cases p-values were obtained by likelihood ratio testing of the model with the effect in question against the model without the effect in question. A significant p-value was defined as $p < 0.05$. T-statistics are reported for each model, similar to the F-statistic that is often reported for such models.

Ribbon volume distributions were compared using Kolmogorov-Smirnov two sample tests ("kstest2" in MATLAB 2018a). A Bonferroni correction was applied to adjust the significance level for multiple comparisons (18 comparisons, adjusted p-value = 0.0028).

RESULTS

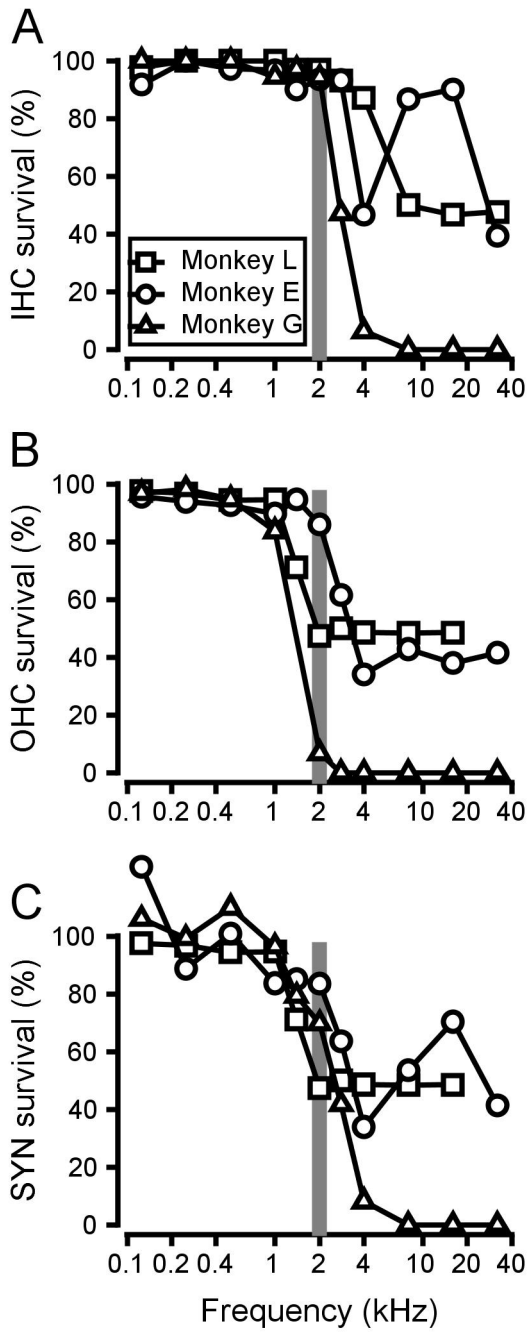

FIGURE A1 – Hair cell and synapse survival after exposure to 141/146 dB SPL noise A. Inner hair cell survival as a function of frequency place in the cochlea for monkeys Li (□), Ec (○) and Gat (△). The grey box represents the frequency band of the noise exposure. B and C are similar to panel A, but for outer hair cells (B) and cochlear ribbon synapses (C).

Hair cell survival after exposure to 120 dB noise.

Figure A2 Confocal microscopic images (XY projection) of cochlear outer hair cells and inner hair cells at the 5.6kHz frequency place in a control (A) and in noise exposed subjects (B: 2 months, C: 10 months post-exposure). OHC = outer hair cell. IHC = inner hair cell. IHC/OHC presynaptic puncta are labeled with the CtBP2 immunolabel (red) and postsynaptic glutamate receptor puncta in opposing auditory nerve fibers are labeled with the GluA2 immunolabel (green). Myo7a labels cell bodies (grey).

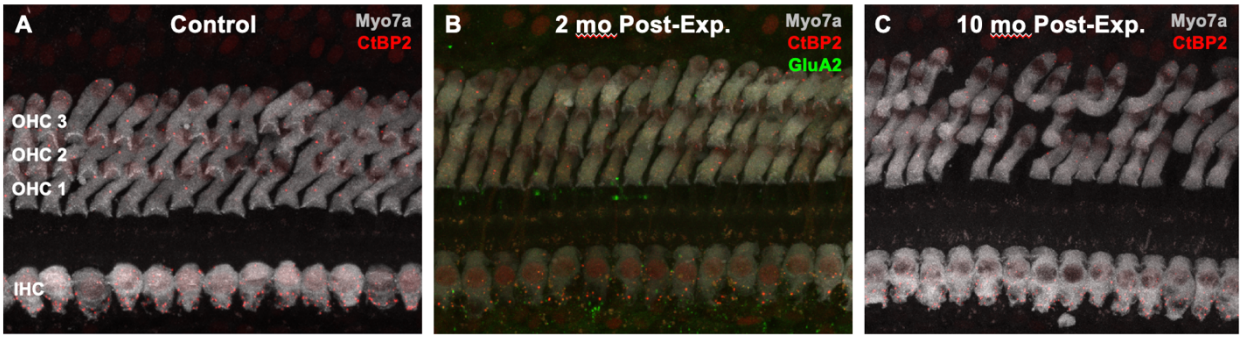

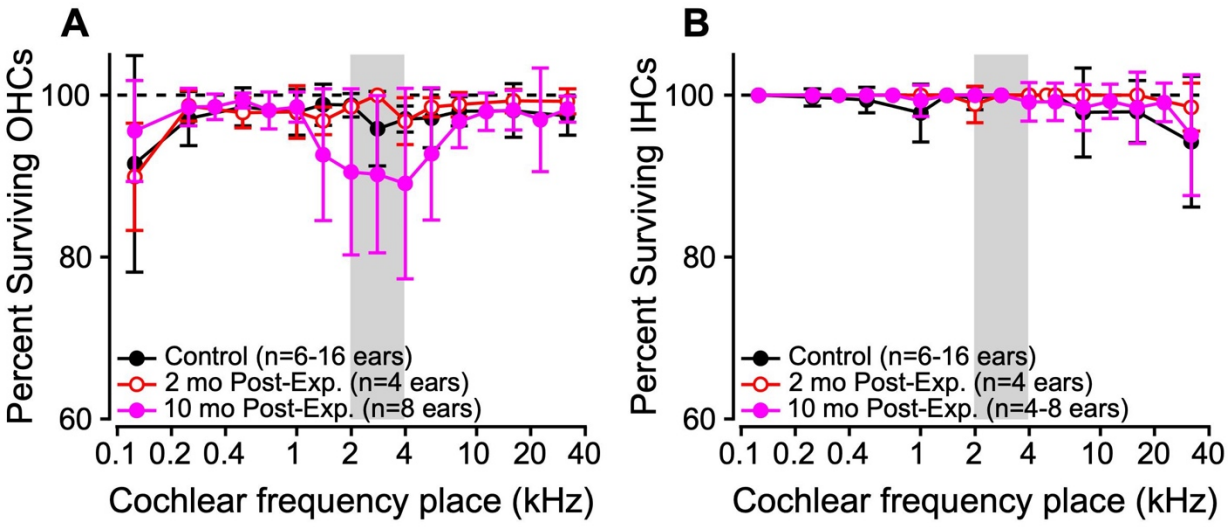

Figure A3. Outer hair cell survival (A) and inner hair cell survival (B) as a function of cochlear frequency place in controls (black, *n* = 6-16 ears per frequency) and at 2 (red, *n* = 4 ears) and 10 (pink, *n* = 8 ears) months post-exposure. Error bars indicate ± 1 standard deviation from the mean. Gray boxes illustrate the noise exposure band.

Synapse survival and volume after exposure to 120 dB noise

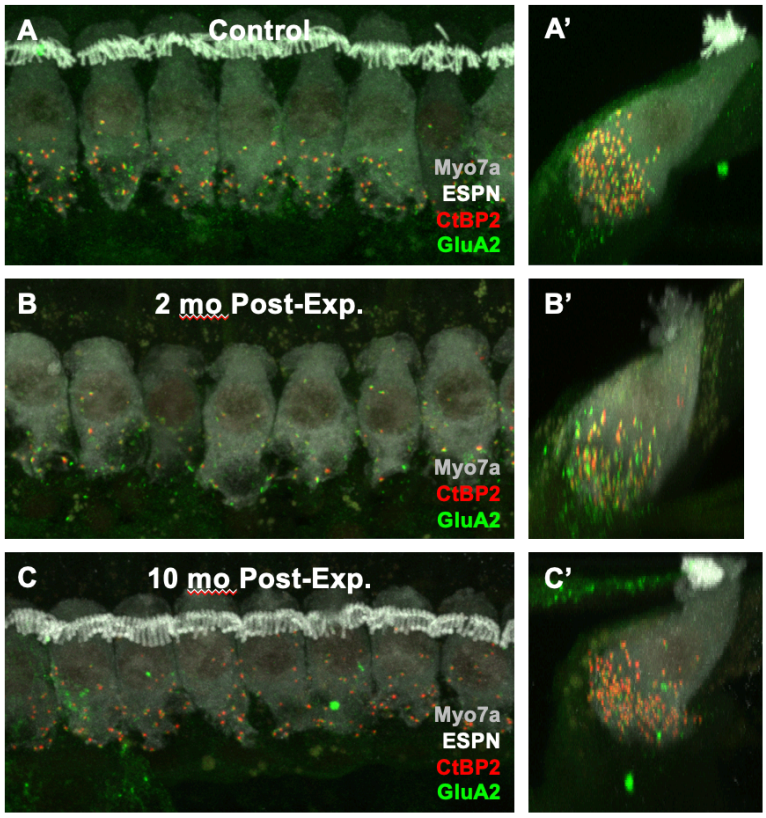

Figure A4. Confocal microscopic images of cochlear inner hair cells at the 5.6kHz frequency place in a control and in subjects 2 months post-exposure and 10 months post-exposure to the 120 dB noise exposure. A,B,C: XY projection. A',B',C': YZ projection. IHC presynaptic puncta are labeled with the CtBP2 immunolabel (red) and postsynaptic glutamate receptor puncta in opposing auditory nerve fibers are labeled with the GluA2 immunolabel (green). Cell bodies are labeled with Myo7a. Efferent terminals were labeled with ESPN.

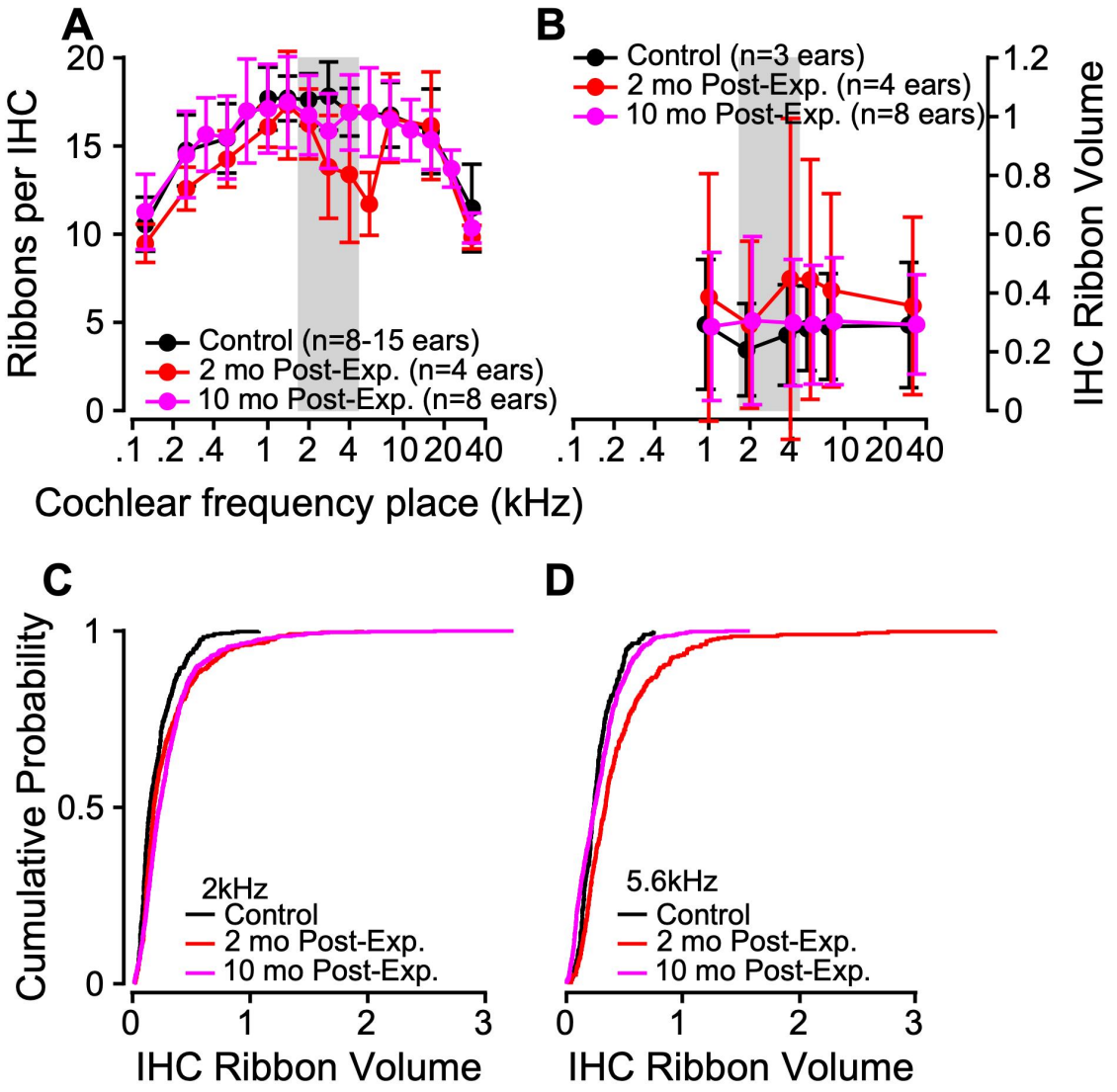

Figure A5. A,B. Mean ribbons per inner hair cell (A) and mean inner hair cell ribbon volume (B) as a function of cochlear frequency place in controls (black, n = 8-15 ears per frequency) and at 2 (red, n = 4 ears) and 10 (pink, n = 8 ears) months post-exposure. Error bars indicate ± 1 standard deviation from the mean. C,D. Cumulative distribution functions of IHC ribbon volume at 2 kHz and 5.6 kHz cochlear frequency places.

Model form: *IHC Ribbon Count_2 Month ~ Exposure + Frequency;* $R^2 = 0.35$

Linear mixed effects model for IHC ribbon count in controls vs. 2 months post-exposure

Variable	***T-statistic (df)***	***p-value***
Exposure	-2.15 (183)	0.033
Frequency	-3.00 (183)	0.003

Model form: *IHC Ribbon Count_10 Month ~ Frequency;* $R^2 = 0.41$

Linear mixed effects model for IHC ribbon count in controls vs. 10 months post-exposure

Variable	***T-statistic (df)***	***p-value***
Exposure	-0.23 (226)	0.815
Frequency	-3.68 (226)	<0.001

Statistical confirmation of synapse volume increase via 2-sample Kolmogorov-smirnov statistical tests

Frequency (kHz)	**2 Mo Post-Exp.**		**10 Mo Post-Exp.**	
	K-statistic	***p-value***	***K-statistic***	***p-value***
1	0.105	0.007	0.086	0.018
2	0.148	<0.000	0.212	<0.000
4	0.209	<0.000	0.098	0.010
5.6	0.257	<0.000	0.159	<0.000
8	0.168	<0.000	0.049	0.552
32	0.131	0.026	0.104	0.087

Outer hair cell ribbon volume after exposure to 120 dB noise

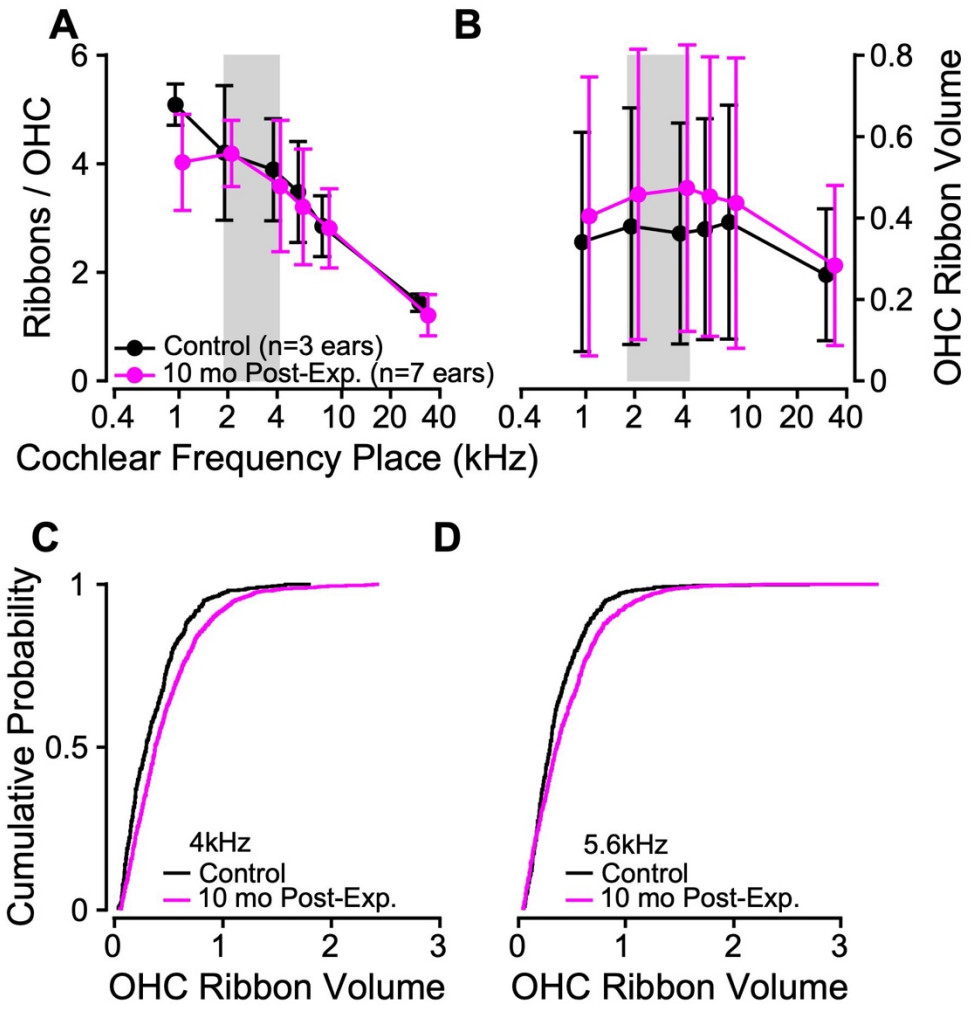

Figure A6. A,B. Ribbons per outer hair cell (A) and mean outer hair cell ribbon volume (B) as a function of cochlear frequency place in controls (black, n = 3 ears per frequency) and at 10 (pink, n = 7 ears) months post-exposure. Error bars indicate ± 1 standard deviation from the mean. C,D. Cumulative distribution functions of OHC ribbon volume at 4kHz and 5.6 kHz cochlear frequency places.

Results of KS-tests comparing outer hair cell ribbon volume between exposed and control monkeys

Frequency (kHz)	***K-statistic***	***p-value***
1	0.098	<0.001
2	0.097	<0.001
4	0.151	<0.001
5.6	0.129	<0.001
8	0.085	0.013
32	0.062	0.635

Audiometric threshold shift following noise exposure

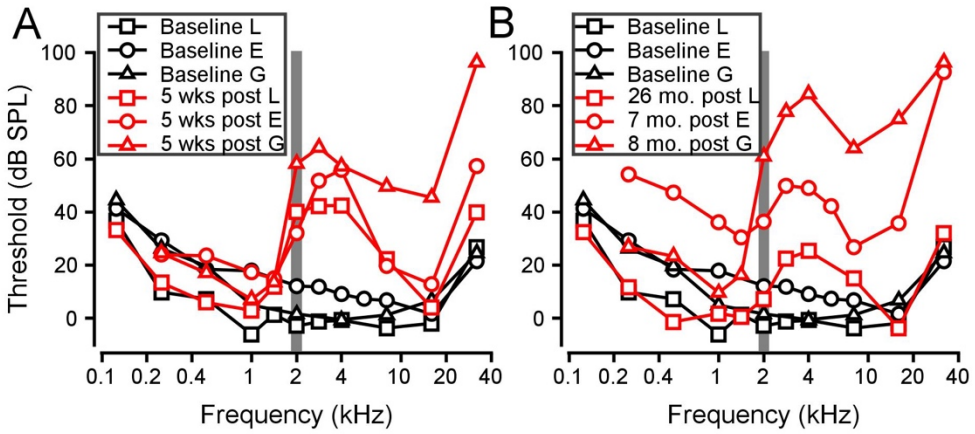

FIGURE A7 – Permanent audiometric shift after 141/146 dB SPL noise exposure. Audiograms for monkeys Li (□), Ec (○), and Gat (△) pre-exposure (black) and post- noise exposure (red). A. Initial audiometric shift measured at 5 weeks post noise exposure for each monkey. B. Secondary audiometric shift measured at time-points after MMR and SRM data collection for Monkeys Li and Ec, but near MMR collection for Monkey Gat.

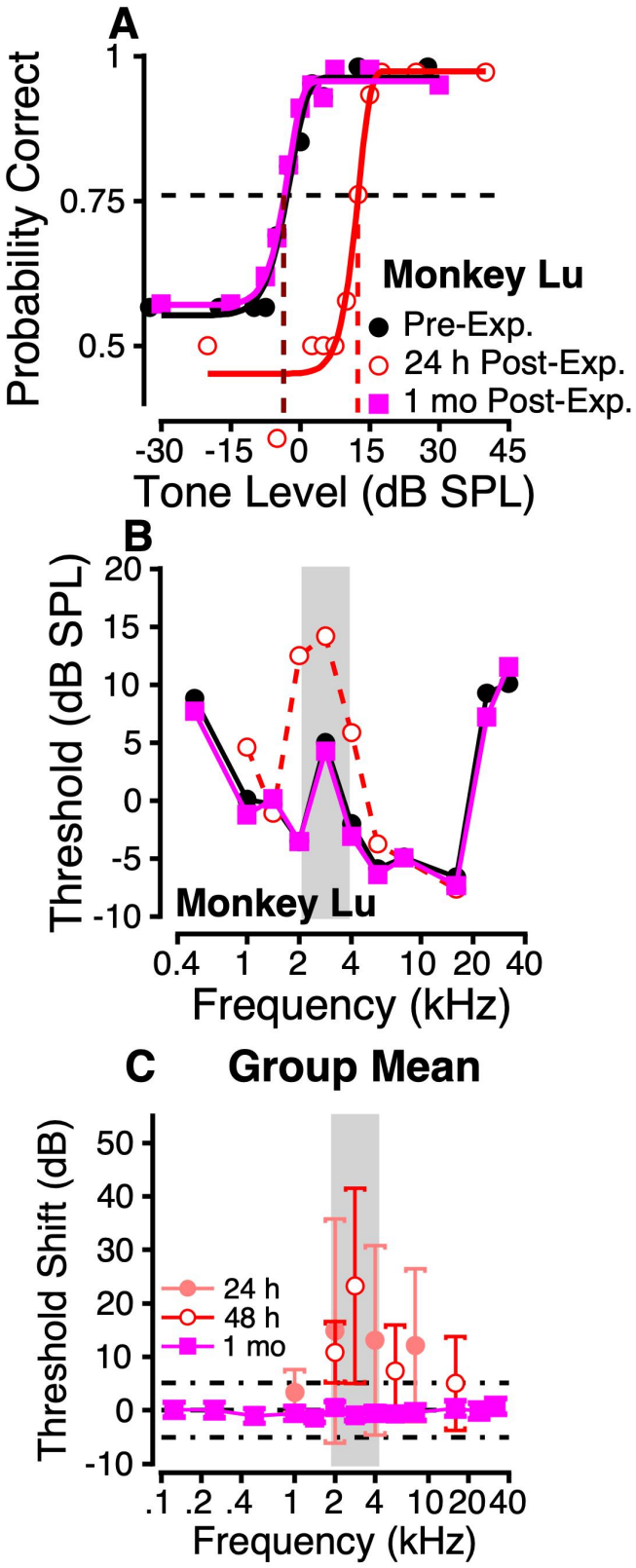

Figure A8 - Temporary threshold shift following exposure to 120 dB SPL noise. A. Example psychometric functions from female monkey Lu pre exposure (black), 24 hours post exposure (red), and 1 month post exposure (pink). B. Example audiogram from monkey Lu, following same format as A. C. Threshold shift of all monkeys exposed to 120 dB noise as a function of tone frequency.

BIBLIOGRAPHY

Adams, J.C. (1986). Neuronal Morphology in the Human Cochlear Nucleus. Arch. Otolaryngol. Neck Surg. *112*, 1253–1261.

Amaro, D., Ferreiro, D.N., Grothe, B., and Pecka, M. (2021). Source identity shapes spatial preference in primary auditory cortex during active navigation. Curr. Biol. *31*, 3875-3883.e5.

Arbogast, T.L., Mason, C.R., and Kidd, G. (2005). The effect of spatial separation on informational masking of speech in normal-hearing and hearing-impaired listeners. J. Acoust. Soc. Am. *117*, 2169–2180.

Arlinger, S., and Gustaffson, H.A. (1991). Masking of Speech by Amplitude-Modulated Noise. J. Sound Vib. 441–445.

Arnsten, A.F.T., Datta, D., Leslie, S., Yang, S.-T., Wang, M., and Nairn, A.C. (2019). Alzheimer's-like pathology in aging rhesus macaques: Unique opportunity to study the etiology and treatment of Alzheimer's disease. Proc. Natl. Acad. Sci. *116*, 26230–26238.

Asokan, M.M., Williamson, R.S., Hancock, K.E., and Polley, D.B. (2018). Sensory overamplification in layer 5 auditory corticofugal projection neurons following cochlear nerve synaptic damage. Nat. Commun. *9*, 1–10.

Asokan, M.M., Williamson, R.S., Hancock, K.E., and Polley, D.B. (2021). Inverted central auditory hierarchies for encoding local intervals and global temporal patterns. Curr. Biol. 1–9.

Bacon, S.P., and Grantham, D.W. (1989). Modulation masking: Effects of modulation frequency, depth, and phase. J. Acoust. Soc. Am. *85*, 2575–2580.

Bacon, S.P., Opie, J.M., and Montoya, D.Y. (1998). the Effects of Hearing Loss and Noise Masking on the Masking Release for Speech. J. Speech, Lang. Hear. Res. *41*, 549–563.

Bakay, W.M.H., Anderson, L.A., Garcia-Lazaro, J.A., McAlpine, D., and Schaette, R. (2018). Hidden hearing loss selectively impairs neural adaptation to loud sound environments. Nat. Commun. *9*.

Bartlett, E.L., and Wang, X. (2007). Neural representations of temporally modulated signals in the auditory thalamus of awake primates. J. Neurophysiol. *97*, 1005–1017.

Batteau, D.W. (1967). The role of the pinna in human localization. Proc. R. Soc. London. Ser. B. Biol. Sci. *168*, 158–180.

Becker, L., Schnee, M.E., Niwa, M., Sun, W., Maxeiner, S., Talaei, S., Kachar, B., Rutherford, M.A., and Ricci, A.J. (2018). The presynaptic ribbon maintains vesicle populations at the hair cell afferent fiber synapse. Elife *7*, 1–26.

Bee, M.A. (2008). Finding a mate at a cocktail party: spatial release from masking improves acoustic mate recognition in grey treefrogs. Anim. Behav. *75*, 1781–1791.

Beitel, R.E., Schreiner, C.E., Cheung, S.W., Wang, X., and Merzenich, M.M. (2003). Reward-dependent plasticity in the primary auditory cortex of adult monkeys trained to discriminate temporally modulated signals. Proc. Natl. Acad. Sci. U. S. A. *100*, 11070–11075.

Beitel, R.E., Schreiner, C.E., and Vollmer, M. (2020). Spectral plasticity in monkey primary auditory cortex limits performance generalization in a temporal discrimination task. J. Neurophysiol.

Bendor, D., and Wang, X. (2008). Neural response properties of primary, rostral, and rostrotemporal core fields in the auditory cortex of marmoset monkeys. J. Neurophysiol. *100*, 888–906.

Benichoux, V., Ferber, A., Hunt, S., Hughes, E., and Tollin, D. (2018). Across species "natural ablation" reveals the brainstem source of a noninvasive biomarker of binaural hearing. J. Neurosci. *38*, 8563–8573.
Benson, M., Greene, N.T., Peacock, J., and Tollin, D.J. (2020). Noise-Induced Cochlear Synaptopathy in Guinea Pig. Assoc. Res. Otolaryngol. Midwinter Meet.
Benson, M.A., Peacock, J., Greene, N., and Tollin, D. (2022). Binaural brainstem and spatial hearing deficits in a guinea pig model of noise-Induced cochlear synaptopathy. J. Acoust. Soc. Am. *151*, A258–A258.
Besser, J., Festen, J.M., Goverts, S.T., Kramer, S.E., and Pichora-Fuller, M.K. (2015). Speech-in-speech listening on the LiSN-S test by older adults with good audiograms depends on cognition and hearing acuity at high frequencies. Ear Hear. *36*, 24–41.
Best, V., Marrone, N., Mason, C.R., and Kidd, G. (2012). The influence of non-spatial factors on measures of spatial release from masking. J. Acoust. Soc. Am. *131*, 3103–3110.
Best, V., Mason, C.R., Swaminathan, J., Roverud, E., and Kidd, G. (2017). Use of a glimpsing model to understand the performance of listeners with and without hearing loss in spatialized speech mixtures. J. Acoust. Soc. Am. *141*, 81–91.
Bharadwaj, H.M., Verhulst, S., Shaheen, L., Liberman, M.C., and Shinn-Cunningham, B.G. (2014). Cochlear neuropathy and the coding of supra-threshold sound. Front. Syst. Neurosci. *8*, 1–18.
Bharadwaj, H.M., Masud, S., Mehraei, G., Verhulst, S., and Shinn-Cunningham, B.G. (2015). Individual Differences Reveal Correlates of Hidden Hearing Deficits. J. Neurosci. *35*, 2161–2172.
Bharadwaj, H.M., Mai, A.R., Simpson, J.M., Choi, I., Heinz, M.G., and Shinn-Cunningham, B.G. (2019). Non-Invasive Assays of Cochlear Synaptopathy – Candidates and Considerations. Neuroscience *407*, 53–66.
Boemio, A., Fromm, S., Braun, A., and Poeppel, D. (2005). Hierarchical and asymmetric temporal sensitivity in human auditory cortices. Nat. Neurosci. *8*, 389–395.
Bohlen, P.A., Dylla, M.E., Timms, C., and Ramachandran, R. (2014). Detection of modulated tones in modulated noise by non-human primates. JARO - J. Assoc. Res. Otolaryngol. *15*, 801–821.
Bramhall, N., Beach, E., Epp, B., LePrell, C.G., Lopez-Poveda, E.A., Plack, C., Schaette, R., Verhulst, S., and Canlon, B. (2019). The search for noise-induced cochlear synaptopathy in humans: Mission impossible? Hear. Res. *377*, 88–103.
Bramhall, N.F., Niemczak, C.E., Kampel, S.D., Billings, C.J., and McMillan, G.P. (2020). Evoked potentials reveal noise exposure–related central auditory changes despite normal audiograms. Am. J. Audiol. *29*, 152–164.
Brand, A., Behrend, O., Marquardt, T., McAlpine, D., and Grothe, B. (2002). Precise inhibition is essential for microsecond interaural time difference coding. Nature *417*, 543–547.
Bregman, A.S. (1994). Auditory Scene Analysis: The perceptual organization of sound. MIT Press.
Britten, K.H., Newsome, W.T., Shadlen, M.N., Celebrini, S., and Movshon, J.A. (1996). A relationship between behavioral choice and the visual responses of neurons in macaque MT. Vis. Neurosci. *13*, 87–100.
Bronkhorst, Aw., and Plomp, Rjtj. (1992). Effect of multiple speechlike maskers on binaural speech recognition in normal and impaired hearing. J. Acoust. Soc. Am. *92*, 3132–3139.
Brown, A.D., and Tollin, D.J. (2016). Slow temporal integration enables robust neural coding and perception of a cue to sound source location. J. Neurosci. *36*, 9908–9921.

Bryman, G.S., Liu, A., and Do, M.T.H. (2020). Optimized Signal Flow through Photoreceptors Supports the High-Acuity Vision of Primates. Neuron *108*, 335-348.e7.
Buran, B.N., Strenzke, N., Neef, A., Gundelfinger, E.D., Moser, T., and Liberman, M.C. (2010). Onset Coding Is Degraded in Auditory Nerve Fibers from Mutant Mice Lacking Synaptic Ribbons. J. Neurosci. *30*, 7587–7597.
Burger, R.M., and Pollak, G.D. (1998). Analysis of the Role of Inhibition in Shaping Responses to Sinusoidally Amplitude-Modulated Signals in the Inferior Colliculus. *22*.
Burke, K., Screven, L.A., Kobrina, A., Charlton, P.E., Schrode, K., Villavisanis, D.F., Dent, M.L., and Lauer, A.M. (2022). Effects of Noise Exposure and Aging on Behavioral Tone Detection in Quiet and Noise by Mice. Eneuro *9*, ENEURO.0391-21.2022.
Burton, J.A., Dylla, M.E., and Ramachandran, R. (2018). Frequency selectivity in macaque monkeys measured using a notched-noise method. Hear. Res. *357*, 73–80.
Burton, J.A., Valero, M.D., Hackett, T.A., and Ramachandran, R. (2019a). The use of nonhuman primates in studies of noise injury and treatment. J. Acoust. Soc. Am. *146*, 3770–3789.
Burton, J.A., Valero, M.D., Hackett, T.A., and Ramachandran, R. (2019b). The use of nonhuman primates in studies of noise injury and treatment. J. Acoust. Soc. Am. *3770*.
Burton, J.A., Mackey, C.A., Macdonald, K.S., Hackett, T.A., and Ramachandran, R. (2020). Changes in audiometric threshold and frequency selectivity correlate with cochlear histopathology in macaque monkeys with permanent noise-induced hearing loss. Hear. Res. *398*, 108082.
Carhart, R., Tillman, T.W., and Johnson, K.R. (1968). Effects of Interaural Time Delays on Masking by Two Competing Signals. J. Acoust. Soc. Am. *43*, 1223–1230.
Caspary, D.M., Ling, L., Turner, J.G., and Hughes, L.F. (2008). Inhibitory neurotransmission, plasticity and aging in the mammalian central auditory system. J. Exp. Biol. *211*, 1781–1791.
Cavanagh, J.F., Wiecki, T. V, Kochar, A., and Frank, M.J. (2014). Eye tracking and pupillometry are indicators of dissociable latent decision processes. J. Exp. Psychol. Gen. *143*, 1476–1488.
Chakrabarti, R., Jung, S., Michanski, S., Neef, A., Wichmann, C., Jaime Tobón, L.M., Grabner, C., Jean, P., Neef, J., Picher, M.M., et al. (2018). The synaptic ribbon is critical for sound encoding at high rates and with temporal precision. Elife *7*, 1–39.
Chambers, A.R., Pilati, N., Balaram, P., Large, C.H., Kaczmarek, L.K., and Polley, D.B. (2017). Pharmacological modulation of Kv3.1 mitigates auditory midbrain temporal processing deficits following auditory nerve damage. Sci. Rep. *7*, 1–15.
Christison-Lagay, K.L., and Cohen, Y.E. (2014). Behavioral correlates of auditory streaming in rhesus macaques. Hear. Res. *309*, 17–25.
Clack, T.D. (1966). Effect of Signal Duration on the Auditory Sensitivity of Humans and Monkeys (Macaca mulatta). J. Acoust. Soc. Am. *40*, 1140–1146.
Clark, W.W. (1979). Absolute threshold and response latency for the chinchilla as a function of stimulus duration. J. Acoust. Soc. Am. *65*, S54–S55.
Clock, A.E., Salvi, R.J., Saunders, S.S., and Powers, N.L. (1993). Neural correlates of temporal integration in the cochlear nucleus of the chinchilla. Hear. Res. *71*, 37–50.
Clock Eddins, A., Salvi, R.J., Wang, J., and Powers, N.L. (1998). Threshold-duration functions of chinchilla auditory nerve fibers. Hear. Res. *119*, 135–141.
Cohen, Y.E., Cohen, I.S., and Gifford, G.W. (2004). Modulation of LIP Activity by Predictive Auditory and Visual Cues. Cereb. Cortex *14*, 1287–1301.

Cooper, J.C., and Gates, G.A. (1991). Hearing in the elderly-the framingham cohort, 1983-1985: Part II. prevalence of central auditory processing disorders. Ear Hear. *12*, 304–311.
Costalupes, J.A. (1983). Temporal integration of pure tones in the cat. Hear. Res. *9*, 43–54.
Dai, L., Best, V., and Shinn-Cunningham, B.G. (2018). Sensorineural hearing loss degrades behavioral and physiological measures of human spatial selective auditory attention. Proc. Natl. Acad. Sci. 1–10.
Dallos, P., and Fay, R.R. (2012). The cochlea (Springer Science & Business Media).
Darwin, C.J., and Hukin, R.W. (2000). Effectiveness of spatial cues, prosody, and talker characteristics in selective attention. J. Acoust. Soc. Am. *107*, 970–977.
Dau, T., Kollmeier, B., and Kohlrausch, A. (1997). Modeling auditory processing of amplitude modulation. I. Detection and masking with narrow-band carriers. J. Acoust. Soc. Am. *102*, 2892–2905.
Davis, K.A. (2005). Contralateral effects and binaural interactions in dorsal cochlear nucleus. JARO - J. Assoc. Res. Otolaryngol. *6*, 280–296.
Davis, A.C., and Hoffman, H.J. (2019). Hearing loss: rising prevalence and impact. Bull. World Health Organ. *97*, 646.
Davis, K.A., Ramachandran, R., and May, B.J. (1999). Single-unit responses in the inferior colliculus of decerebrate cats. II. Sensitivity to Interaural Level Differences. J. Neurophysiol. *82*, 152–163.
Dawes, P., Emsley, R., Cruickshanks, K.J., Moore, D.R., Fortnum, H., Edmondson-Jones, M., McCormack, A., and Munro, K.J. (2015). Hearing loss and cognition: the role of hearing AIDS, social isolation and depression. PLoS One *10*, e0119616.
Delb, W., Strauss, D.J., Hohenberg, G., and Plinkert, P.K. (2003). The binaural interaction component (BIC) in children with central auditory processing disorders (CAPD). Int. J. Audiol. *42*, 401–412.
Dent, M.L., Larsen, O.N., and Dooling, R.J. (1997). Free-field binaural unmasking in budgerigars (Melopsittacus undulatus). Behav. Neurosci. *111*, 590.
Devore, S., Ihlefeld, A., Hancock, K., Shinn-Cunningham, B.G., and Delgutte, B. (2009). Accurate Sound Localization in Reverberant Environments Is Mediated by Robust Encoding of Spatial Cues in the Auditory Midbrain. Neuron *62*, 123–134.
DiNino, M., Holt, L.L., and Shinn-Cunningham, B.G. (2021). Cutting Through the Noise: Noise-Induced Cochlear Synaptopathy and Individual Differences in Speech Understanding Among Listeners With Normal Audiograms. Ear Hear.
Dooling, R.J., and Searcy, M.H. (1981). Amplitude Modulation Thresholds for the Parakeet. J. Comp. Physiol. *143*, 383–388.
Downer, J.D., Niwa, M., and Sutter, M.L. (2015). Task Engagement Selectively Modulates Neural Correlations in Primary Auditory Cortex. J. Neurosci. *35*, 7565–7574.
Downer, J.D., Niwa, M., and Sutter, M.L. (2017). Hierarchical differences in population coding within auditory cortex. J. Neurophysiol. *118*, 717–731.
Downer, J.D., Bigelow, J., Runfeldt, M.J., and Malone, B.J. (2021). Temporally precise population coding of dynamic sounds by auditory cortex. J. Neurophysiol. *126*, 148–169.
Drakopoulos, F., Vasilkov, V., Osses Vecchi, A., Wartenberg, T., and Verhulst, S. (2022). Model-based hearing-enhancement strategies for cochlear synaptopathy pathologies. Hear. Res. *424*, 108569.
Drullman, R., Festen, J.M., and Plomp, R. (1994). Effect of reducing slow temporal modulations on speech reception. J. Acoust. Soc. Am. *95*, 2670–2680.
Dubno, J.R., Horwitz, A.R., and Ahlstrom, J.B. (2002). Benefit of modulated maskers for

speech recognition by younger and older adults with normal hearing. J. Acoust. Soc. Am. *111*, 2897–2907.
Dylla, M.E., Hrnicek, A., Rice, C., and Ramachandran, R. (2013). Detection of tones and their modification by noise in nonhuman primates. JARO - J. Assoc. Res. Otolaryngol. *14*, 547–560.
Eggermont, J.J. (2017). Acquired hearing loss and brain plasticity. Hear. Res. *343*, 176–190.
Evans, E.F., and Nelson, P.G. (1973). The responses of single neurones in the cochlear nucleus of the cat as a function of their location and the anaesthetic state. Exp. Brain Res. *4*, 402–427.
Fay, R.R. (1982). Neural Mechanisms of an Auditory Temporal Discrimination by the Goldfish. J. Comp. Physiol. 201–216.
Festen, J.M., and Plomp, R. (1981). Relations between auditory functions in normal hearing. J. Acoust. Soc. Am. *70*, 356–369.
Festen, J.M., and Plomp, R. (1990). Effects of fluctuating noise and interfering speech on the speech-reception threshold for impaired and normal hearing. J. Acoust. Soc. Am. *88*, 1725–1736.
Fettiplace, R., and Fuchs, P.A. (1999). Mechanisms of hair cell tuning. Annu. Rev. Physiol. *61*, 809.
Formby, C. (1985). Differential sensitivity to tonal frequency and to the rate of amplitude modulation of broadband noise by normally hearing listeners. J. Acoust. Soc. Am. *78*, 70–77.
Formby, C., and Muir, K. (1988). Modulation and gap detection for broadband and filtered noise signals. J. Acoust. Soc. Am. *84*, 545–550.
Francis, A. (2010). Improved segregation of simultaneous talkers differentially affects perceptual and cognitive capacity demands for recognizing speech. Attention, Perception, Psychophys. *72*, 501–516.
Freyman, R.L., Balakrishnan, U., and Helfer, K.S. (2001). Spatial release from informational masking in speech recognition. J. Acoust. Soc. Am. *109*, 2112–2122.
Fuchs, P.A., and Glowatzki, E. (2015). Synaptic studies inform the functional diversity of cochlear afferents. Hear. Res. *330*, 18–25.
Füllgrabe, C., Berthommier, F., and Lorenzi, C. (2006). Masking release for consonant features in temporally fluctuating background noise. Hear. Res. *211*, 74–84.
Furman, A.C., Kujawa, S.G., and Liberman, M.C. (2013). Noise-induced cochlear neuropathy is selective for fibers with low spontaneous rates. J. Neurophysiol. *110*, 577–586.
Garcia-Sifuentes, Y., and Maney, D.L. (2021). Reporting and misreporting of sex differences in the biological sciences. Elife *10*, 1–3.
de Gee, J.W., Tsetsos, K., Schwabe, L., Urai, A.E., McCormick, D., McGinley, M.J., and Donner, T.H. (2020). Pupil-linked phasic arousal predicts a reduction of choice bias across species and decision domains. Elife *9*, e54014.
Gelfand, S.A., Ross, L., and Miller, S. (1988). Sentence reception in noise from one versus two sources: Effects of aging and hearing loss. J. Acoust. Soc. Am. *83*, 248–256.
George, E.L.J., Festen, J.M., and Houtgast, T. (2006). Factors affecting masking release for speech in modulated noise for normal-hearing and hearing-impaired listeners. J. Acoust. Soc. Am. *120*, 2295–2311.
Gerken, G., Bhat, V., and Hutchison-Clutter, M. (1990). Auditory temporal integration and the power function model. J. Acoust. Soc. Am. *88*, 767–778.
Gibson, D.J., Young, E.D., and Costalupes, J.A. (1985). Similarity of dynamic range adjustment

in auditory nerve and cochlear nuclei. J. Neurophysiol. *53*, 940–958.
Gifford, G.W., and Cohen, Y.E. (2005). Spatial and non-spatial auditory processing in the lateral intraparietal area. Exp. Brain Res. *162*, 509–512.
Gilkey, R.H., and Good, M.D. (1995). Effects of Frequency on Free-Field Masking. Hum. Factors *37*, 835–843.
Goldberg, J.M., and Brown, P.B. (1969). Response of binaural neurons of dog superior olivary complex to dichotic tonal stimuli: some physiological mechanisms of sound localization. J. Neurophysiol. *32*, 613–636.
Gopal, K. V, and Pierel, K. (1999). Binaural interaction component in children at risk for central auditory processing disorders. Scand. Audiol. *28*, 77–84.
Green, D.M., and Swets, J.A. (1966). Signal detection theory and psychophysics. (Oxford, England: John Wiley).
Greene, N.T., Anbuhl, K.L., Ferber, A.T., DeGuzman, M., Allen, P.D., and Tollin, D.J. (2018). Spatial hearing ability of the pigmented Guinea pig (Cavia porcellus): Minimum audible angle and spatial release from masking in azimuth. Hear. Res. *365*, 62–76.
Griffiths, T.D., Lad, M., Kumar, S., Holmes, E., McMurray, B., Maguire, E.A., Billig, A.J., and Sedley, W. (2020). How Can Hearing Loss Cause Dementia? Neuron *108*, 401–412.
Groh, J.M., Kelly, K.A., and Underhill, A.M. (2003). A Monotonic Code for Sound Azimuth in Primate Inferior Colliculus. J. Cogn. Neurosci. *15*, 1217–1231.
Grose, J.H., Buss, E., and Elmore, H. (2019). Age-Related Changes in the Auditory Brainstem Response and Suprathreshold Processing of Temporal and Spectral Modulation. Trends Hear. *23*, 1–11.
Grothe, B., Pecka, M., and McAlpine, D. (2010). Mechanisms of sound localization in mammals. Physiol. Rev. *90*, 983–1012.
Guest, H., Munro, K.J., Prendergast, G., Howe, S., and Plack, C.J. (2017). Tinnitus with a normal audiogram : Relation to noise exposure but no evidence for cochlear synaptopathy. Hear. Res. *344*, 265–274.
Guest, H., Munro, K.J., Prendergast, G., Millman, R.E., and Plack, C.J. (2018). Impaired speech perception in noise with a normal audiogram : No evidence for cochlear synaptopathy and no relation to lifetime noise exposure. Hear. Res. *364*, 142–151.
Hackett, T.A. (2011). Information flow in the auditory cortical network. Hear. Res. *271*, 133–146.
Hackett, T.A., Stepniewska, I., and Kaas, J.H. (1998). Thalamocortical Connections of the Parabelt Auditory Cortex in Macaque. J. Comp. Neurol. *400*, 271–286.
Hackett, T.A., de la Mothe, L.A., Camalier, C.R., Falchier, A., Lakatos, P., Kajikawa, Y., and Schroeder, C.E. (2014). Feedforward and feedback projections of caudal belt and parabelt areas of auditory cortex: Refining the hierarchical model. Front. Neurosci. *8*, 1–21.
Han, E.X., Fernandez, J.M., Swanberg, C., Shi, R., and Bartlett, E.L. (2021). Longitudinal auditory pathophysiology following mild blast-induced trauma. J. Neurophysiol. *126*, 1172–1189.
Harris, K.C., Ahlstrom, J.B., Dias, J.W., Kerouac, L.B., McClaskey, C.M., Dubno, J.R., and Eckert, M.A. (2021). Neural Presbyacusis in Humans Inferred from Age-Related Differences in Auditory Nerve Function and Structure. J. Neurosci. *41*, 10293–10304.
Hauser, M.D. (1989). Ontogenetic changes in the comprehension and production of vervet monkey (Cercopithecus aethiops) vocalizations. J. Comp. Psychol. *103*, 149–158.
Hauser, S.N., Burton, J.A., Mercer, E.T., and Ramachandran, R. (2018). Effects of noise

overexposure on tone detection in noise in nonhuman primates. Hear. Res. *357*, 33–45.
Hawkins, J.E., and Stevens, S.S. (1950). The Masking of Pure Tones and of Speech by White Noise. J. Acoust. Soc. Am. *22*, 6–13.
Hawkins, J.E., Johnsson, L.G., Stebbins, W.C., Moody, D.B., and Coombs, S.L. (1976). Hearing loss and cochlear pathology in monkeys after noise exposure. Acta Otolaryngol. *81*, 337–343.
Heffner, H.E., and Heffner, R.S. (2018). The evolution of mammalian hearing. In AIP Conference Proceedings, p.
Heffner, R.S., and Heffner, H.E. (1992). Evolution of sound localization in mammals. In The Evolutionary Biology of Hearing, (Springer), pp. 691–715.
Heil, P. (2014). Towards a Unifying Basis of Auditory Thresholds: Binaural Summation. J. Assoc. Res. Otolaryngol. *234*, 219–234.
Heil, P., Neubauer, H., Brown, M., and Irvine, D.R.F. (2008). Towards a unifying basis of auditory thresholds: Distributions of the first-spike latencies of auditory-nerve fibers. Hear. Res. *238*, 25–38.
Heil, P., Matysiak, A., and Neubauer, H. (2017). A probabilistic Poisson-based model accounts for an extensive set of absolute auditory threshold measurements. Hear. Res. *353*, 135–161.
Henry, K.S., Neilans, E.G., Abrams, K.S., Idrobo, F., and Carney, L.H. (2016). Neural correlates of behavioral amplitude modulation sensitivity in the budgerigar midbrain. J. Neurophysiol. *115*, 1905–1916.
Henry, K.S., Abrams, K.S., Forst, J., Mender, M.J., Neilans, E.G., Idrobo, F., and Carney, L.H. (2017). Midbrain Synchrony to Envelope Structure Supports Behavioral Sensitivity to Single-Formant Vowel-Like Sounds in Noise. JARO - J. Assoc. Res. Otolaryngol. *18*, 165–181.
Hernández-Pérez, R., Rojas-Hortelano, E., and de Lafuente, V. (2020). Integrating Somatosensory Information Over Time. Neuroscience *433*, 72–80.
Hewitt, M.J., and Meddis, R. (1994). A computer model of amplitude-modulation sensitivity of single units in the inferior colliculus. J. Acoust. Soc. Am. *95*, 2145–2159.
Hickman, T.T., Hashimoto, K., Liberman, L.D., and Liberman, M.C. (2020a). Synaptic migration and reorganization after noise exposure suggests regeneration in a mature mammalian cochlea. Sci. Rep. *10*, 1–15.
Hickman, T.T., Hashimoto, K., Liberman, L.D., and Liberman, M.C. (2020b). Synaptic migration and reorganization after noise exposure suggests regeneration in a mature mammalian cochlea. Sci. Rep. *10*, 1–14.
Hickman, T.T., Hashimoto, K., Liberman, L.D., and Liberman, M.C. (2021). Cochlear Synaptic Degeneration and Regeneration After Noise: Effects of Age and Neuronal Subgroup. Front. Cell. Neurosci. *15*.
Hildreth, J.D. (1973). Bloch's law and a temporal integration model for simple reaction time to light. Percept. Psychophys. *14*, 421–432.
Hind, S.E., Haines-Bazrafshan, R., Benton, C.L., Brassington, W., Towle, B., and Moore, D.R. (2011). Prevalence of clinical referrals having hearing thresholds within normal limits. Int. J. Audiol. *50*, 708–716.
Hoglen, N.E.G., Larimer, P., Phillips, E.A.K., Malone, B.J., and Hasenstaub, A.R. (2018). Amplitude modulation coding in awake mice and squirrel monkeys. J. Neurophysiol. *119*, 1753–1766.
Holt, M.M., and Schusterman, R.J. (2007). Spatial release from masking of aerial tones in

pinnipeds. J. Acoust. Soc. Am. *121*, 1219–1225.
Huk, A.C., and Shadlen, M.N. (2005). Neural Activity in Macaque Parietal Cortex Reflects Temporal Integration of Visual Motion Signals during Perceptual Decision Making. J. Neurosci. *25*, 10420–10436.
Ihlefeld, A., Chen, Y.W., and Sanes, D.H. (2016). Developmental Conductive Hearing Loss Reduces Modulation Masking Release. In Trends in Hearing, pp. 1–14.
Ingham, N.J., and McAlpine, D. (2005). GABAergic inhibition controls neural gain in inferior colliculus neurons sensitive to interaural time differences. J. Neurosci. *25*, 6187–6198.
Jakien, K.M., Kampel, S.D., Stansell, M.M., and Gallun, F.J. (2017). Validating a rapid, automated test of spatial release from masking. Am. J. Audiol. *26*, 507–518.
Jay, M.F., and Sparks, D.L. (1987). Sensorimotor integration in the primate superior colliculus. I. Motor convergence. J. Neurophysiol. *57*, 22–34.
Johnson, J.S., Yin, P., O'Connor, K.N., and Sutter, M.L. (2012). Ability of primary auditory cortical neurons to detect amplitude modulation with rate and temporal codes: Neurometric analysis. J. Neurophysiol. *107*, 3325–3341.
Joris, P.X., and Yin, T.C.T. (1992). Responses to amplitude-modulated tones in the auditory nerve of the cat. J. Acoust. Soc. Am. *91*, 215–232.
Joris, P.X., Carney, L.H., Smith, P.H., and Yin, T.C. (1994). Enhancement of neural synchronization in the anteroventral cochlear nucleus. I. Responses to tones at the characteristic frequency. J. Neurophysiol. *71*, 1022–1036.
Joris, P.X., Schreiner, C.E., and Rees, A. (2004). Neural Processing of Amplitude-Modulated Sounds. Physiol. Rev. *84*, 541–577.
Joris, P.X., Bergevin, C., Kalluri, R., Mc Laughlin, M., Michelet, P., van der Heijden, M., and Shera, C.A. (2011). Frequency selectivity in Old-World monkeys corroborates sharp cochlear tuning in humans. Proc. Natl. Acad. Sci. *108*, 17516–17520.
Juarez-Salinas, D.L., Engle, J.R., Navarro, X.O., and Recanzone, G.H. (2010). Hierarchical and Serial Processing in the Spatial Auditory Cortical Pathway Is Degraded by Natural Aging. J. Neurosci. *30*, 14795–14804.
JUFANG, H. (1997). Long-latency neurons in auditory cortex involved in temporal integration: Physiological and anatomical experiments. Neurosci. Res. *28*, S216–S216.
Jun, E.J., Bautista, A.R., Nunez, M.D., Allen, D.C., Tak, J.H., Alvarez, E., and Basso, M.A. (2021). Causal role for the primate superior colliculus in the computation of evidence for perceptual decisions. Nat. Neurosci. *24*, 1121–1131.
Kavanagh Moore, J. (1980a). The primate cochlear nuclei: Loss of lamination as a phylogenetic process. J. Comp. Neurol. *193*, 609–629.
Kavanagh Moore, J. (1980b). The primate cochlear nuclei: Loss of lamination as a phylogenetic process. J. Comp. Neurol. *193*, 609–629.
Kelly-Ballweber, D., and Dobie, R.A. (1984). Binaural interaction measured behaviorally and electrophysiologically in Young and old adults. Int. J. Audiol. *23*, 181–194.
Kelly, J.B., Cooke, J.E., Gilbride, P.C., Mitchell, C., and Zhang, H. (2006). Behavioral limits of auditory temporal resolution in the rat: Amplitude modulation and duration discrimination. J. Comp. Psychol. *120*, 98–105.
Kemp, S. (1984). Reaction time to a tone in noise as a function of the signal-to-noise ratio and tone level. Percept. Psychophys. *36*, 473–476.
Kemp, S., and Irwin, R.J. (1979). Reaction Time to the Start and End of Weak Signals in Noise (Routledge).
Kietzman, M.L., and Gillam, B.J. (1972). Visual temporal integration and simple reaction time.

Percept. Psychophys. *11*, 333–340.
Krishna, B.S., and Semple, M.N. (2000). Auditory Temporal Processing: Responses to Sinusoidally Amplitude-Modulated Tones in the Inferior Colliculus. J. Neurophysiol. *84*, 255–273.
Krueger, C., and Tian, L. (2004). A comparison of the general linear mixed model and repeated measures ANOVA using a dataset with multiple missing data points. Biol. Res. Nurs. *6*, 151–157.
Kujawa, S.G., and Liberman, M.C. (2009). Adding Insult to Injury : Cochlear Nerve Degeneration after " Temporary " Noise-Induced Hearing Loss. J. Neurosci. *29*, 14077–14085.
Lamb, T.D., Collin, S.P., and Pugh, E.N. (2007). Evolution of the vertebrate eye: opsins, photoreceptors, retina and eye cup. Nat. Rev. Neurosci. *8*, 960–976.
Landegger, L.D., Psaltis, D., and Stankovic, K.M. (2016). Human audiometric thresholds do not predict specific cellular damage in the inner ear. Hear. Res. *335*, 83–93.
Langner, G., and Schreiner, C.E. (1988). Periodicity coding in the inferior colliculus of the cat. I. Neuronal mechanisms. J. Neurophysiol. *60*, 1799–1822.
Laumen, G., Ferber, A.T., Klump, G.M., and Tollin, D.J. (2016). The Physiological Basis and Clinical Use of the Binaural Interaction Component of the Auditory Brainstem Response. Ear Hear. *37*, e276–e290.
Lee, J. (1994). Amplitude Modulation Rate Discrimination With Sinusoidal Carriers. J. Acoust. Soc. Am. *4*, 2140–2147.
Lemus, L., Hernández, A., and Romo, R. (2009a). Neural codes for perceptual discrimination of acoustic flutter in the primate auditory cortex. Proc. Natl. Acad. Sci. U. S. A. *106*, 9471–9476.
Lemus, L., Hernández, A., and Romo, R. (2009b). Neural encoding of auditory discrimination in ventral premotor cortex. Proc. Natl. Acad. Sci. U. S. A. *106*, 14640–14645.
Lentz, J.J., and Valentine, S. (2015). Across-frequency processing of modulation phase differences in hearing-impaired listeners. J. Acoust. Soc. Am. *138*, EL205–EL211.
Liberman, L.D., and Liberman, M.C. (2015). Dynamics of cochlear synaptopathy after acoustic overexposure. JARO - J. Assoc. Res. Otolaryngol. *16*, 205–219.
Lin, F.R., Metter, E.J., O'Brien, R.J., Resnick, S.M., Zonderman, A.B., and Ferrucci, L. (2011). Hearing loss and incident dementia. Arch. Neurol. *68*, 214–220.
Liu, A.S.K., Tsunada, J., Gold, J.I., and Cohen, Y.E. (2015). Temporal integration of auditory information is invariant to temporal grouping cues. ENeuro *2*.
Liu, L., Wang, H., Shi, L., Almuklass, A., He, T., Aiken, S., Bance, M., Yin, S., and Wang, J. (2012). Silent Damage of Noise on Cochlear Afferent Innervation in Guinea Pigs and the Impact on Temporal Processing. PLoS One *7*, 1–11.
Lonsbury-Martin, B.L., and Martin, G.K. (1981). Effects of moderately intense sound on auditory sensitivity in rhesus monkeys: behavioral and neural observations. J. Neurophysiol. *46*, 563–586.
Lonsbury-Martin, B.L., Martin, G.K., and Bohne, B.A. (1987). Repeated TTS exposures in monkeys: Alterations in hearing, cochlear structure, and single-unit thresholds. J. Acoust. Soc. Am. *81*, 1507–1518.
Loomba, S., Straehle, J., Gangadharan, V., Heike, N., Khalifa, A., Motta, A., Ju, N., Sievers, M., Gempt, J., Meyer, H.S., et al. (2022). Connectomic comparison of mouse and human cortex. Science (80-.). *377*, eabo0924.
Lopez-Poveda, E.A. (2014). Why do I hear but not understand? Stochastic undersampling as a

model of degraded neural encoding of speech. Front. Neurosci. *8*, 1–7.
Lopez-Poveda, E.A., and Barrios, P. (2013). Perception of stochastically undersampled sound waveforms: A model of auditory deafferentation. Front. Neurosci. *7*, 1–13.
Lorenzi, C., Micheyl, C., and Berthommier, F. (1995). Neuronal correlates of perceptual amplitude-modulation detection. Hear. Res. *90*, 219–227.
Lütkenhöner, B. (2011). Auditory signal detection appears to depend on temporal integration of subthreshold activity in auditory cortex. Brain Res. *1385*, 206–216.
Mackey, C., Tarabillo, A., and Ramachandran, R. (2021a). Three psychophysical metrics of auditory temporal integration in macaques. J. Acoust. Soc. Am. *150*, 3176–3191.
Mackey, C.A., McCrate, J., MacDonald, K.S., Feller, J., Liberman, L.D., Liberman, M.C., Hackett, T.A., and Ramachandran, R. (2021b). Correlations between cochlear pathophysiology and behavioral measures of temporal and spatial processing in noise exposed macaques. Hear. Res. *401*, 108156.
Mackey, C.A., Dylla, M.E., Bohlen, P.A., Hrnicek, A., Mayfield, J., and Ramachandran, R. (2022). Correlations between behavior and neuronal responses in the cochlear nucleus (CN) and inferior colliculus of behaving monkeys. BioRxiv.
Macmillan, N.A., and Creelman, C.D. (2004). Detection theory: A user's guide. Psychol. Press.
Malmierca, M.S., and Hackett, T.A. (2010). The Oxford Handbook of Auditory Science: The Auditory Brain. 9–42.
Marmel, F., Cortese, D., and Kluk, K. (2020). The ongoing search for cochlear synaptopathy in humans: Masked thresholds for brief tones in Threshold Equalizing Noise. Hear. Res. *392*, 107960.
Marr, D., Poggio, T., and Brenner, S. (1979). A computational theory of human stereo vision. Proc. R. Soc. London. Ser. B. Biol. Sci. *204*, 301–328.
Marrone, N., Mason, C.R., and Kidd Jr, G. (2008). Tuning in the spatial dimension: Evidence from a masked speech identification task. J. Acoust. Soc. Am. *124*, 1146–1158.
Mast, T. (1973). Dorsal Cochlear Nucleus of the Chinchilla: Excitation by Contralateral Sound. Brain Res. *62*, 61–70.
Matthews, G., and Fuchs, P. (2010). The diverse roles of ribbon synapses in sensory neurotransmission. Nat. Rev. Neurosci. *11*, 812–822.
Maxwell, B.N., Richards, V.M., and Carney, L.H. (2020). Neural fluctuation cues for simultaneous notched-noise masking and profile-analysis tasks: Insights from model midbrain responses. J. Acoust. Soc. Am. *147*, 3523–3537.
McDermott, J., and Hauser, M.D. (2007). Nonhuman primates prefer slow tempos but dislike music overall. Cognition *104*, 654–668.
Miller, J., and Ulrich, R. (2003). Simple reaction time and statistical facilitation: A parallel grains model. Cogn. Psychol. *46*, 101–151.
Monaghan, J.J.M., Garcia-Lazaro, J.A., McAlpine, D., and Schaette, R. (2020). Hidden Hearing Loss Impacts the Neural Representation of Speech in Background Noise. Curr. Biol. *30*, 4710-4721.e4.
Moody, D.B. (1994). Detection and discrimination of amplitude-modulated signals by macaque monkeys. J. Acoust. Soc. Am. *95*, 3499–3510.
Moody, D.B., Stebbins, W.C., Hawkins, J.E., and Johnsson, L.G. (1978). Hearing loss and cochlear pathology in the monkey (Macaca) following exposure to high levels of noise. Arch. Otorhinolaryngol. *220*, 47–72.
Moore, B.C.J. (1996). Perceptual Consequences of Cochlear Hearing Loss and their Implications for the Design of Hearing Aids. Ear Hear. *17*, 133–161.

Moore, J.K. (2000). Organization of the human superior olivary complex. Microsc. Res. Tech. *51*, 403–412.
Moore, B.C.J., and Sęk, A.P. (2019). Discrimination of the phase of amplitude modulation applied to different carriers: Effects of modulation rate and modulation depth for young and older subjects. J. Acoust. Soc. Am. *146*, 1696–1704.
Moore, J.K., Osen, K.K., Storm-Mathisen, J., and Ottersen, O.F. (1996). γ-Aminobutyric acid and glycine in the baboon cochlear nuclei: An immunocytochemical colocalization study with reference to interspecies differences in inhibitory systems. J. Comp. Neurol. *369*, 497–519.
Mowery, T.M., Caras, M.L., Hassan, S.I., Wang, D.J., Dimidschstein, J., Fishell, G., and Sanes, D.H. (2019). Preserving inhibition during developmental hearing loss rescues auditory learning and perception. J. Neurosci. *39*, 0749–19.
Murray, C.A., de Larrea-Mancera, E.S.L., Glicksohn, A., Shams, L., and Seitz, A.R. (2020). Revealing multisensory benefit with diffusion modeling. J. Math. Psychol. *99*, 102449.
Nelson, P.C., and Carney, L.H. (2004). A phenomenological model of peripheral and central neural responses to amplitude-modulated tones. J. Acoust. Soc. Am. *116*, 2173–2186.
Nelson, P.C., and Carney, L.H. (2007). Neural rate and timing cues for detection and discrimination of amplitude-modulated tones in the awake rabbit inferior colliculus. J. Neurophysiol. *97*, 522–539.
Nelson, P.C., Smith, Z.M., and Young, E.D. (2009). Wide-Dynamic-Range Forward Suppression in Marmoset Inferior Colliculus Neurons Is Generated Centrally and Accounts for Perceptual Masking. J. Neurosci. *29*, 2553–2562.
Ng, C., and Recanzone, G.H. (2017). Age-Related Changes in Temporal Processing of Rapidly-Presented Sound Sequences in the Macaque Auditory Cortex. Cereb. Cortex 1–22.
Nieuwenhuis, S., Forstmann, B.U., and Wagenmakers, E.-J. (2011). Erroneous analyses of interactions in neuroscience: a problem of significance. Nat. Neurosci. *14*, 1105–1107.
Nityananda, V., and Bee, M.A. (2012). Spatial release from masking in a free-field source identification task by gray treefrogs. Hear. Res. *285*, 86–97.
Niwa, M., Johnson, J.S., O'Connor, K.N., and Sutter, M.L. (2012a). Active Engagement Improves Primary Auditory Cortical Neurons' Ability to Discriminate Temporal Modulation. J. Neurosci. *32*, 9323–9334.
Niwa, M., Johnson, J.S., O'Connor, K.N., and Sutter, M.L. (2012b). Activity Related to Perceptual Judgment and Action in Primary Auditory Cortex. J. Neurosci. *32*, 3193–3210.
Niwa, M., Johnson, J.S., O'Connor, K.N., and Sutter, M.L. (2013). Differences between Primary Auditory Cortex and Auditory Belt Related to Encoding and Choice for AM Sounds. J. Neurosci. *33*, 8378–8395.
Noda, T., and Takahashi, H. (2015). Anesthetic effects of isoflurane on the tonotopic map and neuronal population activity in the rat auditory cortex. Eur. J. Neurosci. *42*, 2298–2311.
O'Connor, K.N., Barruel, P., Hajalilou, R., and Sutter, M.L. (1999). Auditory temporal integration in the rhesus macaque (Macaca mulatta). J. Acoust. Soc. Am. *106*, 954–965.
O'Connor, K.N., Johnson, J.S., Niwa, M., Noriega, N.C., Marshall, E.A., and Sutter, M.L. (2011). Amplitude modulation detection as a function of modulation frequency and stimulus duration: Comparisons between macaques and humans. Hear. Res. *277*, 37–43.
Parthasarathy, A., Herrmann, B., and Bartlett, E.L. (2019). Aging alters envelope representations of speech-like sounds in the inferior colliculus. Neurobiol. Aging *73*,

30–40.
Parthasarathy, A., Hancock, K.E., Bennett, K., Degruttola, V., and Polley, D.B. (2020a). Bottom-up and top-down neural signatures of disordered multi-talker speech perception in adults with normal hearing. Elife *9*, 1–22.
Parthasarathy, A., Hancock, K.E., Bennett, K., Degruttola, V., and Polley, D.B. (2020b). Bottom-up and top-down neural signatures of disordered multi-talker speech perception in adults with normal hearing. Elife *9*, 1–23.
Paul, B.T., Bruce, I.C., and Roberts, L.E. (2017). Evidence that hidden hearing loss underlies amplitude modulation encoding deficits in individuals with and without tinnitus. Hear. Res. *344*, 170–182.
Peacock, J., Mackey, C.A., Benson, M.A., Burton, J.A., Greene, N.T., Ramachandran, R., and Tollin, D.J. (2021). The Binaural Interaction Component in Rhesus Macaques (Macaca mulatta). Eneuro *8*, ENEURO.0402-21.2021.
Penikis, K.B. (2020). Temporal Coding of Sensory Information by Neural Populations in the Olfactory and Auditory Systems. New York University.
Plomp, R., and Bouman, M.A. (1959). Relation between Hearing Threshold and Duration for Tone Pulses. J. Acoust. Soc. Am. *31*, 749–758.
Prinsloo, K.D., and Lalor, E.C. (2022). General auditory and speech-specific contributions to cortical envelope tracking revealed using auditory chimeras. J. Neurosci. JN-RM-2735-20.
Raab, D.H. (1962). Effect of Stimulus-Duration on Auditory Reaction-Time. Am. J. Psychol. *75*, 298.
Rajala, A.Z., Jenison, R.L., and Populin, L.C. (2017). Neural correlate of auditory spatial attention allocation in the superior colliculus. J. Neurophysiol. jn.00854.2017.
Ramachandran, R. (2018). Subcortical neural correlates of behavior in the auditory system. J. Acoust. Soc. Am. *144*, 1899.
Ramachandran, R., Davis, K. a, and May, B.J. (1999). Single-unit responses in the inferior colliculus of decerebrate cats. I. Classification based on frequency response maps. J. Neurophysiol. *82*, 152–163.
Ramachandran, R., Davis, K.A., and May, B.J. (2000). Rate representation of tones in noise in the inferior colliculus of decerebrate cats. JARO - J. Assoc. Res. Otolaryngol. *1*, 144–160.
Ratcliff, R., and Murdock, B.B. (1976). Retrieval processes in recognition memory. Psychol. Rev. *83*, 190–214.
Ratcliff, R., Huang-Pollock, C., and McKoon, G. (2018). Modeling individual differences in the go/no-go task with a diffusion model. Decision *5*, 42–62.
Resnik, J., and Polley, D.B. (2017). Fast-spiking GABA circuit dynamics in the auditory cortex predict recovery of sensory processing following peripheral nerve damage. Elife *6*, 1–14.
Resnik, J., and Polley, D.B. (2021). Cochlear neural degeneration disrupts hearing in background noise by increasing auditory cortex internal noise. Neuron *109*, 984-996.e4.
Rhode, W.S. (1994). Temporal coding of 200% amplitude modulated signals in the ventral cochlear nucleus of cat. Hear. Res. *77*, 43–68.
Rhode, W.S., Roth, G.L., and Recio-spinoso, A. (2010). Response properties of cochlear nucleus neurons in monkeys. Hear. Res. *259*, 1–15.
Richards, D.G., and Wiley, R.H. (1980). Reverberations and Amplitude Fluctuations in the Propagation of Sound in a Forest: Implications for Animal Communication. Am. Nat. *115*, 381–399.
Rocchi, F., and Ramachandran, R. (2018). Neuronal adaptation to sound statistics in the

inferior colliculus of behaving macaques does not reduce the effectiveness of the masking noise. J. Neurophysiol. jn.00875.2017.
Rocchi, F., and Ramachandran, R. (2020). Foreground stimuli and task engagement enhance neuronal adaptation to background noise in the inferior colliculus of macaques. J. Neurophysiol. *124*, 1315–1326.
Rocchi, F., Dylla, M.E., Bohlen, P.A., and Ramachandran, R. (2017). Spatial and temporal disparity in signals and maskers affects signal detection in non-human primates. Hear. Res. *344*, 1–12.
Rosen, S. (1992). Temporal information in speech. Phil. Trans. R. Soc. Lond. B *336*, 367–373.
Rowland, B.A., and Stein, B.E. (2007). Multisensory integration produces an initial response enhancement. Front. Integr. Neurosci. *1*, 1–8.
Rowland, B.A., Quessy, S., Stanford, T.R., and Stein, B.E. (2007). Multisensory integration shortens physiological response latencies. J. Neurosci. *27*, 5879–5884.
Rubio, M.E., Gudsnuk, K.A., Smith, Y., and Ryugo, D.K. (2008). Revealing the molecular layer of the primate dorsal cochlear nucleus. Neuroscience *154*, 99–113.
Ruggles, D., Bharadwaj, H.M., and Shinn-Cunningham, B.G. (2011). Normal hearing is not enough to guarantee robust encoding of suprathreshold features important in everyday communication. Proc. Natl. Acad. Sci. U. S. A. *108*, 15516–15521.
Ryan, A.F., and Miller, J. (1977). Effects of Behavioral Performance on Single-Unit Firing Patterns in Inferior Colliculus of the Rhesus Monkey. J. Neurophysiol. *40*.
Ryan, A.F., and Miller, J. (1978). Single Unit Responses in the Inferior Colliculus of the Awake and Performing Rhesus Monkey *. Exp. Brain Res. *407*, 389–407.
Saberi, K., Dostal, L., Sadralodabai, T., Bull, V., and Perrott, D.R. (1991). Free-field release from masking. J. Acoust. Soc. Am. *90*, 1355–1370.
Sachs, M.B., and Abbas, P.J. (1974). Rate versus level functions for auditory-nerve fibers in cats: Tone-burst stimuli. J. Acoust. Soc. Am. *56*, 1835–1847.
Sammeth, C.A., Greene, N.T., Brown, A.D., and Daniel, T.J. (2020). Normative Study of the Binaural Interaction Component of the Human Auditory Brainstem Response as a Function of Interaural Time Differences. Ear Hear. 1–15.
Sanders, J.W., and Honig, E.A. (1967). Brief Tone Audiometry: Results in Normal and Impaired Ears. Arch. Otolaryngol. - Head Neck Surg. *85*, 640–647.
Sayles, M., Füllgrabe, C., and Winter, I.M. (2013). Neurometric amplitude-modulation detection threshold in the guinea-pig ventral cochlear nucleus. J. Physiol. *591*, 3401–3419.
Schumacher, J.W., Schneider, D.M., and Woolley, S.M.N. (2011). Anesthetic state modulates excitability but not spectral tuning or neural discrimination in single auditory midbrain neurons. J. Neurophysiol. *106*, 500–514.
Schwaber, M.K., Garraghty, P.E., and Kaas, J.H. (1993). Neuroplasticity of the adult primate auditory cortex following cochlear hearing loss. Am. J. Otol. *14*, 252–258.
Shaheen, L.A., and Liberman, M.C. (2018). Cochlear Synaptopathy Changes Sound-Evoked Activity Without Changing Spontaneous Discharge in the Mouse Inferior Colliculus. Front. Syst. Neurosci. *12*, 1–19.
Shaheen, L., Valero, M.D., and Liberman, M.C. (2015). Towards a Diagnosis of Cochlear Neuropathy with Envelope Following Responses. JARO - J. Assoc. Res. Otolaryngol. *16*, 727–745.
Shaheen, L.A., Slee, S.J., and David, S. V. (2021). Task engagement improves neural discriminability in the auditory midbrain of the marmoset monkey. J. Neurosci. *41*,

284–297.
Sheft, S., and Yost, W.A. (1990). Temporal integration in amplitude modulation detection. J. Acoust. Soc. Am. *88*, 796–805.
Shi, L., Liu, L., He, T., Guo, X., Yu, Z., Yin, S., and Wang, J. (2013). Ribbon synapse plasticity in the cochleae of guinea pigs after noise-induced silent damage. PLoS One *8*.
Shinn-Cunningham, B.G. (2008). Object-based auditory and visual attention. Trends Cogn. Sci. *12*, 182–186.
Slee, S.J., and David, S. V. (2015). Rapid Task-Related Plasticity of Spectrotemporal Receptive Fields in the Auditory Midbrain. J. Neurosci. *35*, 13090–13102.
Smith, P.H., and Rhode, W.S. (1987). Characterization of HRP-labeled globular bushy cells in the cat anteroventral cochlear nucleus. J. Comp. Neurol. *266*, 360–375.
Song, Q., Shen, P., Li, X., Shi, L., Liu, L., Wang, J., Yu, Z., Stephen, K., Aiken, S., Yin, S., et al. (2016). Coding deficits in hidden hearing loss induced by noise: The nature and impacts. Sci. Rep. *6*, 1–13.
Spezio, M.L., Keller, C.H., Marrocco, R.T., and Takahashi, T.T. (2000). Head-related transfer functions of the Rhesus monkey. Hear. Res. *144*, 73–88.
Stahl, A.N., Mondul, J.A., Alek, K.A., Hackett, T.A., and Ramachandran, R. (2022). Audiologic characterization using clinical physiological measures: Normative data from macaque monkeys. Hear. Res. 108568.
Stebbins, W.C. (1982). Concerning The Need for More Sophisticated Animal Models in Sensory Behavioral Toxicology. Environ. Health Perspect. *44*, 77–85.
Stevens, H.E., and Wickesberg, R.E. (1999). Ensemble responses of the auditory nerve to normal and whispered stop consonants. Hear. Res. *131*, 47–62.
Suthakar, K., and Liberman, M.C. (2021). Auditory-nerve responses in mice with noise-induced cochlear synaptopathy. J. Neurophysiol. *126*, 2027–2038.
Suthakar, K., and Liberman, M.C. (2022). Noise masking in cochlear synaptopathy: auditory brainstem response vs. auditory nerve response in mouse. J. Neurophysiol. *127*, 1574–1585.
Suthakar, K., Liberman, M.C., Laboratories, E., Eye, M., Surgery, N., and Disorders, O.C. Auditory-Nerve Responses in Mice with Noise-Induced Cochlear Synaptopathy.
Swets, J. (1973). The Relative Operating Characteristic in Psychology. Science (80-.). *334*, 1415–1420.
Tanner, W.P., and Swets, J. (1954). A decision-making theory of visual detection. Psychol. Rev. *61*, 401–409.
Thome, A., Marrone, D.F., Ellmore, T.M., Chawla, M.K., Lipa, P., Ramirez-Amaya, V., Lisanby, S.H., McNaughton, B.L., and Barnes, C.A. (2017). Evidence for an Evolutionarily Conserved Memory Coding Scheme in the Mammalian Hippocampus. J. Neurosci. *37*, 2795 LP – 2801.
Tollin, D.J. (2003). The lateral superior olive: A functional role in sound source localization. Neuroscientist *9*, 127–143.
Tollin, D.J., and Yin, T.C.T. (2005). Interaural phase and level difference sensitivity in low-frequency neurons in the lateral superior olive. J. Neurosci. *25*, 10648–10657.
Tremblay, K.L., Pinto, A., Fischer, M.E., Klein, B.E.K., Klein, R., Levy, S., Tweed, T.S., and Cruickshanks, K.J. (2015). Self-Reported Hearing Difficulties Among Adults With Normal Audiograms. Ear Hear. *36*, e290–e299.
Trevino, M., Escabi, C.D., Zang, A., Pawlowski, K., and Lobarinas, E. (2022). Effect of Selective Carboplatin-Induced Inner Hair Cell Loss on Temporal Integration in Chinchillas. J.

Assoc. Res. Otolaryngol.
Tsunada, J., Liu, A.S.K., Gold, J.I., and Cohen, Y.E. (2015). Causal contribution of primate auditory cortex to auditory perceptual decision-making. Nat. Neurosci. *19*, 135–142.
Tsunada, J., Cohen, Y.E., and Gold, J.I. (2019). Post-decision processing in primate prefrontal cortex influences subsequent choices on an auditory decision-making task. Elife *8*, 1–21.
Tsunozaki, M., and Bautista, D.M. (2009). Mammalian somatosensory mechanotransduction. Curr. Opin. Neurobiol. *19*, 362–369.
Valero, M.D., Burton, J.A., Hauser, S.N., Hackett, T.A., Ramachandran, R., and Liberman, M.C. (2017). Noise-induced cochlear synaptopathy in rhesus monkeys (Macaca mulatta). Hear. Res. *353*, 213–223.
Vélez, A., Höbel, G., Gordon, N.M., and Bee, M.A. (2012). Dip listening or modulation masking? Call recognition by green treefrogs (Hyla cinerea) in temporally fluctuating noise. J. Comp. Physiol. *198*, 891–904.
Verhulst, S., Ernst, F., Garrett, M., and Vasilkov, V. (2018). Suprathreshold Psychoacoustics and Envelope-Following Response Relations: Normal-Hearing, Synaptopathy and Cochlear Gain Loss. Acta Acust. United with Acust. *104*, 800–803.
Verschooten, E., Desloovere, C., and Joris, P.X. (2018). High-resolution frequency tuning but not temporal coding in the human cochlea. PLoS Biol. *16*, e2005164.
Viemeister, N.F. (1979). Temporal modulation transfer functions based upon modulation thresholds. J. Acoust. Soc. Am. *66*, 1364–1380.
Viemeister, N.F., and Wakefield, G.H. (1991). Temporal integration and multiple looks. J. Acoust. Soc. Am. *90*, 858–865.
Viemeister, N.F., Shivapuja, B.G., and Recio, A. (1992). Physiological Correlates of Temporal Integration. In Auditory Physiology and Perception, (Elsevier), pp. 323–330.
Viswanathan, V., Shinn-Cunningham, B.G., and Heinz, M.G. (2022). Speech Categorization Reveals the Role of Early-Stage Temporal-Coherence Processing in Auditory Scene Analysis. J. Neurosci. *42*, 240–254.
Wakefield, G.H., and Viemeister, N.F. (1990). Discrimination of modulation depth of sinusoidal amplitude modulation (SAM) noise. J. Acoust. Soc. Am. *88*, 1367–1373.
Wallace, M.T., Wilkinson, L.K., and Stein, B.E. (1996). Representation and integration of multiple sensory inputs in primate superior colliculus. J. Neurophysiol. *76*, 1246–1266.
Wang, X., Lu, T., Bendor, D., and Bartlett, E.L. (2008). Neural coding of temporal information in auditory thalamus and cortex. Neuroscience *154*, 294–303.
Wang, Y., Abrams, K.S., Carney, L.H., and Henry, K.S. (2021). Midbrain-Level Neural Correlates of Behavioral Tone-in-Noise Detection: Dependence on Energy and Envelope Cues. J. Neurosci. *41*, 7206–7223.
Ward, W.D., and Duvall, A.J. (1971). Behavioral and Ultrastructural Correlates of Acoustic Trauma. Ann. Otol. Rhinol. Laryngol. *80*, 881–896.
Watson, A.B. (1979). Probability summation over time. Vision Res. *19*, 515–522.
Watson, C.S., and Gengel, R.W. (1969). Signal Duration and Signal Frequency in Relation to Auditory Sensitivity. J. Acoust. Soc. Am. *46*, 989–997.
Webster, D.B., and Fay, R.R. (2013). The mammalian auditory pathway: neuroanatomy (Springer Science & Business Media).
Wiecki, T., Sofer, I., and Frank, M. (2013). HDDM: Hierarchical Bayesian estimation of the Drift-Diffusion Model in Python. Front. Neuroinform. *7*.
Willott, J.F., and Lu, S.-M. (1982). Noise-induced hearing loss can alter neural coding and increase excitability in the central nervous system. Science (80-.). *216*, 1331–1334.

Winer, J.A., and Schreiner, C.E. (2005). The inferior colliculus.
Wong, S.J., Abrams, K.S., Amburgey, K.N., Wang, Y., and Henry, K.S. (2019). Effects of selective auditory-nerve damage on the behavioral audiogram and temporal integration in the budgerigar. Hear. Res. *374*, 24–34.
Wood, K.C., Town, S.M., and Bizley, J.K. (2019). Neurons in primary auditory cortex represent sound source location in a cue-invariant manner. Nat. Commun. *10*, 1–15.
World Health Organization, W.H. (2018). Addressing the rising prevalence of hearing loss.
Wu, P., O'Malley, J.T., de Gruttola, V., and Liberman, M.C. (2020). Age-Related Hearing Loss Is Dominated by Damage to Inner Ear Sensory Cells, Not the Cellular Battery That Powers Them. J. Neurosci. *40*, 6357–6366.
Wu, P., O'Malley, J.T., de Gruttola, V., and Liberman, M.C. (2021). Primary Neural Degeneration in Noise-Exposed Human Cochleas: Correlations with Outer Hair Cell Loss and Word-Discrimination Scores. J. Neurosci. *41*, 4439–4447.
Yao, J., and Sanes, D. (2022). Transformation of acoustic information to sensory decisions in parietal cortex. BioRxiv.
Yao, J.D., and Sanes, D.H. (2021). Temporal Encoding is Required for Categorization, But Not Discrimination. Cereb. Cortex *31*, 2886–2897.
Yao, J.D., Gimoto, J., Constantinople, C.M., and Sanes, D.H. (2020). Parietal Cortex Is Required for the Integration of Acoustic Evidence. Curr. Biol. *30*, 3293-3303.e4.
Yao, J.D., Zemlianova, K.O., Hocker, D.L., Savin, C., Constantinople, C.M., Chung, S., and Sanes, D.H. (2022). Transformation of acoustic information to sensory decision variables in the parietal cortex. BioRxiv 2022.07.05.498869.
Yin, P., Johnson, J.S., O'Connor, K.N., and Sutter, M.L. (2011). Coding of amplitude modulation in primary auditory cortex. J. Neurophysiol. *105*, 582–600.
Yost, W.A. (1991). Auditory image perception and analysis: The basis for hearing. Hear. Res. *56*, 8–18.
Zion Golumbic, E., Ding, N., Bickel, S., Lakatos, P., Schevon, C.A., McKhann, G.M., Goodman, R.R., Emerson, R., Mehta, A.D., Simon, J.Z., et al. (2013). Mechanisms underlying selective neuronal tracking of attended speech at a "cocktail party." Neuron *77*, 980–991.